



Universidade do Minho
Escola de Engenharia

Catarina Gonçalves Fernandes Gomes

Passive Blade Ice Protection Using Icephobic Surfaces



Universidade do Minho

Escola de Engenharia

Catarina Gonçalves Fernandes Gomes

Passive Blade Ice Protection Using Icephobic Surfaces

Dissertação de Mestrado

Mestrado Integrado em Engenharia Mecânica

Trabalho efetuado sob a orientação do:

Professor Doutor Eurico Augusto Rodrigues de Seabra

DIREITOS DE AUTOR E CONDIÇÕES DE UTILIZAÇÃO DO TRABALHO POR TERCEIROS

Este é um trabalho académico que pode ser utilizado por terceiros desde que respeitadas as regras e boas práticas internacionalmente aceites, no que concerne aos direitos de autor e direitos conexos.

Assim, o presente trabalho pode ser utilizado nos termos previstos na licença abaixo indicada.

Caso o utilizador necessite de permissão para poder fazer um uso do trabalho em condições não previstas no licenciamento indicado, deverá contactar o autor, através do RepositóriUM da Universidade do Minho

Licença concedida aos utilizadores deste trabalho



Atribuição-NãoComercial

CC BY-NC

<https://creativecommons.org/licenses/by-nc/4.0/>

ACKNOWLEDGMENTS

Several people supported and contributed, either with their knowledge or with their presence, to the development of this Master's dissertation. As such, some acknowledgment must be addressed.

First and foremost, I would like to thank my supervisors at Vestas, Julian Anaya and Shane McGuire, for all the advice, accessibility and continuous support throughout all the work. Additionally, I would like to thank Professor Eurico Seabra, my academic supervisor, who was always available to answer my questions.

To Professor Vitor Carneiro for his help setting up my experimental facilities and for his constant support, fundamental for the development of this project. I would also like to thank the engineer Filipe Marques for the help he gave me in the initial phase of the work, spending a lot of his time accompanying me.

A big thanks to Doctor Armando Ferreira for all the help he always offered and for guiding me in the right direction and to Doctor Pedro Martins for all the hours he spent with me for the preparation of the coatings and for all the knowledge he passed on to me.

Thank you to my Vestas colleagues, who always made me feel integrated and provided me with a healthy and happy work environment.

A special thank you to my friends of "Frangos" and "Players", the first ones for making my academic experience unforgettable and the second ones because although we have chosen different paths, every weekend they cross each other again.

Last but not least, I would like to express my deep gratitude to my family, especially my mother and sister for all the unconditional support and for all the sacrifices they made for me to provide me with everything I needed throughout my life. For all the care, help and love, a very sincere thank you.

STATEMENT OF INTEGRITY

I hereby declare having conducted this academic work with integrity. I confirm that I have not used plagiarism or any form of undue use of information or falsification of results along the process leading to its elaboration.

I further declare that I have fully acknowledged the Code of Ethical Conduct of the University of Minho.

Universidade do Minho, 18 de janeiro de 2023

ABSTRACT

Ice accumulation on blade surfaces severely limits the normal operation of wind turbine generators. At present, commercially available technologies to mitigate this problem consist of expensive, energy hungry heating elements. An alternative is the implementation of icephobic coatings. The icephobicity of a surface can be quantified by measuring how strongly ice adheres to it. This simple statement implies rather complex tasks: creating artificial ice on a surface and removing the ice from the surface in a measurable and reproducible way.

In the present research, a comprehensive study was conducted to characterize ice adhesion strength over various surfaces by using a custom-built shear strength tester. The studied surfaces include both laboratory developed and commercially available coatings. In addition, the contact angles for all the surfaces were also measured to correlate the wettability and the measured ice adhesion, that is, hydrophobicity with the icephobicity.

Furthermore, two numerical simulations were performed to identify the measurement uncertainties of the ice adhesion test model and to analyse the effects of the aerodynamical forces that operate in a commercial turbine.

The main results drawn from this work are that there is no direct relationship between icephobicity and hydrophobicity and that icing prevention on wind turbine blades by coating alone is not realistically enough. The alternative that best applies is the combination of an active ice mitigation system with the application of these coatings.

Keywords: Hydrophobicity; Ice adhesion strength; icephobicity; shear stress; wind turbine blades.

RESUMO

A acumulação de gelo nas superfícies das pás limita severamente a operação normal das turbinas eólicas. Atualmente, as tecnologias comercialmente disponíveis para mitigar este problema consistem em elementos de aquecimento dispendiosos e que consomem muita energia. Uma alternativa é a implementação de revestimentos “gelofóbicos”. A “gelofobicidade” de uma superfície pode ser quantificada medindo o seu grau de aderência ao gelo. Esta simples afirmação implica tarefas bastante complexas: criar gelo artificial numa superfície e remover o gelo da superfície de forma mensurável e reproduzível.

No presente projeto, foi realizado um estudo abrangente para analisar a resistência de várias superfícies à aderência do gelo, através de um equipamento de medição de tensão de corte adaptado. As superfícies estudadas incluem tanto revestimentos desenvolvidos em laboratório como revestimentos disponíveis comercialmente. Adicionalmente, também foram medidos os ângulos de contacto para todas as superfícies de forma a correlacionar a molhabilidade e a aderência de gelo medida, ou seja, a hidrofobicidade com a “gelofobicidade”.

Para além disso, foram realizadas duas simulações numéricas para identificar as incertezas de medição do modelo de teste de aderência do gelo e para analisar os efeitos das forças aerodinâmicas a que uma turbina comercial está sujeita.

Os principais resultados retirados deste trabalho são a não existência de uma relação direta entre a gelofobicidade e a hidrofobicidade e que a prevenção da formação de gelo nas pás das turbinas eólicas através da utilização única destes revestimentos não é suficientemente realista. Uma alternativa que melhor se aplica é a combinação de um sistema de mitigação do gelo ativo com a aplicação de revestimentos gelofóbicos.

Palavras-Chave: Hidrofobicidade; força de adesão do gelo; gelofobicidade; tensão de corte; pás das turbinas eólicas.

TABLE OF CONTENTS

Acknowledgments.....	ii
Abstract.....	iv
Resumo.....	v
List of Figures.....	ix
List of Tables.....	xiii
List of Abbreviations and Symbols.....	xiv
1. Introduction	1
1.1. Motivation	2
1.2. Objectives	2
1.3. Dissertation Structure.....	3
2. Literature Review.....	4
2.1. Wind Resources and Energy	4
2.2. Phases of Icing.....	5
2.3. Icing Types.....	6
2.3.1. Atmospheric Icing.....	6
2.4. Impact of Icing.....	8
2.4.1. Full stop of the turbine.....	8
2.4.2. Aerodynamic loss	9
2.4.3. Overloading	10
2.4.4. Human Safety Risks.....	10
2.4.5. Measurement Errors.....	10
2.4.6. Overproduction	10
2.5. Icing Mitigation Systems.....	10
2.5.1. Active Methods	11

2.5.2.	Passive Methods.....	16
2.6.	Hybrid Strategy	20
2.7.	Vestas Cold Climate Solutions	21
2.8.	Icephobic Surfaces.....	22
2.8.1.	Definition of Icephobicity.....	22
2.8.2.	Types of Icephobic Coatings.....	23
2.9.	Hydrophobic and Superhydrophobic Coatings.....	24
2.9.1.	Surface Wettability and Contact Angle	25
2.9.2.	Surface Roughness.....	27
2.9.1.	Water and Ice Adhesion	30
2.10.	Potential Coating Candidates	32
3.	Methodology	34
3.1.	Materials.....	35
3.1.1.	Substrates.....	35
3.1.2.	Polyvinylidene Fluoride (PVDF)	35
3.1.3.	Titanium Dioxide (TiO ₂).....	35
3.1.4.	Dimethylformamide (DMF)	35
3.1.5.	Wearlon Super F-1	35
3.1.6.	Chemona Multi Coat.....	36
3.1.7.	HIREC 300-W	36
3.2.	Preparation Methods	37
3.3.	Methods.....	41
3.3.1.	Contact Angle Measurement.....	41
3.3.2.	Ice Adhesion Strength Measurement.....	42
3.4.	Numerical Analysis.....	45

3.4.1.	Stress Distribution	45
3.4.2.	Aeromechanical Force Analysis	50
4.	Results and Discussion	53
4.1.	Contact Angle Measurement.....	53
4.2.	Ice Adhesion Strength Measurement.....	55
4.3.	Numerical Analysis.....	62
4.3.1.	Stress Distribution	62
4.3.2.	Aeromechanical Force Analysis	64
5.	Conclusions and Future Work.....	69
5.1.	Main Conclusions.....	69
5.2.	Future Work	71
Annex A:	Summary of Ice Mitigation Methods.....	73
Annex B:	Water Contact Angle Results.....	75
Annex C:	Water Contact Angle Normal Distribution	79
Annex D:	Ice Adhesion Strength Results	80
Annex E:	Ice Adhesion Strength Normal Distribution	89
Annex F:	COMSOL Image Results.....	91
Annex G:	COMSOL Shear Stress Results	115
References	117

LIST OF FIGURES

- Figure 2.1 – Timeline of an icing event [8]. 5
- Figure 2.2 – Classification of the different types of ice. 6
- Figure 2.3 – a) Rime ice on a tree [13]. b) Rime ice accretion over wind turbine blades [14]...... 7
- Figure 2.4 – a) Glaze ice [15]. b) Glaze ice accretion over wind turbine blades [14]. 7
- Figure 2.5 – Airfoil shape altered by ice [8]. 9
- Figure 2.6 – 3D power curve as a function of wind speed and ice load [16]. 9
- Figure 2.7 – Categorization of anti-icing and de-icing systems (ADIS). 11
- Figure 2.8 – Placement of the heating elements on the leading edges of the wind turbine blades [7]. 12
- Figure 2.9 – Hot air injection system [18]. 13
- Figure 2.10 – Working principle of inflated rubber boots [8]. 14
- Figure 2.11 – Electro-Magnetic Expulsion De-icing System [19]. 14
- Figure 2.12 – Ultrasonic de-icing technique currently being tested [21]. 15
- Figure 2.13 – Blade pitch control (adapted from [22]). 17
- Figure 2.14 – Manual ice removal from the wind turbine blade [23]. 17
- Figure 2.15 – Ice removal with hot water sprayed from the helicopter [24]. 18
- Figure 2.16 – Black paint on the wind turbine blade [27]. 19
- Figure 2.17 – Visual representation of the electrothermal elements [30]. 21
- Figure 2.18 – Different features of an icephobic coating (adapted from [35]). 23
- Figure 2.19 – Ice deposition on smooth surfaces (adapted from [37]). 23
- Figure 2.20 – Ice deposition on textured surfaces (adapted from [37]). 24
- Figure 2.21 – Ice deposition on slippery surfaces (adapted from [37]). 24
- Figure 2.22 – a) Lotus leaf effect [36]. Drop of water on a duck feather [37]. 25
- Figure 2.23 – a) Sessile drop on a hydrophilic surface and b) on a hydrophobic surface [45]. .. 26

Figure 2.24 – Balanced contact angle between a triple interface between the liquid (<i>l</i>), the solid (<i>s</i>) and the surrounding vapour (<i>v</i>) (adapted from [46]).	26
Figure 2.25 – Wenzel model (adapted from [51]).	28
Figure 2.26 – The surface roughness amplifies wettability [52].	29
Figure 2.27 – Surface roughness decreases wettability [52].	29
Figure 2.28 – Cassie Baxter model (adapted from [10]).	29
Figure 2.29 – Thermodynamic work of ice adhesion normalized by the surface tension of water W_{aylv} as a function of water contact angle θ [56].	31
Figure 3.1 – Diagram of the adopted methodology.	34
Figure 3.2 – Ice adhesion reduction, AMIL's results [76].	36
Figure 3.3 – Vertical band saw used to cut the blade samples.	37
Figure 3.4 – a) Weighing of samples with a precision balance. b) Percentages of TiO ₂ used (2.5%,5,10%).	38
Figure 3.5 – a) Different percentages of TiO ₂ dispersed in DMF. b) Solutions in an ultrasonic bath.	39
Figure 3.6 – Magnetic stirrer used for complete dissolution.	39
Figure 3.7 – a) Spray painting of the coatings. b) Coatings in the oven at 210°C.	40
Figure 3.8 – Representative scheme of the method of synthesis of TiO ₂ nanoparticles.	40
Figure 3.9 – Dataphysics OCA 15 Plus equipment for contact angle measurement.	41
Figure 3.10 – Horizontal shear test.	42
Figure 3.11 – Complete setup of the vertical shear test.	43
Figure 3.12 – Existing forces according to the platform distance: shear, normal and mixed.	44
Figure 3.13 – a) CAD model in Solidworks. b) 3D printed plastic mold. c) Silicone mold used to create the ice cube.	44
Figure 3.14 – Steps for the formation of the ice cube on the surface of the sample.	44
Figure 3.15 – 3D Finite element model in ANSYS.	46

Figure 3.16 – Meshed FEM model.	47
Figure 3.17 – Fixed support condition.	47
Figure 3.18 – a) Velocity value and direction entered in the software. b) Earth gravity effect condition.	48
Figure 3.19 – x and y displacement condition.	48
Figure 3.20 – Boundary conditions applied in this model.	49
Figure 3.21 – Circular geometry used to recreate the ice shape.	50
Figure 3.22 – Runback ice shape, consulted on [84].	51
Figure 3.23 – Location of the ice drops on the airfoil.	52
Figure 3.24 – Flowchart of numerical analysis steps.	52
Figure 4.1 – Variation of the contact angle and the relative standard deviation of the different coatings.	54
Figure 4.2 – Variation of the ice adhesion strength and the relative standard deviation of the different coatings.	55
Figure 4.3 – Effect of the percentage of TiO_2 nanoparticles in the ice adhesion strength value. .	56
Figure 4.4 – Signal to noise ratio (SNR) calculation based on measurement data [86].	57
Figure 4.5 – Comparison of the contact angle and ice adhesion strength.	59
Figure 4.6 – Shear stress values and distribution at the ice-substrate interface.	62
Figure 4.7 – Normal stress values and distribution at the ice-substrate interface.	63
Figure 4.8 – Torque effect leading to compression at the top and tension at the bottom.	63
Figure 4.9 – Image obtained from the COMSOL software for the circular geometry.	64
Figure 4.10 – Image obtained from the COMSOL software for the runback ice geometry.	64
Figure 4.11 – Variation of the shear stress for the circular geometry with a radius of 1 mm.	65
Figure 4.12 – Variation of the shear stress for the circular geometry with a radius of 5 mm.	65
Figure 4.13 – Variation of the shear stress for the circular geometry with a radius of 10 mm. ..	66

Figure 4.14 – Variation of the shear stress for the runback ice geometry with a height of 1 mm.	66
Figure 4.15 – Variation of the shear stress for the runback ice geometry with a height of 5 mm.	67
Figure 4.16 – Variation of the shear stress for the runback ice geometry with a height of 10 mm.	67
Figure 4.17 – Comparison between the shear stress results taken from the COMSOL software (when the forces are higher) and the results obtained in the ANSYS software.....	68

LIST OF TABLES

Table 2.1 – Wettability conditions of a surface by contact angle measurement (θ) (adapted from [49]). 27

Table 2.2 – Collection of coatings and surfaces presented in the literature for different types of tests. WB stands for wetting behaviour, SH for superhydrophobic, HP for hydrophobic and HF hydrophilic. ARF stands for adhesion reduction factor. 33

Table 3.1 – Chemona Multi Coat composition [77]. 36

Table 3.2 – HIREC 300-W composition [79]. 37

Table 3.3 – Mass/volume used in the preparation of each coating..... 38

Table 3.4 – Laboratory-produced and commercially purchased coatings. 40

Table 3.5 – Mechanical proprieties of ice and PVDF inserted in the software..... 46

Table 3.6 – Maximum values of the forces measured experimentally for each coating. 49

Table 4.1 – Summary of the water contact angle measurements. 53

Table 4.2 – Summary of the ice adhesion strength results..... 55

Table 4.3 – Signal-to-noise ratio calculation for the different tests of the Wearlon coating..... 58

LIST OF ABBREVIATIONS AND SYMBOLS

Abbreviations

CO ₂	Carbon dioxide;
AEP	Annual energy production;
ADIS	Anti-icing and de-icing systems;
SHS	Superhydrophobic surfaces;
CA	Contact angle;
ARF	Adhesion reduction factor;
PTFE	Polytetrafluoroethylene;
PVDF	Polyvinylidene fluoride;
PDMS	Polydimethylsiloxane;
RTV	Room temperature vulcanizing silicone;
TiO ₂	Titanium dioxide;
SiO ₂	Silicon dioxide;
SH	Superhydrophobic;
HP	Hydrophobic;
HF	Hydrophilic;
Si	Silicon;
PMMA	Poly(methyl methacrylate);
PS	Polystyrene;
SLIPS	Slippery liquid-infused porous surfaces;
SLIC	Self-lubricating icephobic coating;
DMF	Dimethylformamide;
(CH ₃) ₂ NC(O)H	Dimethylformamide;
USA	United States of America;

AMIL	Anti-Icing Materials International Laboratory;
DEM	Mechanical engineering department;
IB-S	Institute of Science and Innovation for Bio-Sustainability;
ISO	International Organization for Standardization;
CAD	Computer-aided design;
SD	Standard deviation;
RSD	Relative standard deviation;
CFD	Computational fluid dynamics;
SNR	Signal-to-noise ratio;
AFM	Atomic force microscope.

Symbols

l	Liquid;
s	Solid;
v	Vapour;
θ	Contact angle;
γ_{lv}	Liquid/vapour surface tension;
γ_{sv}	Solid/vapour surface tension;
γ_{ls}	Liquid/solid surface tension;
r	Roughness factor;
A_{real}	Rough interfacial area;
$A_{projected}$	Flat interfacial area;
θ_{rough}	Apparent static angle;

f_s	Solid area fraction;
f_v	Vapour area fraction;
θ_{app}	Apparent angle;
θ_s	Liquid/solid contact angle;
θ_v	Liquid/vapour contact angle;
f	Surface fraction;
i	Ice;
W_a	Thermodynamic work of adhesion;
γ_{iv}	Ice/vapour surface free energy;
γ_{is}	Ice/solid surface free energy;
τ	Ice adhesion strength;
F_S	Applied shear force;
A	Cross-section area;
τ_{ub}	Ice adhesion strength of the uncoated blade;
τ_{cb}	Ice adhesion strength of the coated blade;
A_{signal}	Peak amplitude of the shear stress;
σ_{noise}	Standard deviation of the noise.

1. INTRODUCTION

Non-renewable energies, mostly fossil fuels, have been causing big environmental, social and economic changes all around the world. The scientific analysis and reports on these energy sources and the alarming impacts felt in several areas have led to the international community having increasing concerns in the search for reliable alternatives, over the last couple of years.

Currently, the use of renewable energy resources is seen as vital to achieve sustainable development. Within these, wind energy presents itself as one of the most promising renewable energy sources for massive production of electricity, mainly due to technological advancement in wind turbines, but also to awareness on the part of consumers, as well as government financial incentives.

Within the wind energy industry, the Danish company, Vestas, stands out for being currently the world's largest producer of wind turbines and it is responsible for its design, manufacture, sale, transport and maintenance across the globe. In January 2022, Vestas was named the most sustainable company in the world in the 18th annual Global 100 ranking published by Corporate Knights [1].

Commonly wind turbine farms are located in colder regions, as they have a higher wind energy potential than other regions, due to the higher density of the air. So, these regions are exposed frequently to icing events. Ice accumulation represents the most significant threat to the integrity of wind turbines in cold weather, as the roughness generated from ice accretion on the blades can significantly reduce their aerodynamic performance and consequently the power production of the wind turbine.

Over the years, wind power companies, including Vestas, have developed several ice protection systems to overcome these effects. Although currently available techniques for ice removal are generally effective, they require a high-power consumption, are expensive to operate and time-consuming. Another problem that these systems present is the runback ice, which happens when the water, a consequence of the ice melting on the heated elements, runs back and freezes again.

An optional solution to these icing problems is the use of surfaces with low ice adhesion properties: icephobic coatings. The application of such coatings can help in reducing the shear forces needed to remove the ice from the blades, subsequently, ice can be shed through external forces, such as wind and gravity. Due to the low installation cost and reduction of the power input, a hybrid strategy that combines the current electro-thermal systems and icephobic coatings has attracted more and more attention as a viable strategy for ice mitigation on wind turbine blades. Therefore, the present work focuses on the study

of this option and was carried out in partnership with Vestas, with continuous monitoring throughout its development.

1.1. MOTIVATION

The main motivation behind this project is the existence of few documents and investigations on icephobic coatings. Most research has been published after 2005, making it a new research field. Since its study is still at a primary stage, there is still no consensus in the scientific community on the definition of icephobicity itself.

One approach analysed in the present report focuses on water repellent surfaces, i.e. hydrophobic coatings, for ice mitigation. Nevertheless, the appropriateness of hydrophobicity for anti-icing applications is still controversial, considering that the mechanics of ice and water adhesion are different.

The integration of icephobic coatings in wind turbine blades as a complementary ice mitigation system to the existing ones could bring environmental and economic benefits. Obviously, finding reliable and effective solutions for mitigating or completely impeding the ice adhesion on solid surfaces is an ongoing challenge of substantial industrial and scientific value, further demonstrating the necessity of the present project.

1.2. OBJECTIVES

The aim of this thesis is to study the icephobic performance of different coatings ranging from superhydrophobic to polymer surfaces for wind turbine blade application.

In order to accomplish the main objective of the project, several sub-objectives were also defined:

- Literary review of concepts and previous studies on icephobic coatings;
- Study of the ice adhesion strength by using a shear testing facility;
- Measurement of the water contact angle of each coating;
- Analyze the correlation between surface wettability and ice adhesion strength;
- Development of a numerical model of the ice adhesion experiment;
- Aerodynamic study of the effect of the external forces acting on the airfoil.

1.3. DISSERTATION STRUCTURE

This dissertation consists of 5 Chapters in total. A brief summary of each one is given below:

Chapter 1 brings together general considerations designed to frame the reader in the topic addressed, establishes the objectives to be achieved in the course of this work and describes the structure adopted for the dissertation and its general organization.

The next chapter, Chapter 2, presents a background of the topics that are relevant to understand the scope and importance of the developed work. Initially, a framework is made of wind energy, problems caused by ice, nature and ice formation, and existing ice mitigation systems. Subsequently, icephobic surfaces are addressed, emphasizing their applicability in reducing ice accumulation. Next, hydrophobic surfaces are referred to as potential icephobic surfaces, where several concepts are discussed, including surface wettability, contact angle, roughness and differences between water and ice adhesion. Finally, several scientific articles related to icephobicity are reviewed with respect to their methodology and effectiveness.

Chapter 3 establishes the methodology involved in the project, including the materials and methods used to prepare the blade samples. In this segment is also covered the equipment and conditions used for the quantitative study of ice adhesion strength and water contact angle for the different surfaces. The end of this section introduces a finite element study of the ice adhesion testing model to understand the stress distribution effects at the ice-solid interface and an aerodynamic analysis of the shear stress in an airfoil caused by the external forces to which it is subjected.

Chapter 4 describes the experimental results and their discussions. The values obtained for the ice adhesion strength for each coating are presented and compared to the reference sample. As well, the surfaces are divided into hydrophilic, hydrophobic and superhydrophobic based on their contact angles. Additionally, the ice adhesion characteristics were compared to the contact angle of the surfaces to study the influence of surface wettability on the ice adhesion strength. Furthermore, the results obtained in the numerical simulations are also referred and analysed.

Finally, Chapter 5 discusses the significance and conclusion of this study. Also in this chapter, some suggestions for possible future work are pointed out.

2. LITERATURE REVIEW

This chapter reviews many key aspects relevant to the whole thesis. This involves some explanations regarding some general knowledge about wind turbine technology development and one of the problems that affect its performance, ice accumulation. The last section presents an alternative to the currently most used systems in ice mitigation, with the main objective of reducing energy consumption.

2.1. WIND RESOURCES AND ENERGY

Since early recorded history, people have harnessed the energy of the wind, mostly for their own purposes. It was used by windmills for grinding grain or pumping waters, as well in the sailing ships, as their main source of energy.

Eventually, new ideas and ways of using the energy of the wind would spread around the world. The first known wind turbine used to produce electricity was built in Scotland, in 1887, by Professor James Blyth of Anderson's. A year later, wind energy made it to the United States as Ohio inventor Charles Brush created a wind turbine to provide electricity for his mansion [2].

In 1957 a Danish engineer named Johannes Juul built a horizontal-axis wind turbine. The basics he used from his research and development were very important in the establishment of a wind turbine concept which consisted of a three-bladed, stall-regulated rotor at a fixed speed, with an induction machine drive train. This very simple model had a big success with most of the other countries adapting their models to this prototype [3].

Despite wind power not generating as much electricity as fossil fuels, and thus not being an immediate substitute for petroleum in most applications, all the concerns about the shortages only stacked to the urgency to expand wind power, alongside other renewable energies. Earlier oil crises had already caused many utility and industrial users of petroleum to shift to coal or natural gas, and wind power had already shown great potential for replacing natural gas in electricity generation on a cost basis with the technological advances made in the last years [4], [5].

Nowadays, the main reason for the use of wind turbines to generate electrical power is to lower the CO₂ emissions as much as possible to help limit climate change. Even with that in mind, there is still a lot of discrepancy between the investments made by different countries, and there are a lot of important

factors having their respective impact on the investment of every country. Those factors include firstly the wind potential of the respective country as well as their financial support for the investment and secondly, bureaucratic issues like permissions for construction or local impact in populations, having even some investments being done in offshore sites to avoid this factor [5].

2.2. PHASES OF ICING

In regions with cold climates, available wind power is approximately 10% higher than in other regions due to the increase in air density at lower temperatures [6]. Consequently, wind turbines, particularly the turbine blades, are facing possible icing events, which affect the integrity of the outdoor equipment and are detrimental to turbine performance and durability. The process of ice accumulation or so-called phases of an icing event is important for the understanding of the operation of wind turbines and the ice mitigation systems.

An icing event can be described using meteorological icing, recovery time, incubation time, and instrumental icing (Figure 2.1). From a meteorological point of view, an icing event is the succession of two phases: meteorological icing, when weather conditions (temperature, humidity, wind speed, etc.) lead to the formation of ice, followed by recovery time, which is the time it takes to remove the ice from the blades. From an instrumental point of view, it is also the succession of two phases: incubation time, which is the time before equipment, such as anemometers, can detect the ice, followed by instrumental icing, which is the period when the ice affects the equipment (loss of production). Therefore, incubation time is the period between the beginning of meteorological icing and the beginning of instrumental icing, while recovery time is the period between the end of meteorological icing and the end of instrumental icing [7], [8].

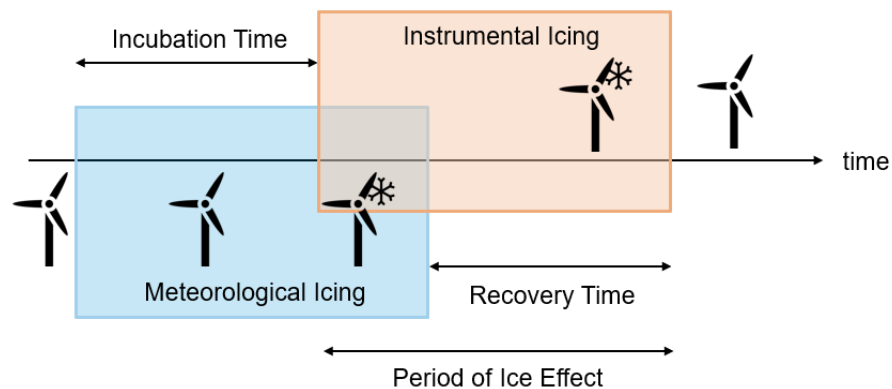


Figure 2.1 – Timeline of an icing event [8].

2.3. ICING TYPES

The type of ice that forms on the surface of wind blades is dependent on several factors like the air temperature, relative humidity, barometric pressure, air density, altitude and wind speed, as well as on the heat balance occurring at the surface. Predicting the type and shape of ice accretion for a specific set of icing conditions is difficult because of the complex interactions between the atmospheric and meteorological parameters [9].

2.3.1. ATMOSPHERIC ICING

Atmospheric icing is defined as the accretion of ice or snow on structures that are exposed to the atmosphere, like wind turbine blades. Three different types of atmospheric icing can be distinguished: in-cloud icing, precipitation icing and frost. The third type, frost, is not believed to significantly impact wind turbines and their loads. In-cloud icing can be further subdivided into rime and glaze and precipitation icing into freezing rain and wet snow [10] [8]. The classification of the different types of ice is illustrated in Figure 2.2.

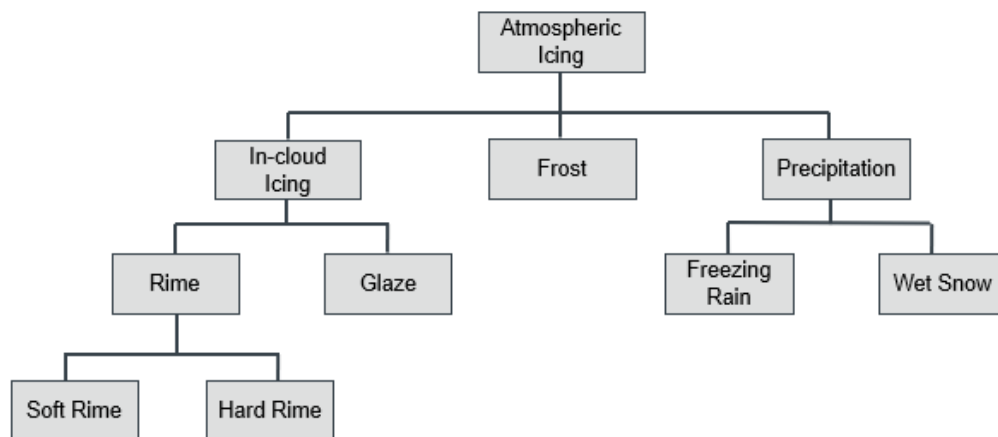


Figure 2.2 – Classification of the different types of ice.

2.3.1.1. IN-CLOUD ICING

In-cloud icing happens when supercooled water droplets hit a surface below 0°C and freeze upon impact. The droplet's temperature can be as low as -30°C and because of their size, they don't freeze in the air. The temperature and size of the droplets determine whether the ice formed will be considered soft rime, hard rime or glaze [11].

- **Rime:** It is formed when the thermal energy released by the formation of ice from the droplets that are impacting the surface is removed quickly enough by wind and radiation

so that no liquid water is present on the surface. Rime appears white and breaks off easier than glaze (Figure 2.3) [12].



Figure 2.3 – a) Rime ice on a tree [13]. b) Rime ice accretion over wind turbine blades [14].

Soft rime forms when the droplet size is small and the water content in the air is low. The resulting accretion will have little adhesion and low density, due to larger gaps between the frozen particles [12].

Hard rime forms with medium droplet size and higher water content in the air. Subsequently, it has a higher density, due to better bonding and smaller air gaps between the frozen particles, which is more difficult to remove [12].

- **Glaze:** it is formed when a portion of the droplets does not freeze upon impact but runs back on the surface and freezes later (Figure 2.4). It is more difficult to remove than rime ice due to its inherent physical properties, including higher adhesion pressure [11].



Figure 2.4 – a) Glaze ice [15]. b) Glaze ice accretion over wind turbine blades [14].

2.3.1.2. PRECIPITATION

Precipitation occurs when – either rain or snow – freezes after hitting the surface. The accretion rate can be much higher than in-cloud icing, which will cause more damage to the blades. Precipitation icing may result in freezing rain or wet snow, depending on how the precipitation is influenced by variations in temperature [12].

- **Freezing rain:** when rain falls on the surface whose temperature is below 0°C. Ice adhesion and density are high when this phenomenon occurs [11].
- **Wet snow:** when snow is slightly liquid at a temperature between 0°C and -3°C and it sticks to the surface. It is easy to remove at first but can be difficult if it freezes on the surface [11].

2.3.1.3. FROST

Frost forms when the water vapour solidifies directly on a cool surface. It often occurs during low winds [11].

2.4. IMPACT OF ICING

Wind turbines operating in cold regions or at high altitudes frequently face icing conditions, which can lead to a significant reduction in the performance of the wind turbine. Many methods have been presented to reduce or eliminate the icing on wind turbine blades, to decrease the economic loss caused by icing and assure their maximum reliability. Prior to addressing ice mitigation measures, the significant problems related directly to icing are discussed.

2.4.1. FULL STOP OF THE TURBINE

In some cases, severe icing has led to the complete stop of the turbine, resulting in significant energy loss. Indeed, downtimes can last several days or weeks, due to the persistent ice on the blades. One example is a turbine in Sweden that was stopped for over 7 weeks, because of icing, in the winter of 2002–2003. The Swedish statistical incident database contains a total of 1337 such ‘stop’ records reported to have occurred between 1998 and 2003, resulting in a total downtime of 161,523 hours. Ninety-two of the incidents (7%) were related to the cold climate and resulted in 8022 hours (5%) of production loss [12].

2.4.2. AERODYNAMIC LOSS

Aerodynamically, the presence of ice could change the surface roughness of the blade and alters the profile of the airfoil, which changes the lift and drag coefficients, causing a reduction in the aerodynamic performance, leading to a severe loss of performance.

Figure 2.5 shows a few examples of airfoil shapes altered by ice. In serious cases, the blade torque will be reduced to zero, and the unit will stop power output completely. Annual production losses are between 0.005% and 50%, depending on the intensity, duration and annual frequency of icing events. Vestas reported an impact of up to 10% on Annual Energy Production (AEP) [8][6].

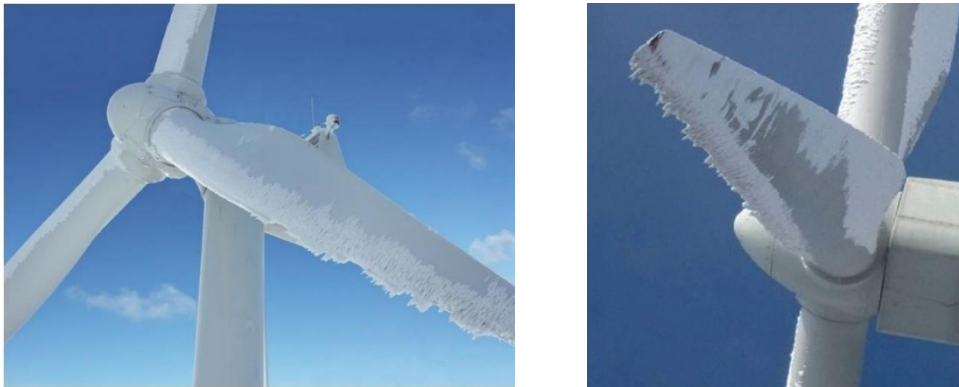


Figure 2.5 – Airfoil shape altered by ice [8].

Based on field measurements and/or models, power curves for wind turbines affected by ice accretion have been developed. For example, Figure 2.6 illustrates a specific 3D power curve that shows energy as a function of wind speed and ice load [16].

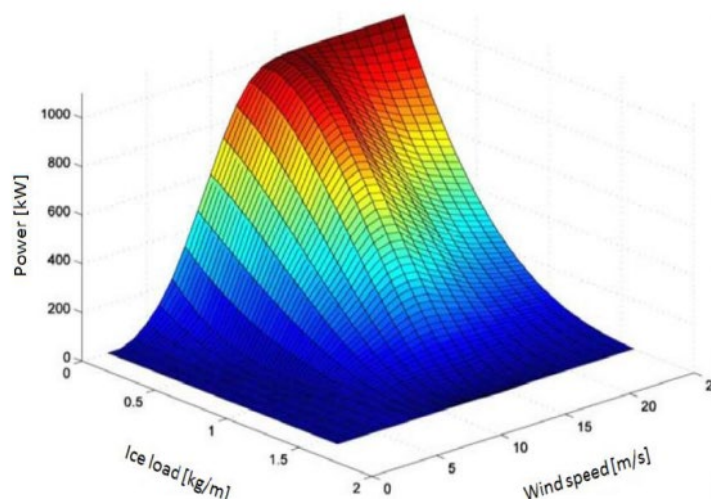


Figure 2.6 – 3D power curve as a function of wind speed and ice load [16].

2.4.3. OVERLOADING

Ice coating on the blade surface will increase the load of the blade and other key components. In addition to this, iced turbine blades become unbalanced. Even though wind turbines are designed to support extreme loads, the fatigue loads will shorten the lifetime of the components. Additional ice masses will cause higher deterministic loads, asymmetric masses will cause unbalance, ice accretion will increase the excitation of edgewise vibrations and resonance may occur due to the changed natural frequencies of the blades, particularly for smaller turbines and lightweight rotor blades [8][17].

2.4.4. HUMAN SAFETY RISKS

Because most of the ice layers are located at the tip of the blade, when the ice layer of the blade melts and falls off, the falling ice has a large centrifugal force, which will make the ice fly out along the rotation direction of the blade, consequently, could damage other units nearby and cause hidden danger to the life safety of workers [17].

2.4.5. MEASUREMENT ERRORS

Blade icing will increase the measurement error of wind speed and direction measuring instruments, causing a wrong reading of the value. In icing conditions, wind speed errors can be as high as 30% [6].

2.4.6. OVERPRODUCTION

Higher air density related to low temperatures and airfoil modifications can lead to the overproduction of wind turbines. Up to 16% of overproduction has been recorded [6].

2.5. ICING MITIGATION SYSTEMS

As mentioned in the previous chapter, the accumulation of ice affects wind turbine operation in various ways, including measurement errors, power losses, mechanical failures and safety hazards.

In recent years, extensive research has been undertaken to identify and model ice prevention methods. Most of these methods are taken from the aviation industry and can be classified into two categories: active and passive. Active methods rely on an external system applied to the blade, while passive methods rely on the physical properties of the blade to prevent ice accumulation. Both methods can also be divided into two strategies: anti-icing and de-icing systems (ADIS) [12]. The categorization of ADIS is presented in Figure 2.7.

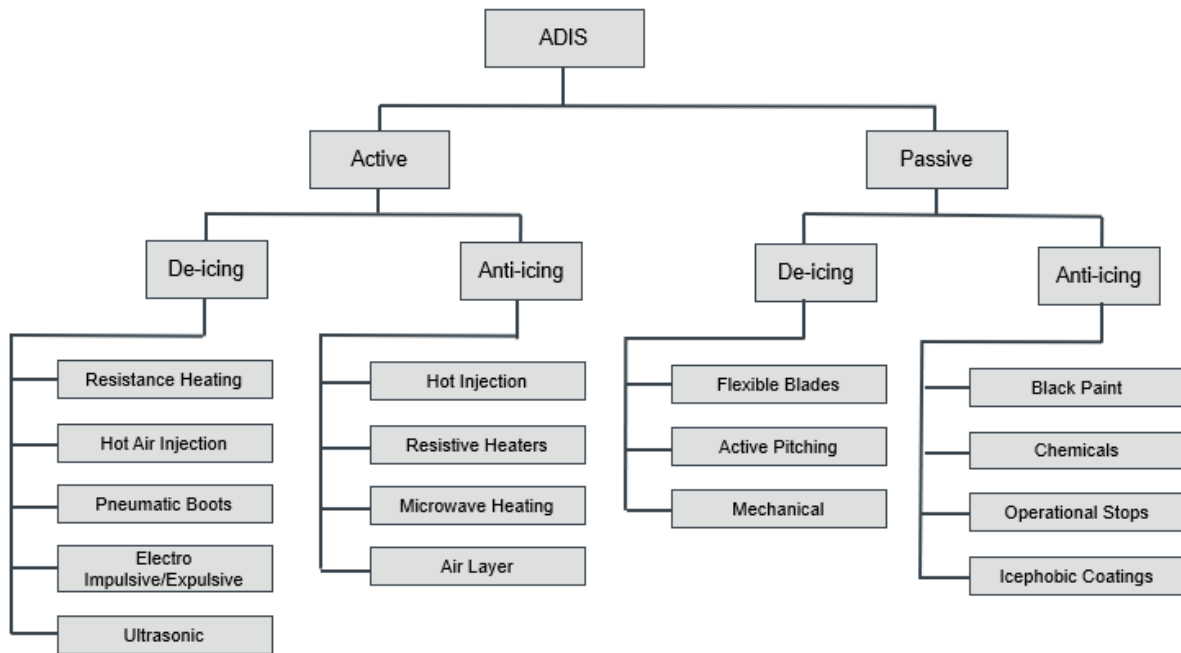


Figure 2.7 – Categorization of anti-icing and de-icing systems (ADIS).

Anti-icing refers to preventing or at least delaying the ice accretion on the blades and requires accurate weather forecasting. While de-icing refers to the removal of ice from the blades. It corresponds to a shortening of the recovery time during an icing event. De-icing requires a reliable method of ice detection [16], [11].

While de-icing systems have been used more widely because they do not require any major change in the design of the wind turbine and its blades, anti-icing systems are considered to be more promising for the future as they do not require the turbine to stop in order to work, and once installed require minimal power. For both research areas, most work is done by turbine manufacturers and only limited information on the technical specifications and performance of these systems is openly available [11].

In this chapter, the existing ice prevention and mitigation techniques are compared, either commercially available or at the research and development stage. A summary of these methods is provided in the Annex A.

2.5.1. ACTIVE METHODS

Active protection methods require supplied energy to perform and include thermal and pneumatic techniques. The characteristics, advantages and inconvenience of each system are presented here.

2.5.1.1. ACTIVE DE-ICING SYSTEMS

The active de-icing systems include electro-thermal heating, hot air injection, pneumatic boots, electro impulsive/expulsive and the ultrasonic system, described below.

Electro-thermal Heating

It consists of an electrical heating element embedded inside the membrane or laminated on the surface (see Figure 2.8). The idea is to create a water film between the ice and the surface. Once created, centrifugal forces will throw the ice away. The heating elements, in the form of thermal pads, electrically heated foils, and metal or carbon fiber electrical elements are mounted on the aerodynamically relevant leading edge of the rotor blade, which is also where most ice accretes.



Figure 2.8 – Placement of the heating elements on the leading edges of the wind turbine blades [7].

The ice detector and blade surface temperature are used to control the operation of the heating system and the additional temperature sensors are installed to protect the blade from permanent damage induced by overheating. This system has the advantage of efficiency close to 100%, because of the direct heating and the energy demand doesn't increase with the size of the blade. However, there are other drawbacks which are the high-power consumption and the risk of lightning strikes. Also, the runback ice, which happens when the water, consequence of the ice melted on the heated elements, runs back after the element and freezes again, can be aerodynamically harmful, because it has a high density and can form a barrier at the edge of the heating element [11][7].

Hot Air Injection

This technique was adapted to wind turbines by Enercon in 2009, and then most recently by Senvion and Vestas. This method consists of blowing warm air into the rotor blade at standstill with special tubes. The heat is transferred through the shell in order to keep the blade free of ice. Again, the idea is

to develop a water film between the ice and the surface. Once developed, it allows centrifugal forces to get rid of the ice (Figure 2.9). It can be used for both anti-icing (Enercon, Servion) and de-icing (Vestas).

One of the benefits of this system is that the leading-edge surface and the blade's aerodynamics are not affected. Another is that with use of a closed circuit, the heating power is reduced significantly compared to an open cycle, where air needs to be heated to the desired temperature starting from the outside temperature. Yet, the thermal efficiency of a closed loop hot air based system will remain rather poor, because a large mass of material has to be heated prior to attending the blade surface. Also, the heat source, often a hot air blower, is located typically at the blade root while the highest heat fluxes are needed at the tip of the blade [11].

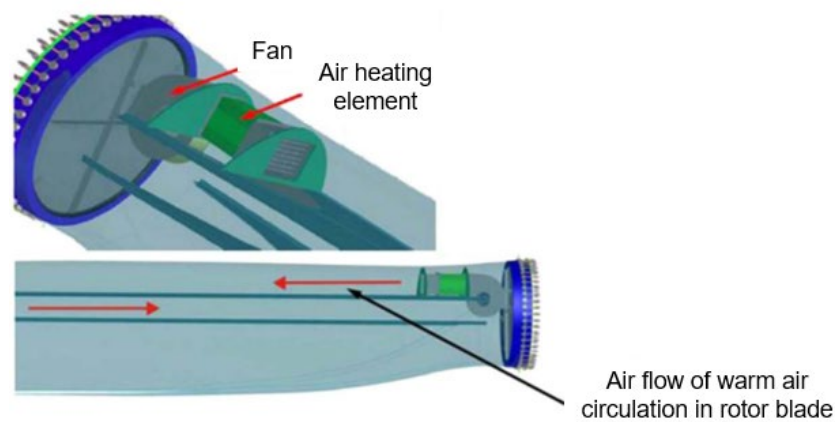


Figure 2.9 – Hot air injection system [18].

Pneumatic Boots

Flexible pneumatic boots inflate to break the ice. In the normal non-inflated state, tubes lay flat and conform to the airfoil surface on which the de-icer is bonded. After the build-up of generally 6 to 13 mm of ice on the surface of the airfoil, de-icers are inflated with compressed air. The inflation cycle lasts for a few seconds to achieve optimal ice shed and prevent additional ice formation on the inflated surface. After the ice has cracked, its bond to the surface is broken and it is removed through centrifugal and aerodynamic forces. De-icers are then allowed to deflate. Vacuum is then applied to ensure that there is no lifting of the surface on the low-pressure side of the airfoil (Figure 2.10).

Despite the use of this system in small aeroplanes, they have not proven pragmatic for wind turbine applications for several reasons, like the increased aerodynamic interference and noise that would be caused by an inflated boot and the additional mechanical complexity associated with such a system would add significantly to the maintenance burden for the 20-year life span of the turbine [12].

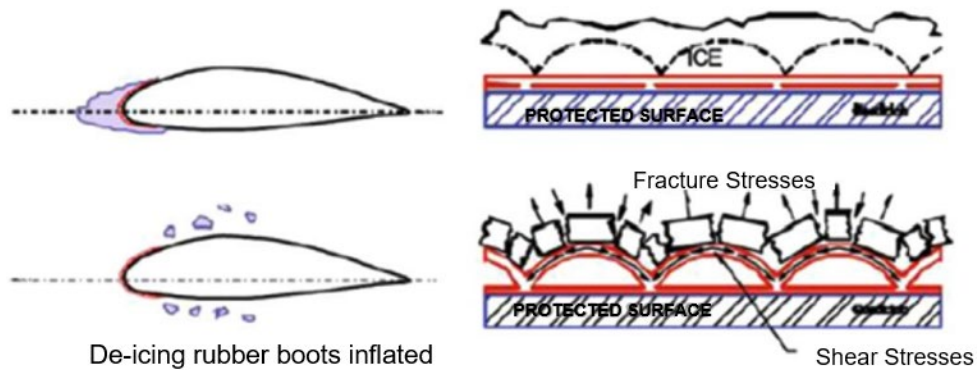


Figure 2.10 – Working principle of inflated rubber boots [8].

Electro Impulsive/Expulsive

It consists of very rapid electromagnetically induced vibration pulses in cycles that flex a metal abrasion shield and crack the ice. A spiral coil is placed near the surface of the profile. When current is applied to the coil, a magnetic field is created between the coil and the thickness of the profile (Figure 2.11). The result is a rapid movement of the surface and the expulsion of the accumulated ice. The system is environmentally friendly, efficient, has low energy consumption and is easily automated, but there remains a lack of practical information and ice expulsion is a potential problem [11] [12].

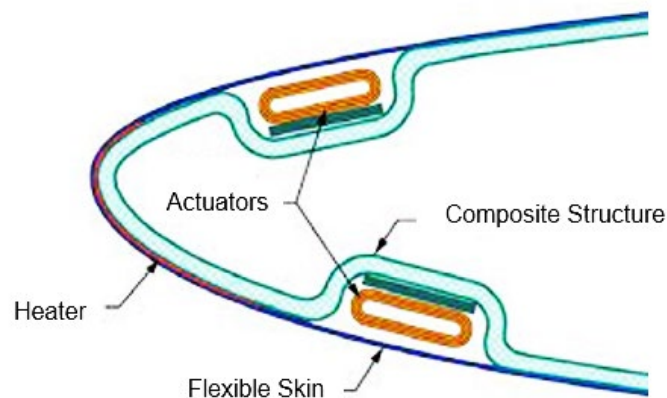


Figure 2.11 – Electro-Magnetic Expulsion De-icing System [19].

Ultrasonic

The idea behind the ultrasonic de-icing technique is based on the fact that the adhesive shear strength of the ice-substrate interface is relatively weak, thus ice could be easily detached when the applied shear force exceeds the adhesive strength of ice. The induction of shear stress over the layered ice-material structure occurs due to the propagation of ultrasonic waves excited by a piezoelectric transducer (Figure 2.12).

Ultrasonic de-icing has raised increasing interest with its energy-saving effect, low running costs, good applicability and environmental conservation. The method has proved efficient on helicopter blades and is a very promising concept for wind turbine blades, but it still needs to be adapted and the delamination risk must be taken care of [8], [20].

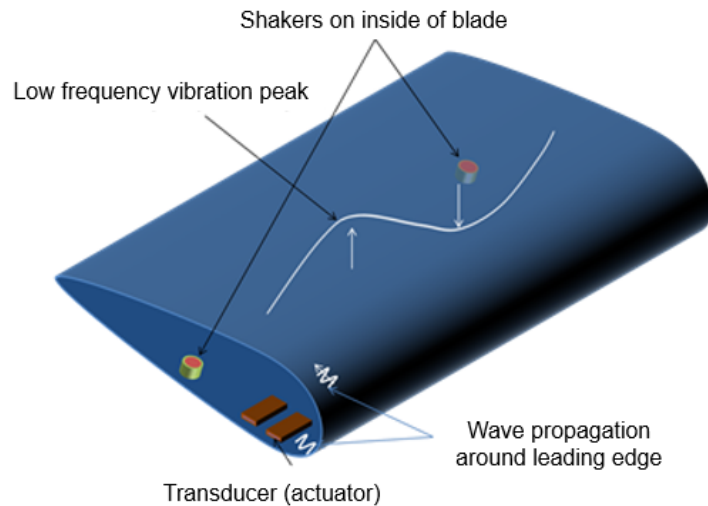


Figure 2.12 – Ultrasonic de-icing technique currently being tested [21].

2.5.1.2. ACTIVE ANTI-ICING SYSTEMS

A proven way to prevent ice built-up is to maintain the surface of interest at a temperature above the freezing point (0°C). Examples of systems that allow this are hot air injection, electro-thermal heating, microwave heating and an air layer system. These thermal methods require an external source of energy, like warm air and heating resistance, described below.

Hot Air Injection

This method has the same operating principle as the one referred in the de-icing systems, the use of hot air flow to heat the leading-edge area of the blades.

The system was tested in Switzerland and has given good results. However, it appears that the hot air injection system is energy intensive and that effectiveness depends on meteorological conditions and blade size [8].

Electro-thermal Heating System

There is no difference in terms of the technology when electro-thermal heating is operated as an anti-icing system instead of the earlier described de-icing system. The difference is that in de-icing mode it is activated only when an ice layer is detected on the blades, usually based on the power curve. As

described in Section 2.5.1.1 the main concerns of this solution are the power consumption and the potential issues caused by runback water [7].

Microwave Heating

This method corresponds in heating the blade's material with microwaves to prevent ice formation. The objective is to maintain the blade surface at a temperature slightly above 0°C, in order to save up some energy that will be used for defrosting. This system allows even heat distribution, consumes less energy, easy to maintain and it is not subject to lightning. The concerns of this technique are safety issues and manufacturing complexity [6][9].

Air Layer

A system where the blade surface is protected by a layer of clean air has been conceived. This system utilizes air flow from inside the blade pushed through rows of small holes near the leading and trailing edges to generate a layer of clean and, if necessary, heated air directly around the blade surface. This layer of air would deflect the majority of water droplets in the air and would melt the few droplets that managed to strike the surface, however, besides the difficult maintenance, there is little published information on this subject [11], [12].

2.5.2. PASSIVE METHODS

Passive techniques are used to prevent ice accumulation without any additional source of energy. The idea behind these techniques is to reduce the operational cost and keep the blades ice-free without any control system or special lightning protection. Passive methods take advantage of the physical properties of the blade surface to eliminate or prevent ice and are similar to active methods in their ability to act as de-icing or anti-icing systems.

2.5.2.1. PASSIVE DE-ICING SYSTEMS

The options for passive de-icing systems are limited and include flexible blades, active pitching and mechanical method.

Flexible Blades

A system designed with blades flexible enough to crack the ice loose has been proposed, as blade flexing is already known to help shed the ice. The disadvantage of trying to crack the ice loose is that thin layers of ice can adhere quite strongly to the blade and may not be brittle enough to crack loose from just

the vibration of the blade, besides that, it would likely also compromise the aerodynamic properties of the blade. This system is still being studied, so information about this method is scarce [9][10].

Active Pitching

Another passive de-icing system is the active pitching (Figure 2.13), which is a semi-active method that uses start/stop cycles to orient the turbine blades into the sun. Though these methods may work in light icing environments, but it has not been scientifically validated and such methods may cause damage to the turbine [6], [12].



Figure 2.13 – Blade pitch control (adapted from [22]).

Mechanical

Mechanical de-icing is a method that directly smashes the ice layer on the blade by machinery or manual (Figure 2.14), and then uses centrifugal force, gravity, vibration and other ways to make the ice break away from the blade surface. This system requires lifting equipment and experts' climbers who manual remove ice from the blades and other structures, as Figure 2.14 points out.

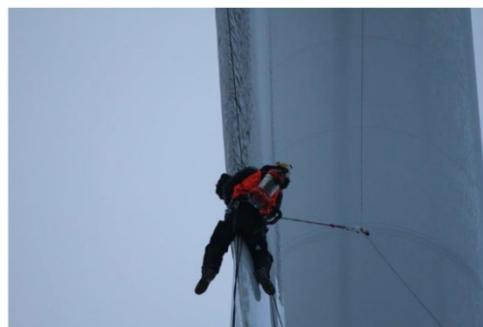


Figure 2.14 – Manual ice removal from the wind turbine blade [23].

This method consumes a lot of time and effort, which makes removal costs and standstill costs very remarkable. In addition, hand removal of the ice can't be conducted if the weather conditions are

harsh and there is always a possibility of injuries due to falling ice. An alternative for manual ice removal is the use of a helicopter (Figure 2.15), which sprays hot water to ice on the wind turbine blades.



Figure 2.15 – Ice removal with hot water sprayed from the helicopter [24].

The benefit of this method is that it can be used for all turbine types. The main disadvantage is that, like the manual de-icing, it cannot be utilized if the weather conditions are too harsh [17][23].

2.5.2.2. PASSIVE ANTI-ICING SYSTEMS

The passive anti-icing methods, including black painting, chemicals, operational stops and icephobic coatings, are usually used to prevent or delay ice formation over wind turbine surfaces.

Black Paint

Painting the rotor blades black (radiant surface?) was one of the first approaches pursued and the idea was that the solar heat from the black colour coated blades would heat up the blades during daylight, causing the ice to melt earlier than with white paint (Figure 2.16). When tested in Yukon (Canada), this method showed immediate and noticeable improvement in performance [25].

Another positive point is the decrease in the number of birds that are killed each year by wind turbines. Painting the blades of a wind turbine black resulted in 70% fewer collision bird victims [26]. However, the black paint only improves performance in areas where icing events are non-frequent and are followed by temperatures above 0°C, or intense sunlight [26]. In summer, the black paint may overheat the blades and affect the properties of glass-fibre reinforced plastics, as they are sensitive to high temperature, consequently, will affect their mechanical properties [8] [7].



Figure 2.16 – Black paint on the wind turbine blade [27].

Chemicals

Chemicals are applied on the surface of the blade in order to lower the freezing of water. These chemicals are pollutants and they need a special application and a lot of maintenance. Furthermore, they cannot remain on the surface of the blade for a long period of time [6].

Operational Stops

This method consists in stopping the wind turbine as soon as the icing event begins. Indeed, when the wind turbine is not operating, smaller amounts of ice will deposit on the blades, therefore, the turbine can be restarted sooner after the icing event. This technique has the advantage of being simple and requires no investment, but it still needs improvement as, for the time being, the benefits are close to zero. The key aspect seems to be the prediction of the icing event. With better detection tools, this technique could yield better results [8].

Icephobic Coatings

Another strategy for ice mitigation on wind turbine blades is the use of special coatings that are able to reduce the shear forces between the ice and the blade's surface. These coatings are called icephobic, as they can prevent ice from sticking to the surface, because of their anti-adherent properties (low surface energy).

Currently, most manufacturers use epoxy or polyester matrix composites reinforced with glass and/or carbon fibres, due to their lower cost. Nonetheless, current research is heading towards nanocomposite coatings, polymers reinforced by minute and nanometre-scale particles.

This approach has several advantages: low cost, easy application and blade maintenance, no special lightning protection needed, protection of the whole surface, allows the reduction of energy consumption and the reducing of the shear forces will also reduce the sensitivity to dirt and insects.

The disadvantages are the large and unsymmetrical accretion during severe icing, leading to instability. The durability of the coatings is also an issue, after a short period of time, the coating can become porous and lose its ability to repel ice. On the other hand, for this method to be really effective, it should be combined with another ice mitigation system.

There are very few studies on this method, most of these techniques are still in the experimental stages, but some have shown promising results. Additionally, detailed information for most of the studies remains proprietary, consequently, most data sheets and chemical compositions are classified and inaccessible [11], [12].

2.6. HYBRID STRATEGY

Advancing the technology for safe and efficient operation of wind turbine blades under atmospheric icing conditions requires the development of novel, effective and low power anti-/de-icing strategies.

As described above, wind turbine ice mitigation can be effectively achieved by using active approaches to electrically heat the blade surfaces, yet it requires an extremely high-power consumption to the electric heating element in order to maintain the blade surface at a high temperature. Another problem is the ice formed from runback water, that has a high density and may be dangerous when shed from the blades in big pieces. It can also accumulate at positions where it may be aerodynamically harmful.

In other terms, in theory, the surface temperature of the blade must be kept above 0°C whenever there is icing, although, to avoid runback water, the water must evaporate, which implies for the heated element temperature to be at least 100°C . Another option would be to extend the size of the area protected by the electric heating element. Both options result in a very high-power consumption for the anti-/de-icing process.

The break-even cost of such a heating system depends on how much energy production is lost due to icing and the price of electricity. Therefore, when the financial benefits of a blade heating system are evaluated, icing time, severity of icing, and potential wind resources need to be known. Based on early work in Europe, thermal anti-icing requires power equal to at least 25% of the turbine's maximum power [12].

As previously mentioned, icephobic coatings have demonstrated the ability to repel water droplets, delay ice nucleation and significantly reduce ice adhesion. Despite these ongoing research activities and

promising results, the findings reported hereafter suggest that coatings alone are not enough to be used for wind turbine operations.

An ideal solution for wind turbine icing mitigation would be a hybrid system, where icephobic coatings would be a complementary option to either thermal or mechanical ice protection methods, for reducing power input and the ecological footprint of these active systems. Also, by coating the entire turbine blade surface with an icephobic coating, it will make the surface water move much faster over the blade surface and roll off swiftly before being refrozen into ice, preventing in this way, the formation of runback ice [28], [29].

In summary, currently, the most commonly used wind turbine anti-/de-icing systems are thermal-based approaches. Although these techniques for ice removal are generally effective, they still need to be improved, as they need a large power supply and, in some cases, the runback water, consequence of heating, can freeze after it passes the heated area. Little attention, however, has been paid to coating strategies, perhaps since such an approach cannot be a standalone solution to icing. Nevertheless, the integration of suitable coatings on aerodynamic and structural surfaces can either enhance the effectiveness of ADIS requirements or lead to a substantial reduction of the energy use [11], [7].

2.7. VESTAS COLD CLIMATE SOLUTIONS

Vestas active system is based on electro-thermal heating elements, that are situated on the leading edge of each blade, from around mid-span to the very tip of the blade (as represented in Figure 2.17).



Figure 2.17 – Visual representation of the electrothermal elements [30].

The control system includes different operational modes allowing the heating elements to separately create the optimal heating level, increasing effectiveness and minimizing energy consumption.

This results in fast and targeted anti-icing action tailored to the specific icing situation. Vestas Anti-Icing System is designed to operate both in rotation and standstill, thereby being applicable from low to high ice severity. This system has two operational modes: anti-icing and de-icing.

- Anti-icing mode: 230-280 kW power available from the wind turbine generator 's own energy production while in rotation.
- De-icing mode: up to 75 kW power from the grid. Mode designed for more severe conditions requiring the turbine to pause operation (30 minutes).

In addition to these systems, Vestas has introduced the siting tool Vestas Ice Assessment, which uses metrological models and algorithms to ensure an industry-leading accurate and precise ice assessment down to turbine level [31], [32].

Like any active ice mitigation system, despite being very efficient, it needs a large input of energy, so it is necessary to consider implementing new alternatives.

2.8. ICEPHOBIC SURFACES

As mentioned earlier in Section 2.5.2.2, due to the low installation cost and almost zero energy consumption, the passive anti-icing approach with icephobic coatings has received more and more attention as a reliable strategy for wind turbine icing mitigation.

2.8.1. DEFINITION OF ICEPHOBICITY

The literature defines icephobicity as the capacity of a surface to repel ice or prevent ice formation, due to its physicochemical properties [33].

Based on this definition, an icephobic coating must be able to reduce ice adhesion strength between ice and a surface, decrease heterogeneous ice nucleation, increase freezing time, rebound supercooled water droplets, inhibit the condensation of water and roll-off supercooled water droplets easily [34]. These features of an icephobic coating are presented in Figure 2.18.

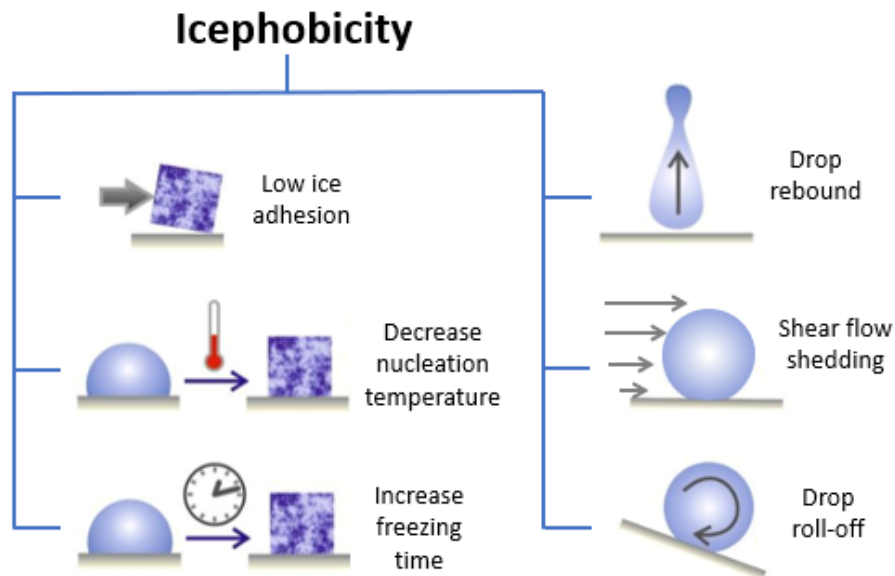


Figure 2.18 – Different features of an icephobic coating (adapted from [35]).

Furthermore, for industrial use, the structural and chemical integrity of icephobic surfaces used in practice must be able to withstand erosion, wear, and other weathering conditions. And, for commercial adoption, these surfaces must be scalable, inexpensive, environmentally friendly, easy to apply and mechanically durable [36].

2.8.2. TYPES OF ICEPHOBIC COATINGS

Taking into account the surface properties, there are several categories of icephobic coatings that will be outlined throughout this section.

2.8.2.1. SMOOTH SURFACES

Smooth elastic surfaces (Figure 2.19) can be icephobic and achieve extremely low ice adhesion strength by tuning surface chemistry, elastic modulus and surface thickness.

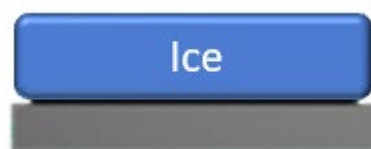


Figure 2.19 – Ice deposition on smooth surfaces (adapted from [37]).

The fabrication process of smooth surfaces is usually straightforward and cost-effective, which can be easily achieved by machining, depositing, molding, spraying, spin-coating and dip coating [37].

2.8.2.2. TEXTURED SURFACES

Textured surfaces with icephobicity (Figure 2.20) contain hierarchical structures, that allow air to get trapped, which will allow the adhesion strength to be lowered [37].

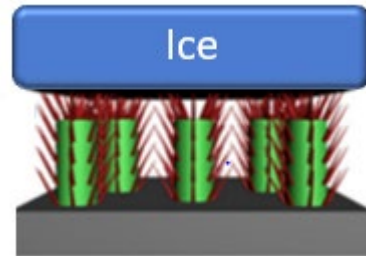


Figure 2.20 – Ice deposition on textured surfaces (adapted from [37]).

The surfaces that fall into this category are the hydrophobic and superhydrophobic, coatings capable of repelling water. These types of surfaces will be detailed later in Chapter 2.9.

2.8.2.3. SLIPPERY SURFACES

Slippery surfaces with icephobicity (Figure 2.21) usually refer to lubricating surfaces, such as organic and aqueous lubricating layers [37]. The layer of liquid lubricant, which is immiscible with water, between ice and the solid surface, reduces the ice adhesion strength to a solid surface.

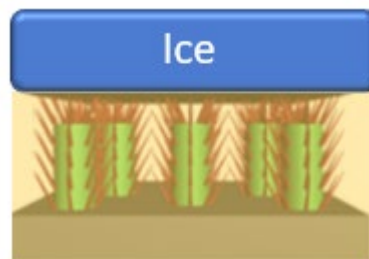


Figure 2.21 – Ice deposition on slippery surfaces (adapted from [37]).

2.9. HYDROPHOBIC AND SUPERHYDROPHOBIC COATINGS

As mentioned above, one type of icephobic coatings are the hydrophobic coatings, surfaces that have the capacity to inhibit the condensation of water and roll-off and rebound supercooled water droplets easily.

Inspired by “the outstanding self-cleaning capability of lotus leaf and duck feather” (Figure 2.22), extensive studies have been conducted in recent years to develop coatings to make superhydrophobic surfaces (SHS) [14].

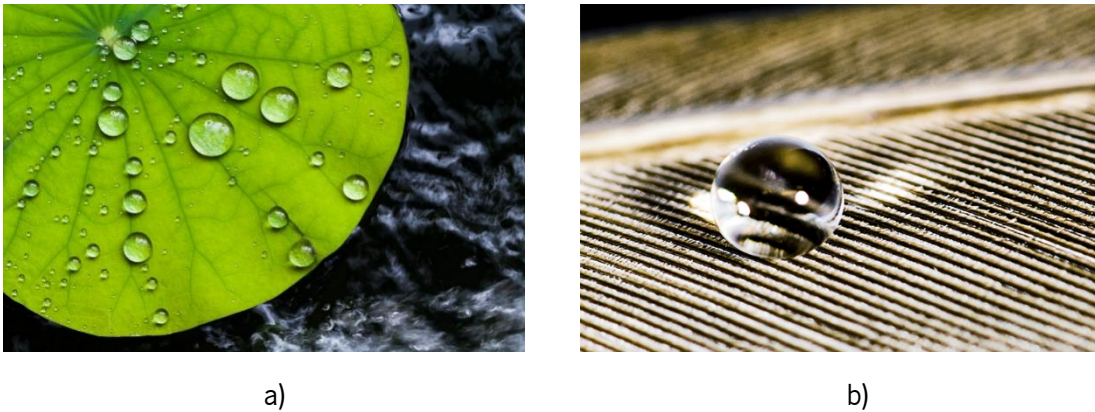


Figure 2.22 – a) Lotus leaf effect [36]. Drop of water on a duck feather [37].

Such coatings have been reported to provide a reduction in normal and shear adhesion of ice to the underlying surface, resulting in a delay in water freezing on surfaces, and to reduce or even completely inhibit nucleation and accumulation of ice and snow on surfaces, because of their low surface energy barrier. The use of a hydrophobic coating on the wind turbine blades can prevent water adsorption on the blades and, therefore, ice formation. For this, these surfaces must meet the following conditions [40]:

1. The hydrophobic coating should effectively reduce the formation of ice and snow;
2. The production of the coating should be simple, cheap, and environmentally friendly;
3. The coating material should be easily mounted or applied to the blade of a wind turbine;
4. This material must be durable to withstand weather conditions.

Even though SHS have been viewed as potential icephobic coatings and shown promising anti-icing performance for protecting outdoor equipment in cold seasons, their biggest obstacle toward real life applications is the durability. The coating, under the actual working environment, is exposed to various conditions including mechanical abrasion, wear, sand and droplet impact, chemical contamination, ambient temperature variation and long-term sun exposure.

In several studies [41]–[43], these surfaces were revealed to be fragile to mechanical shear and usually deteriorated after several trials of the same experiment, subsequently, they fail to mitigate ice for long durations in practical conditions [31][42].

2.9.1. SURFACE WETTABILITY AND CONTACT ANGLE

The wettability of a solid surface can be described by observing the shape of a drop deposited on the surface. A surface having a high wettability (hydrophilic) tends to allow the drop to spread over a relatively wide area, thereby wetting the surface (see Figure 2.23 a). Contrarily, on a surface with low

wettability (hydrophobic), the liquid tends to retain a spherical shape (see Figure 2.23 b) and drops can usually shed from the surface with a slight disturbance.

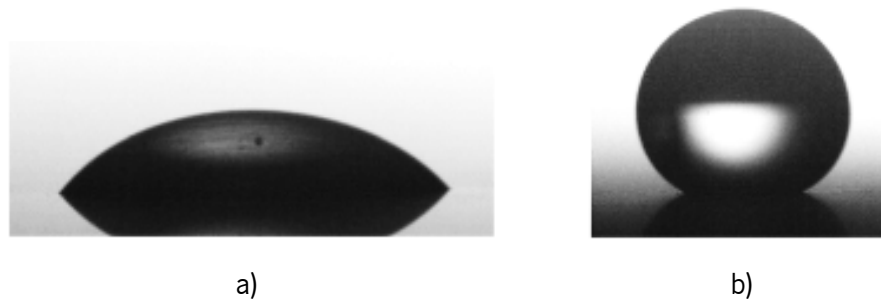


Figure 2.23 – a) Sessile drop on a hydrophilic surface and b) on a hydrophobic surface [45].

When in contact with an ideally solid surface (flat, rigid, smooth and chemically homogeneous) a static liquid drop forms a triple interface between the liquid (l), the solid (s) and the surrounding vapour (v). The typical parameter used to characterize a solid surface wettability is the contact angle (θ), which is the angle formed between the liquid–solid and the liquid–vapour interfaces and can be determined by a balance between the three interfacial surface energy vectors: the liquid/vapour surface tension (γ_{lv}), the solid/vapour surface tension (γ_{sv}) and the liquid/solid surface tension (γ_{ls}), each represented by a vector in Figure 2.24 [45].

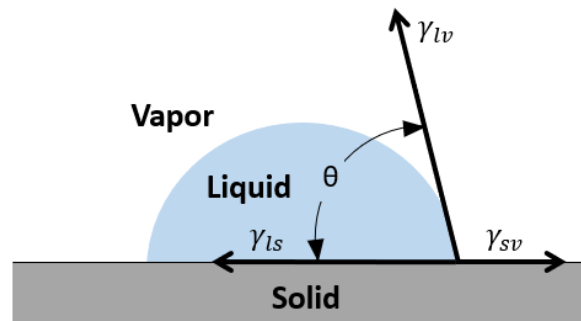


Figure 2.24 – Balanced contact angle between a triple interface between the liquid (l), the solid (s) and the surrounding vapour (v) (adapted from [46]).


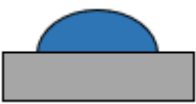

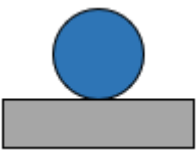
The vectors represent the balance of the forces acting in the triple point interface, and their relation is given by Young's equation (2.1) [47]:

$$\cos \theta = \frac{\gamma_{sv} - \gamma_{ls}}{\gamma_{lv}} \quad (2.1)$$

As evident from Young's equation, lower solid surface energy materials provide higher contact angles while higher surface energy materials have lower contact angles. Thus, lower surface energy materials are preferred for repellent surfaces.

Regarding wettability, and when using water as a liquid, the surfaces can be classified as hydrophilic if the contact angle (CA) is smaller than 90° or hydrophobic if the contact angle is higher than 90° . Surfaces with contact angles close to 0° (less than 10) are classified as superhydrophilic and if the contact angle is higher than 150° then the surface is called superhydrophobic (see Table 2.1) [48].

Table 2.1 – Wettability conditions of a surface by contact angle measurement (θ) (adapted from [49]).

Optical Representation	Macroscopic Result	Contact Angle	Energetic Relationship	Wettability
	Superhydrophilic	$\theta < 10^\circ$	$\gamma_{SV} - \gamma_{LS} = \gamma_{LV}$	Complete wetting
	Hydrophilic	$10^\circ \leq \theta \leq 90^\circ$	$\gamma_{SV} - \gamma_{LS} > 0$	High wettability
	Hydrophobic	$90^\circ \leq \theta \leq 150^\circ$	$\gamma_{SV} - \gamma_{LS} < 0$	Low wettability
	Superhydrophobic	$\theta > 150^\circ$	$\gamma_{SV} - \gamma_{LS} = -\gamma_{LV}$	Non-wettability

2.9.2. SURFACE ROUGHNESS

Despite Young's equation (2.1) being only valid for a sessile drop placed on an ideal, homogeneous and smooth surface, the reality is that there are few solid surfaces that represent these properties at once [48]. In fact, surface roughness is one of the most significant properties that should be taken into consideration when it comes to the superhydrophobic behaviour of surfaces. To describe the effect of roughness on a surface there are two theoretical models that add the roughness parameter to Young's equation: Wenzel model and Cassie-Baxter model.

2.9.2.1. WENZEL STATE

According to Wenzel's theory, proposed in 1936 by Robert Wenzel, when a water drop gets in touch with a low rough surface, it will fill all its voids. Therefore, the surface area available to be in contact with the water is larger than if the surface was completely smooth, as can be observed in Figure 2.25 [50].

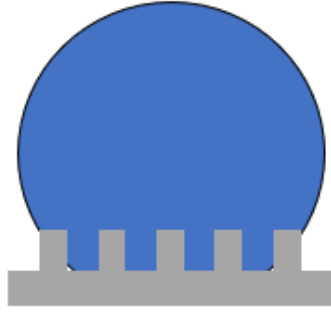


Figure 2.25 – Wenzel model (adapted from [51]).

According to Wenzel, the roughness of a surface is a variable capable of increasing or decreasing the wettability of a surface, so that by increasing the roughness, hydrophobic surfaces will increase their hydrophobicity while hydrophilic surfaces will become more hydrophilic.

In his research, Wenzel proposed a correction factor (r) for contact angle on rough surfaces, which is equal to the ratio of rough interfacial area (A_{real}) over flat interfacial area ($A_{projected}$), as in the equation (2.2):

$$r = \frac{A_{real}}{A_{projected}} \quad (2.2)$$

Therefore, if the surface is rough, then $r > 1$ and if a surface is totally smooth then $r = 1$. However, as smooth as a surface may be, it ends up containing some irregularity, the real area will be greater than the projected area, which makes the roughness parameter always greater than 1.

Substituting the roughness ratio factor, r , in the Young's Equation (2.1), one can obtain the Wenzel's equation (2.3) [28], i.e.,

$$\cos \theta_{rough} = \frac{r(\gamma_{sv} - \gamma_{ls})}{\gamma_{lv}} = r \cos \theta \quad (2.3)$$

Where θ_{rough} represents the apparent static angle that is the angle associated with the rough surface, r represents the roughness factor, and θ represents Young's contact angle (the angle formed if the surface was totally smooth).

From the analysis of the Wenzel's equation (2.3), for a fixed roughness value, it is observed that for $\theta < 90^\circ$ (hydrophilic surface), $\cos \theta_{rough} > \cos \theta$, then the apparent angle will be smaller than the real angle, $\theta_{rough} < \theta$ (Figure 2.26).

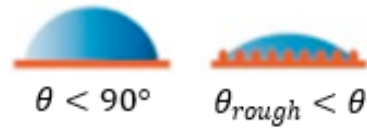


Figure 2.26 – The surface roughness amplifies wettability [52].

For the case $\theta > 90^\circ$ (hydrophobic surface), $\cos \theta_{rough} < \cos \theta$, the apparent angle will be bigger than the real angle, $\theta_{rough} > \theta$ (Figure 2.27).

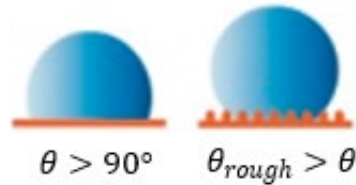


Figure 2.27 – Surface roughness decreases wettability [52].

This analysis that the r factor increases wettability corroborates with the initial prediction of the Wenzel model.

2.9.2.2. CASSIE-BAXTER STATE

Cassie-Baxter model was proposed in 1944, and it assumes that when water gets in contact with a strong rough surface, it relays on air that gets trapped between the water and the surface as can be observed in Figure 2.28, like with duck 's feathers [53].

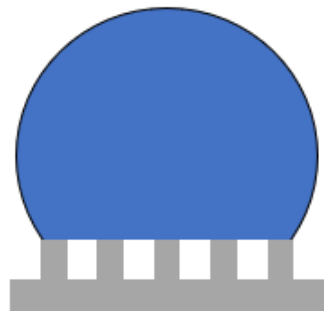


Figure 2.28 – Cassie Baxter model (adapted from [10]).

In the Cassie-Baxter model, there is a link between the fraction of the liquid that comes in contact only with the solid (f_s) and the fraction of the liquid that is in contact only with the vapour (f_v), and the sum of these fractions must correspond to the total apparent contact area of the droplet. The relationship between the ratio of these areas is:

$$f_s + f_v = 1 \quad (2.4)$$

Each of these fractions will contribute in different ways to the apparent contact angle (θ_{app}) result, which can be written as:

$$\cos \theta_{app} = f_s \cos \theta_s + f_v \cos \theta_v \quad (2.5)$$

Where θ_s and θ_v represent the contact angles for the liquid-solid and liquid-vapour, respectively.

For superhydrophobic surfaces, as the water drop is in contact with the surface fractions and the air pockets between the roughness of the surface, $\theta_v = 180^\circ$. Therefore, the equation can be written as:

$$\cos \theta_{app} = f_s \cos \theta_s - f_v \quad (2.6)$$

Resorting to the fact that $f_s + f_v = 1$, the apparent angle (θ_{app}) is given by:

$$\cos \theta_{app} = f(1 + \cos \theta) - 1 \quad (2.7)$$

Where the surface fraction that is in contact with the water drop is now represented by f and θ represents Young's contact angle. When a drop exhibits Cassie-Baxter state behaviour, the surface roughness increases the θ_{app} , whether θ is lower or higher than 90° . So the small contact area between the droplet and the solid surface allows the drop to roll easily over the surface.

For the wind turbine icing scenario, water droplets would impact onto blade surface at high speed up to $\sim 90 \text{ m/s}$ near blade tips for utility-scale wind turbines. The impacted water droplets would readily penetrate the surface textures to promote the transition from the Cassie-Baxter state to fully wetted Wenzel state. Once water freezes within the textures in the Wenzel state, it is extremely difficult to remove the ice, even more than on nontextured surfaces, because of the interlocking between ice and the textures [14][54].

2.9.1. WATER AND ICE ADHESION

The nanoscale mechanisms of ice-adhesion turned out to be highly complex. Menini *et al.* have noted that interactions between ice and substrate is a combination of electrostatic forces, hydrogen bonding, van der Waals forces, and mechanical adhesion [36]. Where Chen *et al.* found that for the hydrophobic surfaces, the interaction between water/ice and the substrate was dominated by van der Waal's forces [37].

Considering ice (i) frozen on a solid (s) it is similar to the case shown in Figure 2.24 except that the water droplet is frozen into ice. To remove the ice from the surface of the solid, the bond (i, s) must be broken, creating two new surfaces (i and s). Assuming an absence of deformations in both the ice

and the solid, the require work to remove the ice can be the thermodynamic work of adhesion, W_a , which is defined as:

$$W_a = \gamma_{sv} + \gamma_{iv} - \gamma_{is} \quad (2.8)$$

Where γ_{sv} is the solid/vapour surface free energy, γ_{iv} the ice/vapour surface free energy and γ_{is} the ice/solid interfacial free energy. Inserting γ_{sv} from equation (2.1) into equation (2.8) leads to:

$$W_a = \gamma_{iv} + \gamma_{lv} \cos \theta + (\gamma_{ls} - \gamma_{is}) \quad (2.9)$$

If the (reasonable) assumption is made that the surface energies of water (liquid) and ice (i.e., frozen water) are approximately the same [55] and that their interfacial energies at the solid surface are also approximately the same ($\gamma_{ls} = \gamma_{is}$), one obtains:

$$W_a \approx \gamma_{lv}(1 + \cos \theta) \quad (2.10)$$

Based on equation (2.10), the thermodynamic work of ice adhesion can be closely approximated by the surface tension of water and the contact angle of water on the solid. This is shown graphically in Figure 2.29.

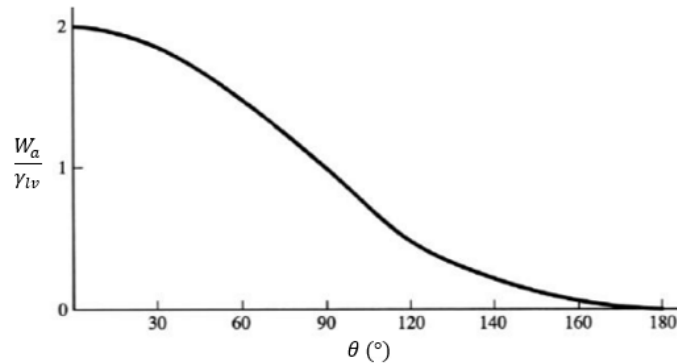


Figure 2.29 – Thermodynamic work of ice adhesion normalized by the surface tension of water $\frac{W_a}{\gamma_{lv}}$ as a function of water contact angle θ [56].

Based on equation (2.10) and Figure 2.29 it can be shown - in an ideal case and with the restrictions addressed above - that a deterministic dependence between the work of adhesion and the contact angle of water does exist. In particular, that the work of adhesion of ice approaches zero when the contact angle approaches 180° . In other words, as the contact angle increases (the more hydrophobic the surface is), the smaller the work of adhesion becomes.

Although hydrophobicity is related to icephobicity, no universal correlation exists between ice adhesion force and water adhesion force on a surface. As water can withstand positive and negative pressures, it cannot support shear stress, a drop under shear stress deforms and de-wets the surface

once the shear force is more than counteract force. However, the scenario is different when the drops freeze, ice can withstand shear and detachment of ice from a surface occurs through fracture. Furthermore, the nominal adhesional force per unit area between ice and a substrate is weaker when the true interface area is less than the apparent one, the texture (roughness) of the surface, including how clean the surface is, determines the ice adhesion.

As most superhydrophobic surfaces are in the so-called Cassie state, the micropores of the substrate that are not filled with water due to hydrophobicity of the substrate surface reduce the effective contact area. Also, the air pockets trapped between the solid and water droplet, when water freezes, become air voids and they can serve as stress concentrators. On the other hand, if the interface includes micropores that are filled with water, Wenzel state, then the true interface area is larger. In such a case, sometimes called 'locking' a purely adhesional failure may become impossible, and the fracture occurs partly cohesionally within the ice material. Special condition, such as supercooled airflow or high humidity can result in a Wenzel wetting state. When water freezes in that state, the ice adhesion strength is increased due to the mechanical interlocking that occurs between the ice and the surface's micro/nano structures. Therefore, the adhesion strength of ice on many materials becomes higher on a microscopically rough surface than on a smooth surface.

Although icephobic properties correlate with high CA, the ability of the hydrophobic surface to sustain a Cassie-Baxter wetting state at subfreezing temperature is the critical parameter for icephobicity. Consequently, some superhydrophobic surfaces can have strong ice adhesion if they cannot maintain a Cassie state. As a result, the association of icephobicity with superhydrophobic surfaces remains debatable [57], [58]. In addition to the contact angle and roughness, there are other factors that affect ice adhesion strength: the nature and purity of the accreted ice (from sea, tap, or demineralized water), which affect the crystalline structure of ice and the possible structural defect, the temperature of the icing condition. Also, the actual temperature of the interface and the surrounding ice, which may contribute to locking in thermal strain energy at the time the ice is detached. To a lesser degree, other factors can influence the interfacial adhesion strength, such as the mechanical properties and the geometries of both substrate and ice [59].

2.10. POTENTIAL COATING CANDIDATES

This chapter points out multiple materials of icephobic coatings, their wetting behaviour, the tests that were carried out for each situation, as well as the value of the adhesion reduction factor (ARF)

compared to the uncoated surface. The most common materials have been fluoropolymers (PTFE, PVDF, PDMS) and silicone-based compounds e.g. RTV silicone rubbers (Table 2.2). The ice adhesion values of these fluoropolymer and silicon rubber coatings have been low, but the drawback of these coatings is their mechanical durability. Therefore, different nanoparticles (TiO_2 and SiO_2) have been added to improve mechanical durability or change the topography of the surface.

Table 2.2 – Collection of coatings and surfaces presented in the literature for different types of tests. WB stands for wetting behaviour, SH for superhydrophobic, HP for hydrophobic and HF hydrophilic. ARF stands for adhesion reduction factor.

Coating	WB	Test	ARF	Reference
PVDF+ SiO_2	SH	Centrifuge ice adhesion test	4.0	[60]
PVDF+ SiO_2	SH	Vertical shear test	8.0	[61]
PDMS+ TiO_2	HP	Push test	5.0	[62]
PTFE	HP	Centrifuge ice adhesion test	2.4	[63]
PTFE	HP	Vertical shear test	7.6	[64]
Hydrocarbon+Si	HF	Push test	2.1	[65]
PMMA	HF	Zero-degree cone test	1.0	[66]
PDMS	HP	Vertical shear test	5.6	[67]
PS + SiO_2	HP	Centrifuge ice adhesion	0.3	[68]
RTV11	SH	Zero-degree cone test	4.4	[66]
SLIPS	HP	Centrifugal ice adhesion	4.5	[69]
SLIC	HP	Tensile ice adhesion	6.8	[70]

Properly functioning icephobic coatings would have great benefits compared to currently utilized anti- and de-icing applications. Icephobic coating would operate without external energy, offer an environmentally friendly option and could be modified for multiple applications. However, the present icephobic coatings still have issues with their durability. The cyclic ice adhesion tests ([71]–[73]) have shown that at least superhydrophobic surfaces will lose their icephobic behaviour during the multiple cycles.

3. METHODOLOGY

The proposed methodology consists of a multi-criterion assessment of the materials using conventional and newly developed laboratory tests. The idea is to obtain comparative results between coatings so that a full assessment can be done on each one.

In this chapter, the materials and tests that were carried out for this project will be briefly described, as well as the methodology applied for the experiments. These tests include contact angle measurements and ice push test, in order to determine their characteristics pertaining to wettability and in repelling ice. Then, two finite-element models of the stress distribution and aerodynamic forces are constructed to perform a quantitative evaluation of the effectiveness of the icephobic coatings to prevent ice adhesion under equivalent external forces as those observed in field conditions. The diagram with the methodology adopted in this project is shown in Figure 3.1.

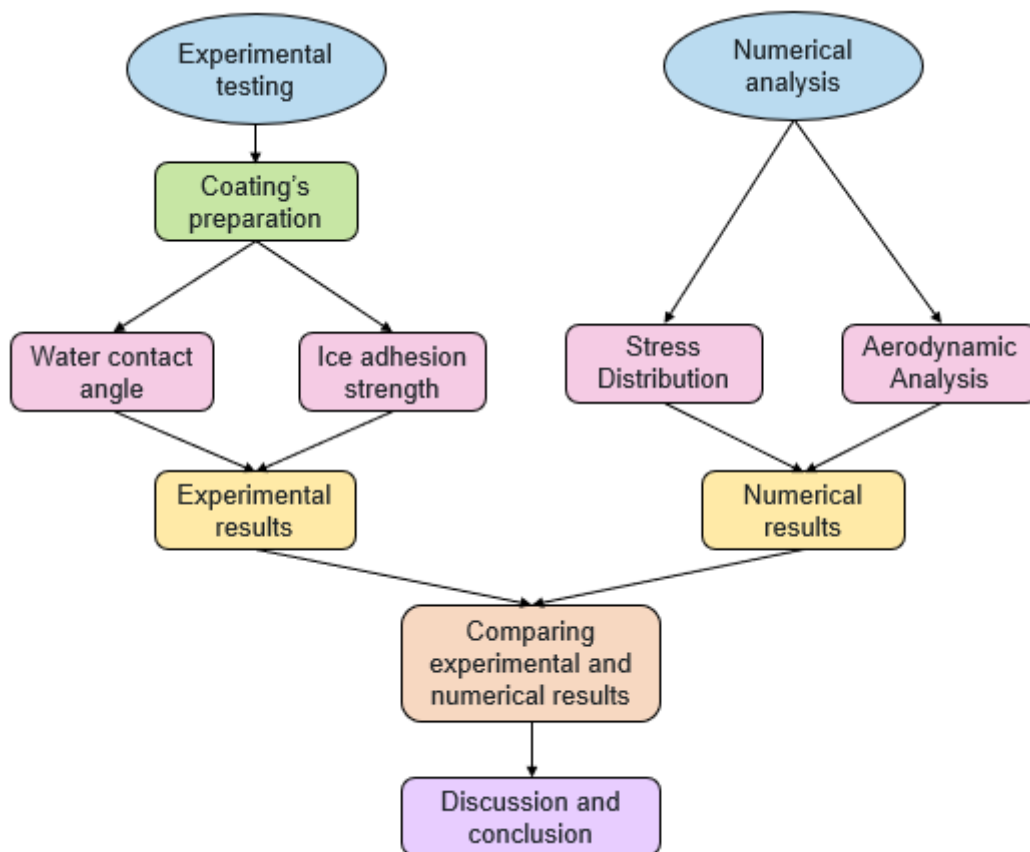


Figure 3.1 – Diagram of the adopted methodology.

3.1. MATERIALS

To verify the efficiency of different coatings in repelling ice, different materials were tested to evaluate the proposed procedure. For purposes of comparison, three commercially available coatings were also tested.

3.1.1. SUBSTRATES

The test was conducted using samples of Vestas wind turbine blades with 5 mm thickness and total surface area of 1000 mm², supplied by the company. The plates are made of fibreglass reinforced epoxy coated with white paint and they were used as a standard base for coating application, representing the baseline or reference.

3.1.2. POLYVINYLIDENE FLUORIDE (PVDF)

Through the literature review ([60], [74], [75]) it can be said that PVDF is an important hydrophobic material, that has been used widely in many fields due to its excellent weathering, chemical corrosion and oxidation resistance. PVDF, purchased from Solvay, was used to create the coatings.

3.1.3. TITANIUM DIOXIDE (TiO₂)

In [60][62] it was noted that the presence of reinforced materials such as nanoparticles, increases the surface roughness of the nanocomposites, thus resulting in higher contact angles. Commercial titanium dioxide nanoparticles, P25 TiO₂, supplied by Evonik were used because of their hydrophobic properties, non-toxicity, availability and mainly because of their excellent self-cleaning effect.

3.1.4. DIMETHYLFORMAMIDE (DMF)

Dimethylformamide, purchased from Merk, is an organic compound with the formula (CH₃)₂NC(O)H, commonly abbreviated as DMF. It is a common solvent, because it is a colourless liquid that is miscible with both water and many organic liquids.

3.1.5. WEARLON SUPER F-1

The commercial coating Wearlon Super F-1, provided by Plastic Maritime Corporation (USA) is a two-component water-based silicone epoxy with increased silicone that enhances the icephobic properties. It is designed for applications that require more non-stick ability without the heavy abrasion. In 2004 it was considered the best non-sacrificial icephobic coating providing an ARF value of 12 (Figure 3.2), by the Anti-Icing Materials International Laboratory (AMIL) [76].

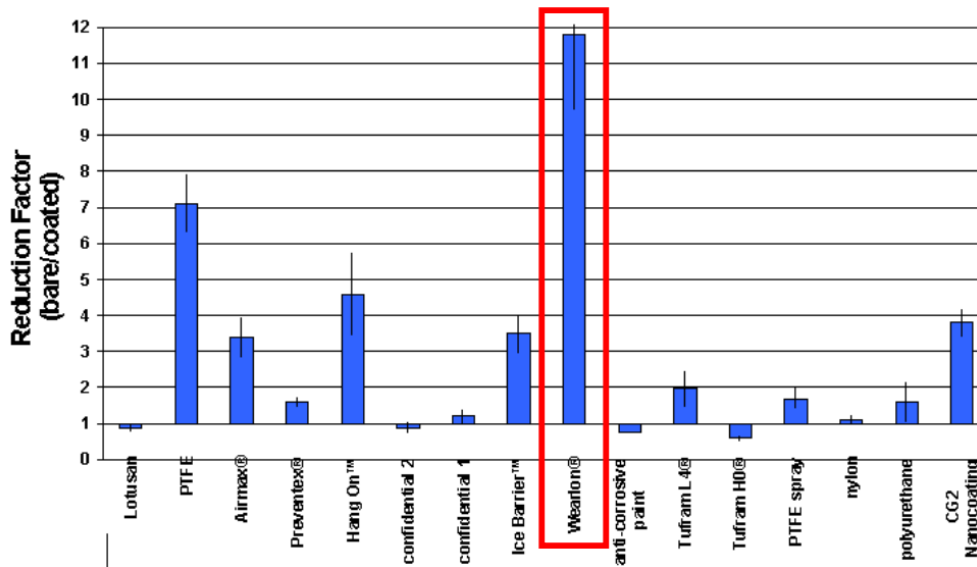


Figure 3.2 – Ice adhesion reduction, AMIL's results [76].

3.1.6. CHEMONA MULTI COAT

Another commercial coating studied was the Multi Coat supplied by Chemona Nanocoat Technologies (Netherlands) which is a hydrophobic nanotechnology-based coating, designed to seal and protect non-porous hard surfaces from dirt and water. Its composition is presented in Table 3.1 [77], [78].

Table 3.1 – Chemona Multi Coat composition [77].

Constituents	Concentration (wt%)
Isopropanol	50 - 100
Zirconium tetrabutanolate	0.5 - 1

3.1.7. HIREC 300-W

HIREC is an advanced water based superhydrophobic coating, developed by NTT Advanced Technology Corporation (Japan), for the protection of equipment against water-related damage. This is achieved as a result of the composition of the HIREC coating material, which combines PTFE particles, fluorinated resin and a small amount of titanium dioxide [79]. Table 3.2 shows the composition of the coating.

Table 3.2 – HIREC 300-W composition [79].

Constituents	Concentration (wt%)
Water	43.8
Polytetrafluoroethylene	40
Fluoro resin	12.2
Ethanol	2.8
Polyoxyethylene	1.1
Titanium dioxide	0.1

3.2. PREPARATION METHODS

For the preparation of the samples, the first step consisted of cutting the blade plates into samples with dimensions of 100 mm by 100 mm, with a vertical band saw (Figure 3.3), located in a laboratory of Mechanical Engineering Department (DEM) of University of Minho.



Figure 3.3 – Vertical band saw used to cut the blade samples.

After that, the substrates were decreased with ethanol, acetone and water and allowed to dry thoroughly prior to the coating application.

To evaluate the influence of TiO_2 nanoparticles, four samples with different weight concentration (0%, 2.5%, 5%, 10%) were utilized to investigate its optimum percentage. The concentrations of nanoparticles were selected based on previous works, in order to avoid their agglomeration and to

guarantee a homogeneous structure with the necessary mechanical properties for these applications. So, for each concentration, the amount of TiO_2 was calculated. The various nanocomposites with the respective concentrations of TiO_2 nanoparticles are gathered in Table 3.3.

Table 3.3 – Mass/volume used in the preparation of each coating.

Sample	PVDF (g)	TiO_2 (g)	DMF (mL)
PVDF + 0% TiO_2	3	-	27
PVDF + 2.5% TiO_2	3	0.07692	27
PVDF + 5% TiO_2	3	0.15789	27
PVDF + 10% TiO_2	3	0.33333	27

So, through a high-precision analytical balance, the quantities were weighed for each solution (Figure 3.4).



a)



b)

Figure 3.4 – a) Weighing of samples with a precision balance. b) Percentages of TiO_2 used (2.5%, 5%, 10%).

After that, the different quantities were dissolved in 27 mL of dimethylformamide and the solutions to be dispersed were placed in an ultrasonic bath for 4 hours (Figure 3.5).

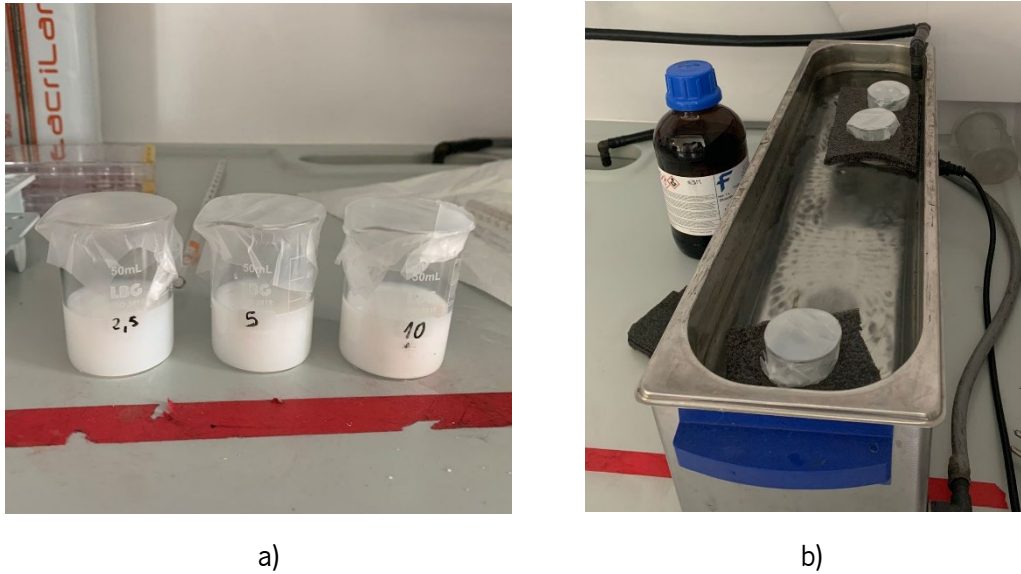


Figure 3.5 – a) Different percentages of TiO_2 dispersed in DMF. b) Solutions in an ultrasonic bath.

Then, 3 g of PVDF was added to the three previous solutions. In addition, 3 g of PVDF were also added for the coating without any percentage of TiO_2 and was also dissolved in 27 mL of DMF. The four solutions were placed under magnetic stirring until complete dissolution (Figure 3.6).



Figure 3.6 – Magnetic stirrer used for complete dissolution.

For the application of the coatings on the blade's samples, a spray gun of 100 mL/min and pressure limited to 20 psi was used (Figure 3.7 a). The gun is activated manually and then the solution is sprayed with the help of compressed air that is released. Through a microscope it was found that the coatings still had some porosity, so the substrates were also dip-coated for 60 s.

Finally, the fabricated coated substrates were placed in an oven at 210°C for 10 minutes (Figure 3.7 b) to remove residual solvents, while the commercial coatings were dried according to the manufacturer instructions. Since DMF is a toxic solvent, the entire process was carried out inside a hotte.

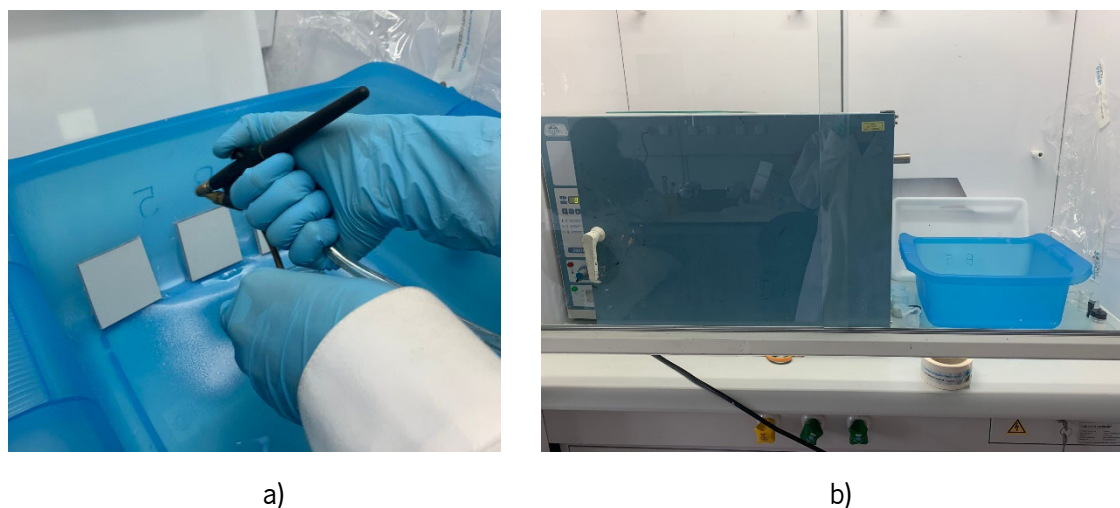


Figure 3.7 – a) Spray painting of the coatings. b) Coatings in the oven at 210°C.

Figure 3.8 represents the general steps of the synthesis process of coatings with TiO₂ nanoparticles.

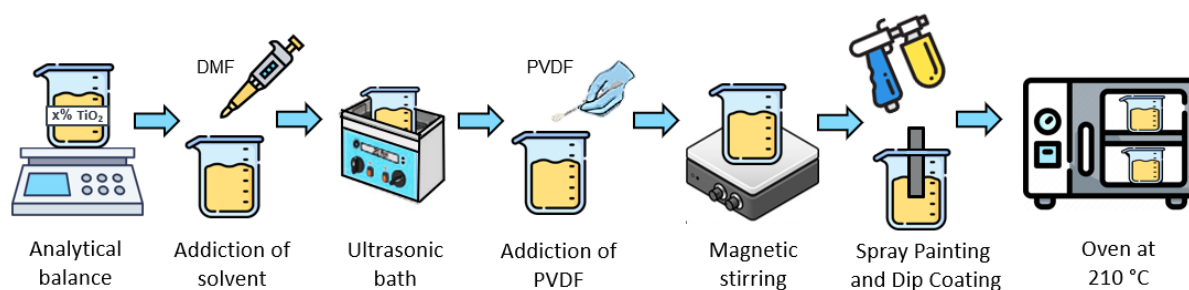


Figure 3.8 – Representative scheme of the method of synthesis of TiO₂ nanoparticles.

The entire procedure was performed at the Institute of Science and Innovation for Bio-Sustainability (IB-S) in Braga. Table 3.4 summarizes all the coatings that will be studied, those manufactured in the laboratory and those acquired commercially.

Table 3.4 – Laboratory-produced and commercially purchased coatings.

Samples	
Fabricated	Commercially Available
PVDF	Wearlon
PVDF + 2.5% TiO ₂	Chemona
PVDF + 5% TiO ₂	HIREC
PVDF + 10% TiO ₂	

3.3. METHODS

In the next sections the tests and equipment used will be described, which include the contact angle measurement test and the ice adhesion strength test.

3.3.1. CONTACT ANGLE MEASUREMENT

When ice forms on a surface from liquid water, the water is the one that first interacts with the surface. For this reason, the study of the wetting behaviour of water on a surface is imperative in a discussion of the interaction of a surface and ice.

To characterize the wettability properties of the coatings, contact angle was measured using sessile drop technique on an optical tensiometer (Dataphysics OCA 15 Plus), represented in Figure 3.9. This system features an automated droplet dispensing system allowing the user to define droplet volume. It features a built-in camera and the Attension software that calculates the contact angle using the Young-Laplace method, which improves accuracy by accounting for the drop's distorted shape due to the weight of the liquid. Static contact angle measurements were performed using a 5 μl droplet of distilled water for 30 seconds under the ambient conditions of the room (relative humidity and temperature), being the average of four measurements calculated.

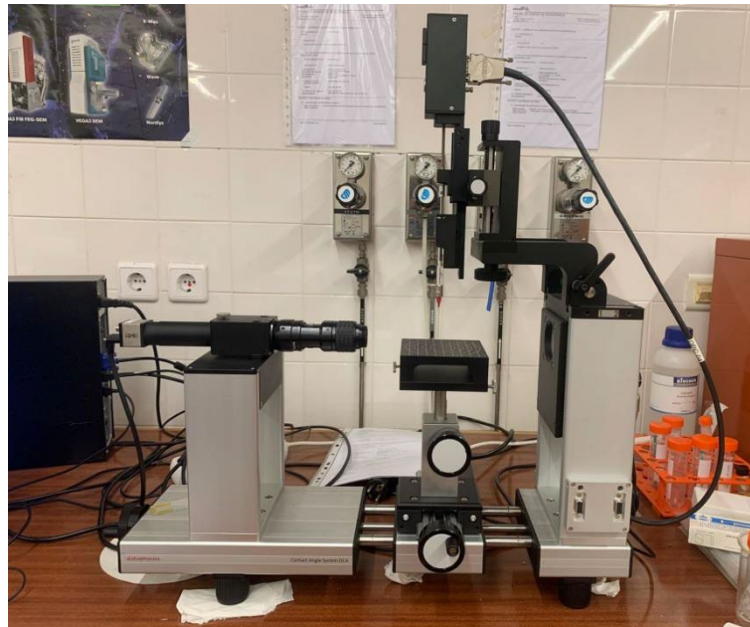


Figure 3.9 – Dataphysics OCA 15 Plus equipment for contact angle measurement.

3.3.2. ICE ADHESION STRENGTH MEASUREMENT

The accumulation of ice on a surface often necessitates ice removal to avoid material or structural failure. Low ice adhesion of a material is therefore a desired property, as surfaces with excellent de-icing properties allow for easy ice removal due to their low ice adhesion strength. Thus, the icephobicity of a surface can be quantified by measuring how strongly ice adheres to it. To complicate matters, testing ice adhesion strength is not straightforward or consistent, this simple statement implies rather complex tasks: creating artificial ice on a surface and removing the ice from the surface in a measurable and reproducible way.

The test performed is an adaptation of one of the most common shear ice adhesion tests, the horizontal pusher test [80], where a statically frozen ice block is pushed until the shear stress at the interface between the ice block and the substrate material is sufficiently large to shed the ice (Figure 3.10).

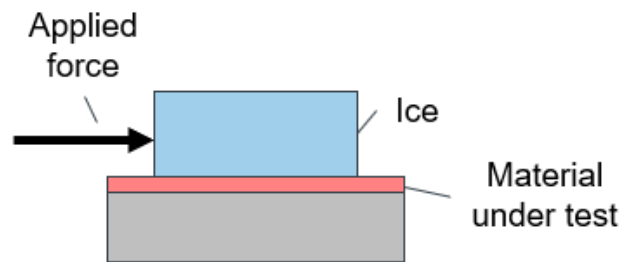


Figure 3.10 – Horizontal shear test.

Although it suffers from a lack of representativeness in the shape and type of ice, the method benefits from its simplicity. The rig is easy to set up, and many tests can be performed in a short time. The results are communicated in terms of ice adhesion strength, the maximum force measured at break is converted into ice adhesion strength by dividing the force by the contact area of the ice/substrate interface.

$$\tau = \frac{F_S}{A} \quad (3.1)$$

Where:

τ = ice adhesion strength in N/mm^2 or MPa ;

F_S = applied shear force in N ;

A = cross-sectional area in mm^2 (constant).

However, this value of ice adhesion strength (τ) is apparent and does not give full account for the mechanisms involved in the delamination process. A better parameter for comparing the ice adhesion characteristics of the different surfaces is the adhesion reduction factor (ARF) that was obtained by dividing the shear stress value of the uncoated blade samples by the shear stress of the coated substrates.

$$ARF_i = \frac{\tau_{ub}}{\tau_{cb}} \quad (3.2)$$

Where:

ARF_i = adhesion reduction factor of coating i ;

τ_{ub} = ice adhesion strength of the uncoated blade sample in kPa ;

τ_{cb} = ice adhesion strength of the coated blade sample in kPa .

Making the adaptation of the horizontal shear test to a vertical shear test, a force parallel to the surface is applied to an ice block preliminarily formed over the substrate, until reaching the maximum force at which debonding occurs, according to the standard ISO 4624. The ice adhesion strength was characterized by a universal mechanical tests Instron® model 8874, in DEM's materials testing laboratory. A representation of the complete setup is shown in Figure 3.11.

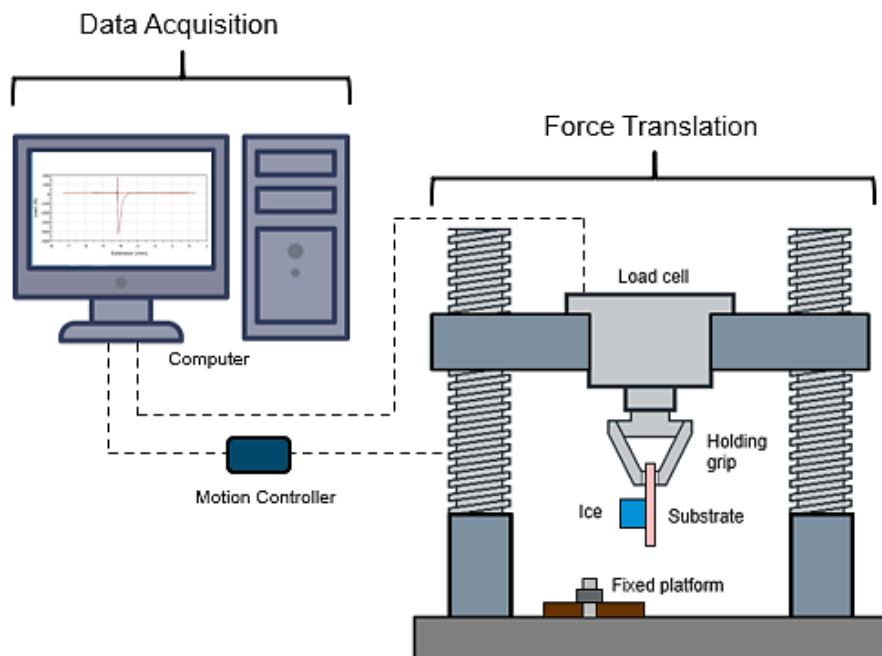


Figure 3.11 – Complete setup of the vertical shear test.

This way, the push-off test is conducted by first fixing an aluminium platform with two screws, which will be used as a stop to separate the ice from the sample. The platform was aligned as close as

possible to the tested sample surface to minimize the torque on the ice cube, trying to ensure that the ice cube is removed through only shear force and not shear and normal (Figure 3.12).

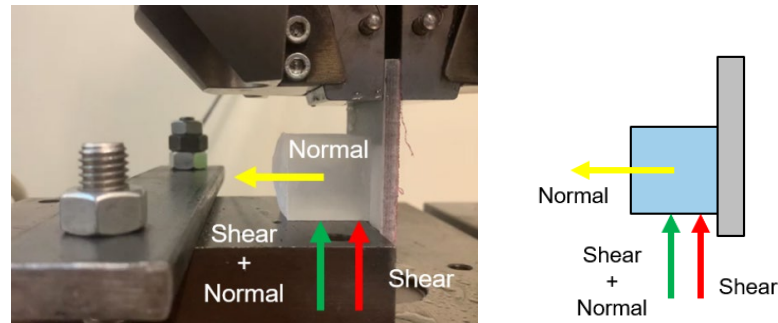


Figure 3.12 – Existing forces according to the platform distance: shear, normal and mixed.

A 3D-printed plastic mold, previously modelled in Solidworks, was used to make the silicone mold to create an approximately 30 mm² ice cube (Figure 3.13).

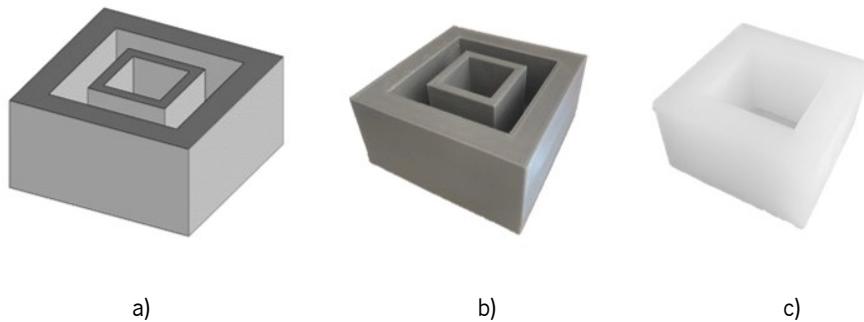


Figure 3.13 – a) CAD model in Solidworks. b) 3D printed plastic mold. c) Silicone mold used to create the ice cube.

Figure 3.14 depicts the formation of the ice cubes. The silicone mold was placed onto the 100 x 100 mm substrates and a syringe was used to inject distilled water into the mold, ensuring that no air bubbles were trapped underneath. The use of distilled water would reduce the effects of solutes or contaminants on ice crystallization, which can cause the ice to undergo heterogeneous ice nucleation. The set was placed in the freezer at -10°C for 24 hours, and pressure from a 200 g metal cylinder was placed on top of the tube to avoid water leakage during freezing. As the ice did not adhere to the silicone mold when the ice was fully formed, the silicone mold could be removed prior to the test and shear force applied directly to the ice block.

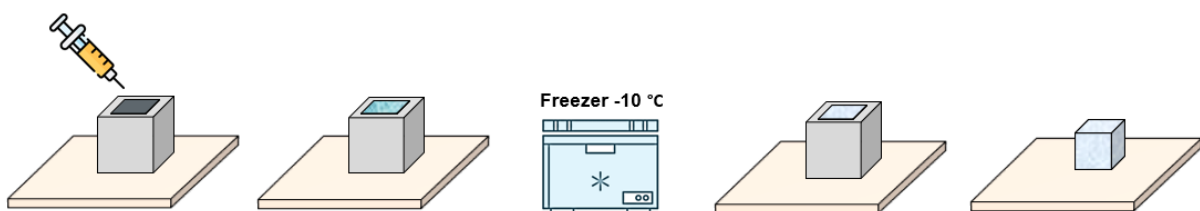


Figure 3.14 – Steps for the formation of the ice cube on the surface of the sample.

Ice-cube substrate was then moved to the testing apparatus and the sample was clamped by a holding grip. The initial conditions were introduced in the software (height = 30 mm, width = 30 mm, thickness = 30 mm) and the impact velocity was set to 0.5 mm/s. The loading curves were recorded while the linear actuator load cell was moved until the ice cube reached the platform and was sheared off the surface. The peak value of the shear force measured was divided by the ice contact area (30 x 30 mm) on the coating surface to obtain the ice adhesion strength (equation 3.1), in negative because the force is applied in the opposite direction to the axis. As the fixed platform distance is small, gravity can be discarded as negligible. Each test surface was measured four times, for a reliable measure, and through the equation (3.1) and (3.2) the average of the measured adhesion strengths and the adhesion reduction factor were calculated. In addition, to verify the accuracy of the results, the standard deviations (SD) and relative standard deviations (RSD) were also calculated. The relative standard deviation consists of the ratio of the standard deviation and the mean, expressed in percentage [81].

3.4. NUMERICAL ANALYSIS

To analyse the viability of the ice adhesion strength test assumptions and effectiveness of the implementation of the icephobic coatings in a wind turbine blade, numerical simulations were developed.

3.4.1. STRESS DISTRIBUTION

Developing a physical model that can predict ice mitigation requires accurate measurement of ice adhesion strength. The standard methods of calculating ice adhesion strength assume a homogenous stress distribution in which the ice adhesion breaking force is considered a cumulative parameter for the ice-solid contact area. However, the accuracy of the ice adhesion strength measurement is influenced by the uncertainty of stress concentration in local regions within the ice-solid interface.

An ideal mechanical strength test is one where only one stress component exists: in reality, complete stress isolation is not achievable. Rather, what exists is a loading case where many stress components are present, but one dominates. In the previous experimental shear test, as the platform was placed as close as possible to the ice cube, most of the interfacial stress is shear, but the normal stress is always, at least, partially there. Most of the time, these secondary stresses are ignored in the calculation and presentation of ice adhesion strength results. Finite element analysis are made to validate whether secondary stresses play a critical role in the measurements and to visualise stress distributions.

The pusher test is reproduced in a linear elastic finite element model, using Explicit Dynamics ANSYS, which is defined in terms of geometry, materials properties, and boundary conditions. The dimensions of the ice block and substrate used in experiments are reproduced, as seen in Figure 3.15.

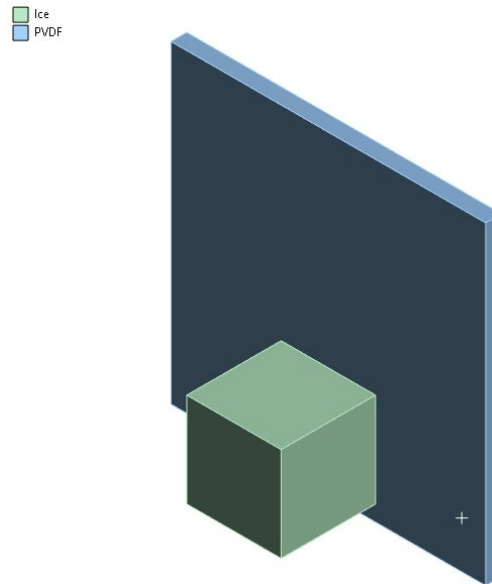


Figure 3.15 – 3D Finite element model in ANSYS.

For the numerical simulation, the study of the substrate with PVDF coating was chosen, intending to facilitate the identification of its mechanical properties. Given the centimetric length scale of the pusher test, the two materials regions were modelled as isotropic linear elastic materials, whose values of the Young's modulus, Poisson ratio and density are listed in Table 3.5.

Table 3.5 – Mechanical properties of ice and PVDF inserted in the software.

Material	Young's Modulus (GPa)	Poisson Ratio	Density (kg/m ³)
Ice [82]	9.33	0.33	897
PVDF [83]	2.15	0.35	1780

The connection between the ice and the PVDF substrate is "bonded", with the condition of "breakable" detachment, the detachment of nodes being conditioned by exceeding a value for shear stress (0.35 MPa), maximum value taken from the experimental results. For this model, the breakable option was set with "Stress Criteria" and then the connection can be broken during the analysis.

As it is a simple geometry, hexahedral elements with 3 mm sizing were used to build the mesh, as shown in Figure 3.16.

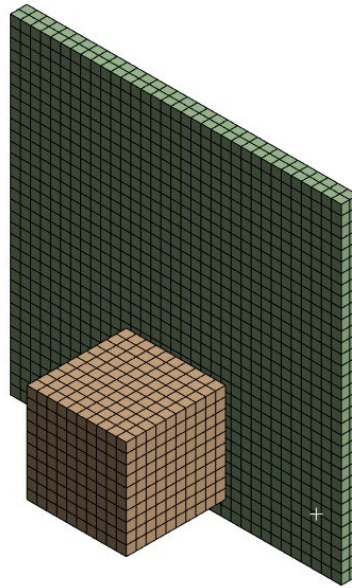


Figure 3.16 – Meshed FEM model.

The boundary conditions used for the model were to approximate the experimental test, with a fixed support at the base of the ice cube, to simulate the platform effect (Figure 3.17).

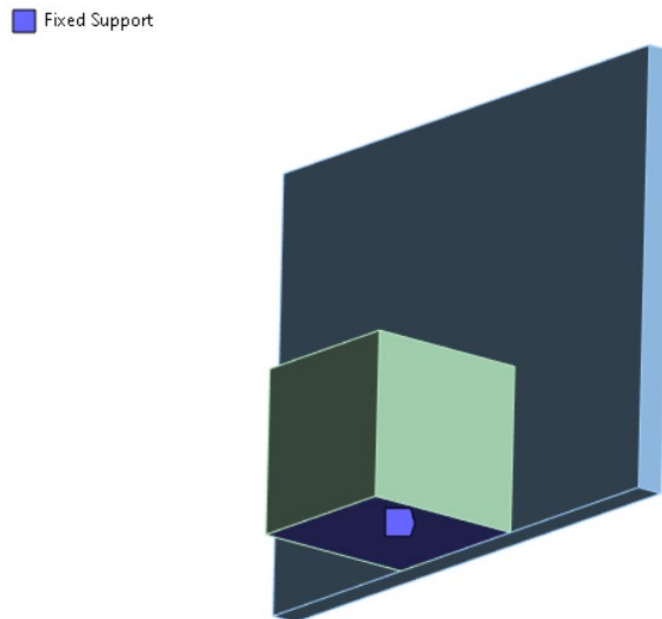


Figure 3.17 – Fixed support condition.

On the substrate, a speed with the same value (0.5 mm/s) and direction as the physical test was applied (Figure 3.18 a). The effect of the earth's gravity was also added to all bodies, with the same direction (Figure 3.18 b).

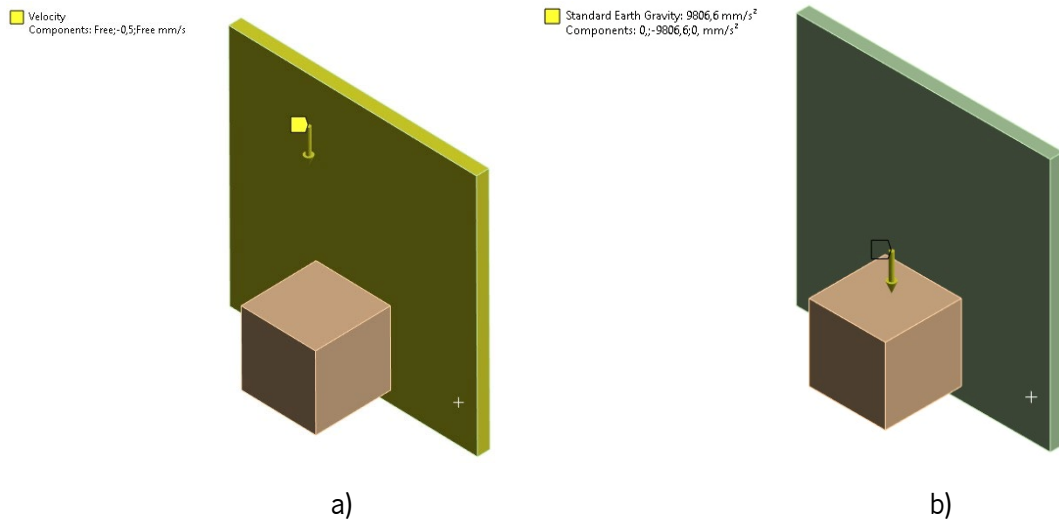


Figure 3.18 – a) Velocity value and direction entered in the software. b) Earth gravity effect condition.

In addition, a x and y free displacement was also applied to the plate (Figure 3.19).

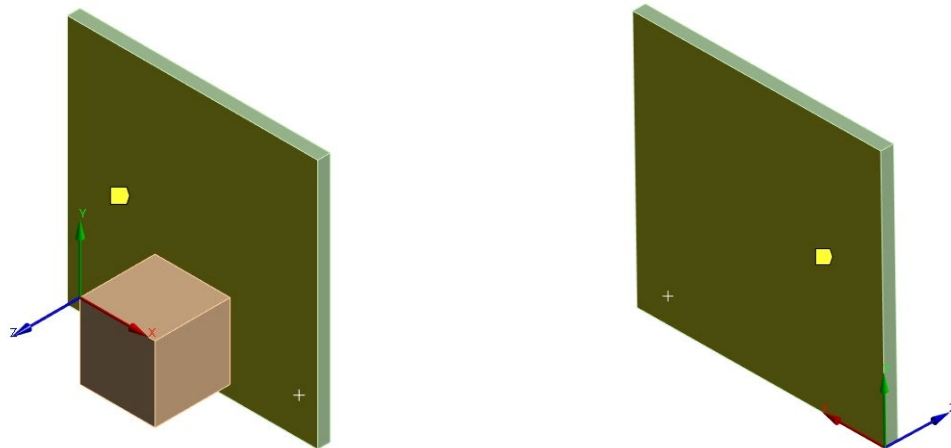


Figure 3.19 – x and y displacement condition.

Finally, the normal and shear stress distribution were calculated.

When using this model for calculating ice/substrate interface strength in this paper, some assumptions were made: the ice and the PVDF surface are perfectly bonded, the van der Waals forces were not considered; the ice is similar to glaze ice, with no porosity or air bubble and homogeneous; the effect of grain size is not taken into account and the test temperature is not examined.

The equipment used in the physical tests considers that the shear stress is the force divided by a specific area, assuming that this value is constant throughout the interface. However, as already mentioned, the distribution of stresses is not homogeneous, rather it is not constant, there are places with greater or lesser stress. So, to obtain the maximum values for each coating, a model similar to the previous one was used.

For the determination of the maximum shear stress of all the coatings, as it was not possible to identify the mechanical properties for each case, it was assumed that the thickness of the coating is very small that could be neglected. Having said that, structural steel was considered for the substrate material in all simulations. The values for the Young's modulus, the Poisson's ratio and density used were 200 GPa, 0.3 and 7850 kg/m³, respectively. The geometric model, type of contact and mesh type and sizing was the same as in the study previous.

The boundary conditions applied in this model (Figure 3.20) were a fixed support at the base and top of the substrate and the effect of gravity in all the bodies.

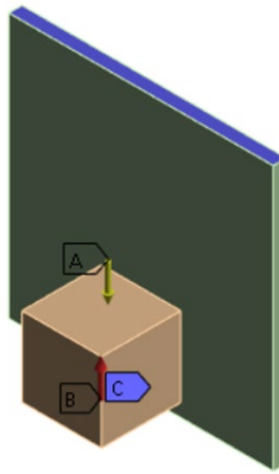


Figure 3.20 – Boundary conditions applied in this model.

Also, a vertical force in the opposite direction to the y-axis (in red) was applied at the base of the ice cube, where the maximum values of the forces measured experimentally for each coating were inserted (Table 3.6).

Table 3.6 – Maximum values of the forces measured experimentally for each coating.

Coating	Measured Maximum Force (N)
Uncoated	788.35
PVDF	309.3
PVDF + 2.5% TiO ₂	392.92
PVDF + 5% TiO ₂	247.36
PVDF + 10% TiO ₂	130.87
Wearlon	36.73
Chemona	115.31
HIREC	435.75

3.4.2. AEROMECHANICAL FORCE ANALYSIS

Removal of ice by aerodynamic forces with icephobic coatings only would make a highly efficient ice protection system, if only it was possible. As the largest stress component for such a loading case would be in shear, a shear ice adhesion analysis can answer the question of whether a surface would be an effective ice protection system in the common aerodynamic shear loading case. In this way, a study of the aerodynamic forces that act on an airfoil was carried out to estimate numerically if those aerodynamical forces are sufficient to detach the ice. For this purpose, a COMSOL CFD model developed by Vestas was modified.

The model represents a 2D blade section located 5 m away from the tip, identical to what it is found in a Vestas 150 m rotor turbine. It resolves the local air velocity surrounding the airfoil taking into account the angle of attack and the ambient air velocity. Discussing it in more detail is out of the scope of this work, but according to Vestas' engineers it is assumed that the pressure field that can be extracted from this simplified model is a sensible approach of the true aerodynamical forces that will operate in a commercial turbine. The turbulent model employed was the $k-\epsilon$ model, the most common to simulate turbulent flow conditions, because of its robustness, economy and reasonable accuracy.

In an initial phase, a simple circular geometry (Figure 3.21) was used to recreate the ice in the blade surface, with three different dimensions (radius = 1; 5; 10 mm) and four different wind velocities (5; 10; 15; 20 mm/s), since this speed range covers the normal operation of a wind turbine.

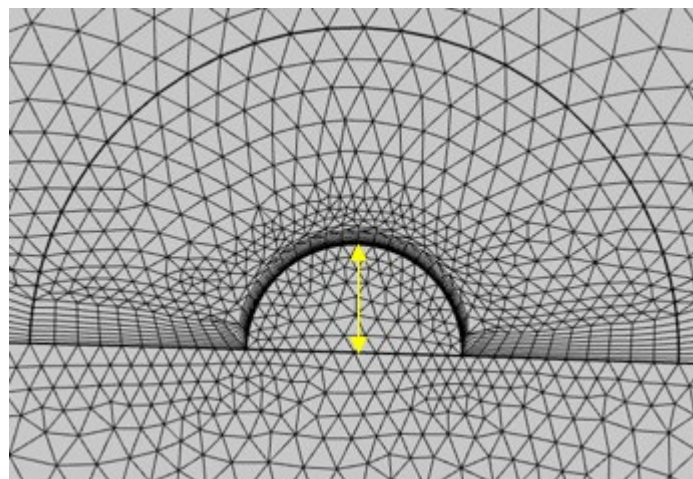


Figure 3.21 – Circular geometry used to recreate the ice shape.

It should be noted that a 2D cut is being used, and therefore the pressure field in the ice correspond not to a semispherical drop of ice, but to half a cylinder running along the aerofoil i.e. the pressure field in the ice surface is being extracted. This pressure field is then used in a linear elastic model, similar to

the one used in ANSYS, but in this case for the ice drop geometry and implemented in COMSOL, also assuming that the materials are isotropic and homogeneous.

Since it was verified that the material of the blade surface had little influence on the results of the shear stress, the material inserted for all the simulations was the same as in the previous study, structural steel. And, for the ice, the same properties were applied.

As one of the essential objectives in adding these coatings to turbine blades is to reduce the accumulation of runback ice, the numerical study in the second part focused on this type of ice shape. However, the runback ice represents a type of ice accretion where very little information is available due to the complexities involved with collecting experimental data. For the geometry design, document [84] was consulted which, through analysis in wind tunnels, managed to remove the geometric format that best represented the realistic runback ice. To study the influence of the ice size, the maximum height (h) of the geometry was alternated by 1; 5 and 10 mm, also with the same previous velocity's values.

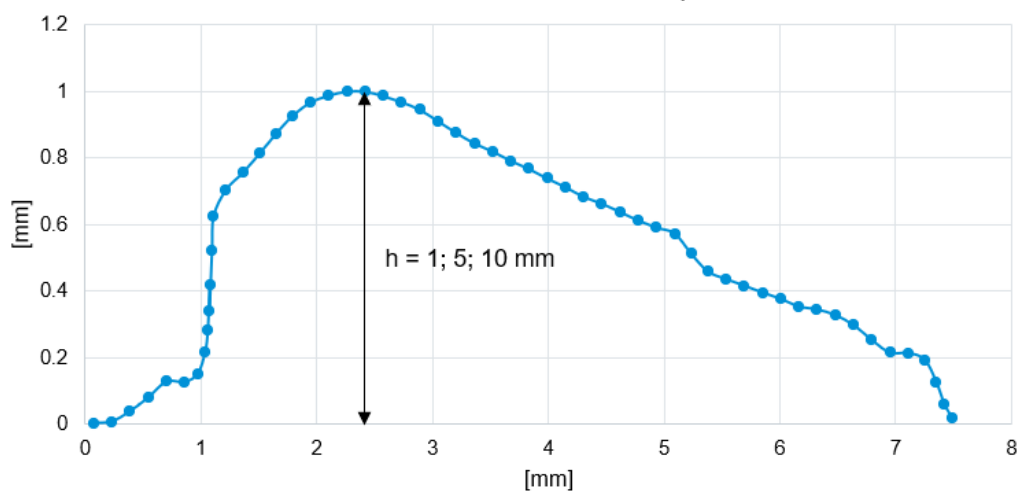


Figure 3.22 – Runback ice shape, consulted on [84].

For a study of the influence of the location, the ice shapes were placed in four different positions, two in the upper part of the airfoil and two in the lower part, at a distance of 30% and 60% of the airfoil length (Figure 3.23). The choice of the ice locations was because as the heating elements are at the leading edge of the blade, the 30% location is where the heating element ends and the 60% is to show a more distant place where ice can accumulate due to the runback water. The spacing between the ice points was to guarantee that the presence of one would not interfere with the result of the other and thus allowing the simulation of the four positions simultaneously, reducing computational time.

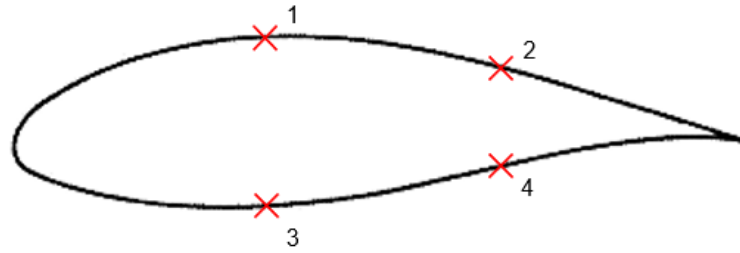


Figure 3.23 – Location of the ice drops on the airfoil.

In that way it was possible to get the maximum and minimum stress values per unit of length at the interface between the airfoil and the ice, for each position.

These values are then compared to the maximum shear values retrieved from the simulations detailed in 3.4.1. to see if the external forces are enough to detach the ice, i.e. superior to the previous ones. Figure 3.24 represents a flowchart of the steps used in numerical analyses.

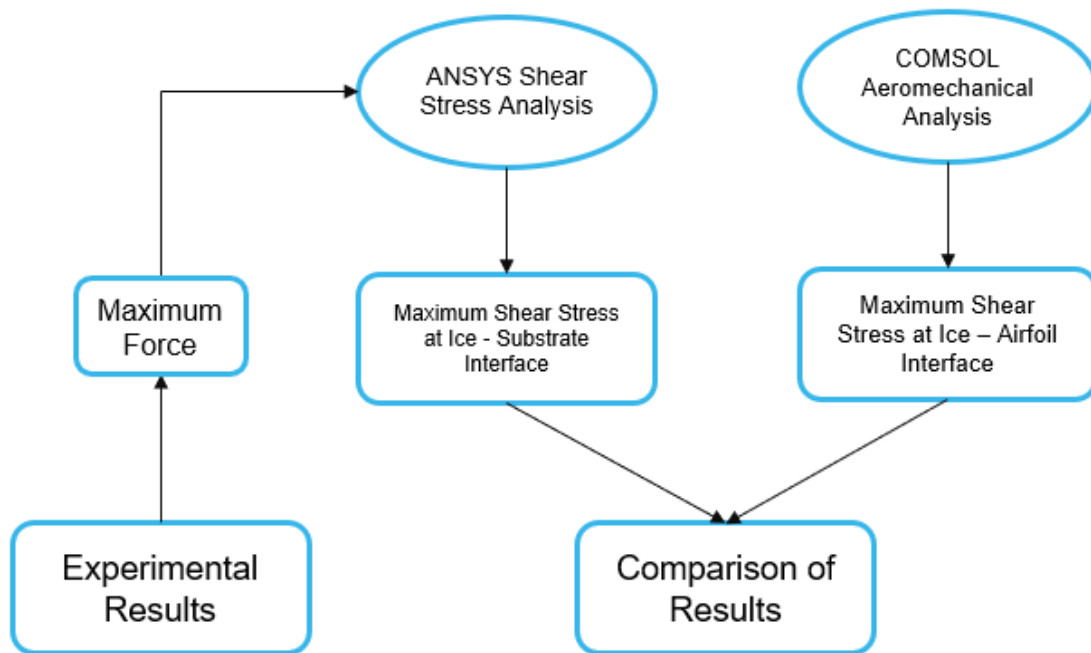


Figure 3.24 – Flowchart of numerical analysis steps.

4. RESULTS AND DISCUSSION

The purpose of this chapter is to present, analyse and relate the results obtained during the experimental and numerical work developed and, as a consequence, to respond to the objectives of this report. Thus, in order to analyse the new characteristics acquired by the samples of the wind turbine blades, the various coatings were compared with the reference samples (without the application of the coating).

4.1. CONTACT ANGLE MEASUREMENT

The analysis of the water contact angle was carried out to evaluate the wettability of the samples, to later relate the water repellency with the ice repellency.

A summary of the measured contact angles is presented in Table 4.1 along with their corresponding water repelling characteristics, as well as a visual representation of its variation in Figure 4.1. Based on the measured contact angles, the surfaces were divided into three categories namely hydrophilic ($CA < 90^\circ$), hydrophobic ($CA > 90^\circ$) and superhydrophobic ($CA > 150^\circ$). The images of the results are detailed in Annex B.

Table 4.1 – Summary of the water contact angle measurements.

Sample	Average CA (°)	SD (±)	RSD (%)	Wetting Property
Uncoated	64.31	2.57	4.00	Hydrophilic
PVDF	90.16	1.33	1.48	Hydrophobic
PVDF + 2.5% TiO ₂	92.84	1.15	1.24	Hydrophobic
PVDF + 5% TiO ₂	96.05	1.13	1.17	Hydrophobic
PVDF + 10% TiO ₂	105.14	5.79	5.51	Hydrophobic
Wearlon	110.71	2.60	2.34	Hydrophobic
Chemona	124.91	3.08	2.47	Hydrophobic
HIREC	151.00	1.15	0.76	Superhydrophobic

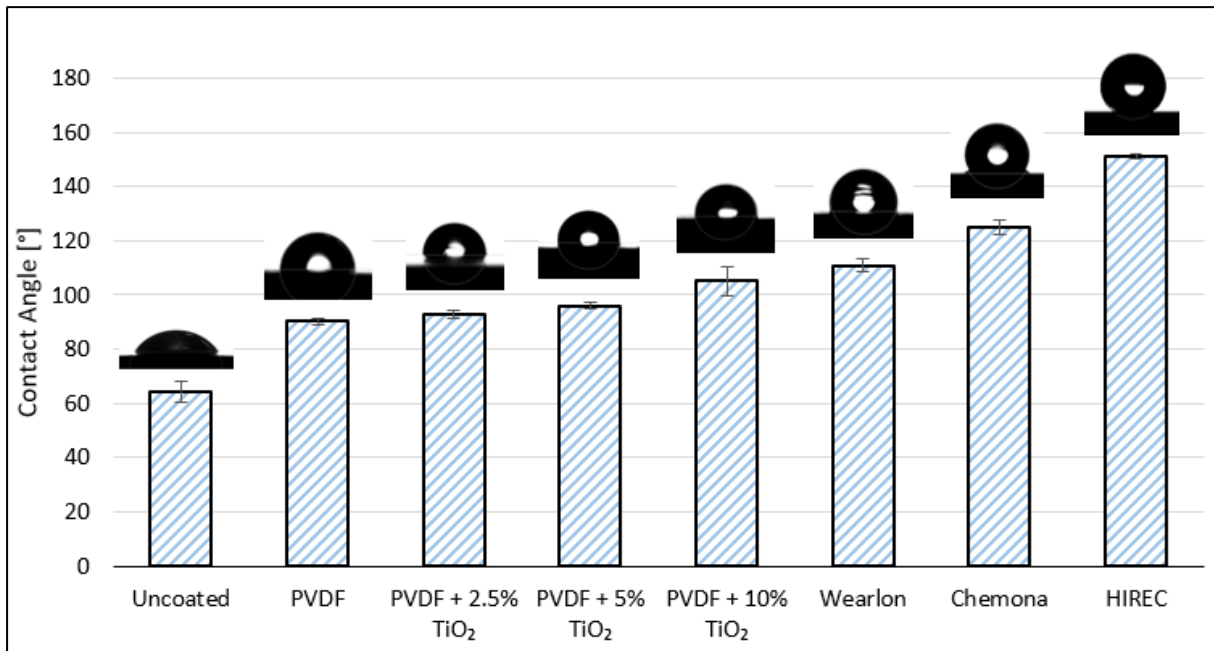


Figure 4.1 – Variation of the contact angle and the relative standard deviation of the different coatings.

As verified in Table 4.1 and Figure 4.1, the relative standard deviation values are satisfactory, because they are all less than 6%, confirming the consistency of the collected results (see Annex C).

Before coating, the surface of the wind turbine blade is hydrophilic, with an average contact angle of $64.31 \pm 2.57^\circ$. With the application of the PVDF on the surface the contact angle increased to 90.16° , indicating that the pure PVDF coating can enhance the hydrophobicity of the wind turbine blade, but it is far away from superhydrophobic.

To further increase the contact angle, the wind turbine blade surface was modified with TiO₂ nanoparticles. According to the data obtained, TiO₂ nanoparticles induce an enhancement in hydrophobicity. The effect observed in Figure 4.1 is thought to an increase in surface roughness, when the TiO₂ content increased, resulting in the lotus effect. Therefore, the surface area in direct contact with the ice/water droplet decreased, leading to a Cassie state.

Regarding the commercial coatings, the Wearlon coating shows a hydrophobic behaviour with a water contact angle of $110.71 \pm 2.60^\circ$ and the Chemona Multi-Coat, as expected, is hydrophobic with a contact angle of $124.91 \pm 3.08^\circ$. Finally, the HIREC coating has the highest value of the measured contact angles, $151.00 \pm 1.15^\circ$, confirming to be superhydrophobic.

From these results, it is possible to see that all the materials' outer surfaces are more hydrophobic than the reference material (uncoated sample).

4.2. ICE ADHESION STRENGTH MEASUREMENT

After measuring the ice adhesion strength four times for each coating, an average of the results was made. The test data and the results of the ice adhesion strength experiments are presented in Table 4.2 and in Figure 4.2. To view the graphs obtained for each coating in more detail Annex D should be consulted.

Table 4.2 – Summary of the ice adhesion strength results.

Sample	Average Ice Adhesion Strength (kPa)	SD (\pm)	RSD (%)	ARF
Uncoated	794.34	116.91	14.72	1.00
PVDF	300.04	33.79	11.26	2.65
PVDF + 2.5% TiO ₂	407.27	24.83	6.10	1.95
PVDF + 5% TiO ₂	224.74	44.98	20.01	3.53
PVDF + 10% TiO ₂	131.20	14.86	11.33	6.05
Wearlon	26.66*	9.75*	36.58*	[29.79; ∞]*
Chemona	105.60	22.24	21.06	7.52
HIREC	449.96	20.32	4.52	1.77

* Not accurately measured

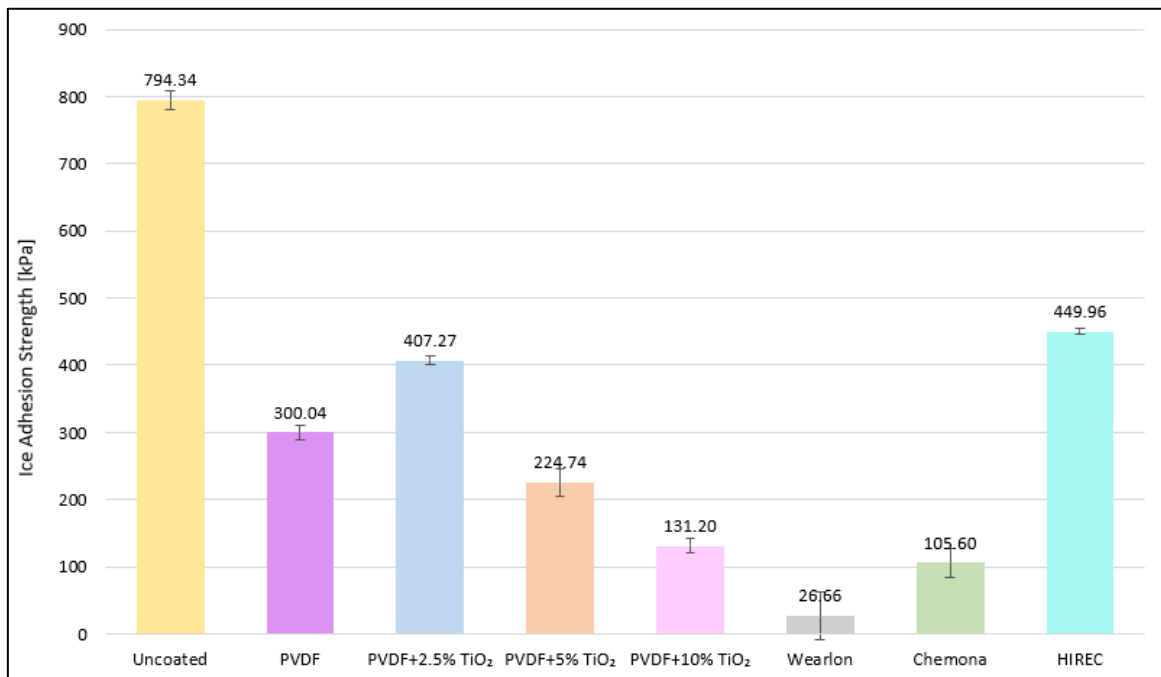


Figure 4.2 – Variation of the ice adhesion strength and the relative standard deviation of the different coatings.

When ice accretion is inevitable, an icephobic surface should possess a low ice adhesion in order to facilitate the removal of the ice layer. For a surface to reduce ice adhesion, it must ensure that a Cassie-Baxter wetting state exists throughout the freezing process. In that state, the air voids present in between the surface's hierarchical structures will reduce the contact area and will act as stress concentration points, reducing the ice adhesion strength. However, transitioning to a Wenzel state prior to or during freezing will cause a reversed effect, in which ice adhesion will increase due to the mechanical interlocking between the ice layer and the surface roughness.

The results depicted in Table 4.2 and Figure 4.2 state that for the uncoated surface, the ice adhesion strength was found to be around 794 kPa, which was the highest value among the measured surfaces. The lowest ice adhesion strengths were observed in the commercial samples, Chemona and Wearlon, with an average of 105.60 kPa and 20.26 kPa, respectively. Since the uncoated sample was the reference, the adhesion reduction factor (ARF) was set to 1.

The study of the effect of surface roughness on the shear stress can be done through the analysis of the graph of Figure 4.3 that relates the percentage of TiO_2 nanoparticles with the ice adhesion strength measured.

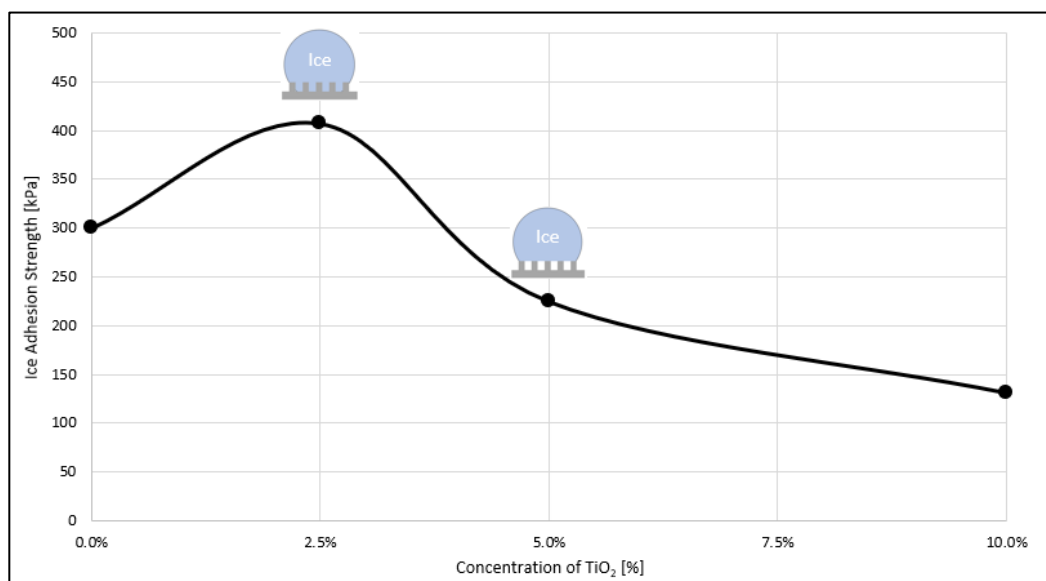


Figure 4.3 – Effect of the percentage of TiO_2 nanoparticles in the ice adhesion strength value.

Some conclusions can be drawn based on these results. In the sample with a percentage of only 2.5% of nanoparticles the adhesion strength increases compared to the sample without any percentage, and from the concentration of 5%, the ice adhesion strength decreased with the increase in titanium dioxide weight. This implies that a Wenzel state was experienced at low temperatures for the 2.5% TiO_2 sample, that not only increases the contact area of the ice and the coating but also makes ice and coating

embedded in each other forming an anchoring effect, which enlarges the ice adhesion strength. By increasing the amount of TiO_2 , the value of adhesion force decreases, this result was attributed to the lower surface energy and enhanced hierarchical structure achieved by the higher content of TiO_2 nanoparticles, where the droplet will freeze on the top of the surface roughness peaks leaving air pockets on the ice-surface interface (Cassie-Baxter state).

As said before, the coatings with the lowest values were the commercial ones, Chemona and Wearlon. The hydrophobic coating, Chemona, showed an average of ice adhesion strength of 105 kPa, revealing a reduction of approximately 7.5 in comparison to the uncoated blade substrate. A peculiar observation was found with the Wearlon coating sample, which exhibited extremely low ice adhesion strength behaviour. During the removal of the mold, the ice cube was more tightly adhered to the mold itself than to the coating, so the test had to be done without removing the mold. As the adhesion of this coatings was very low, during the tests there was not really a detachment, but rather a sliding of the ice cube on the substrate. Because of that, in the first four tests it was not possible to withdraw a concrete result of the ice adhesion strength value, so four more tests were carried out with this coating, however the same behaviour continued to be manifested.

To select the best measurement data, a signal-to-noise ratio study was performed, which is a parameter that compares the level of the desired information to the level of background noise (undesired information), and it is calculated from the following equation [85] [86]:

$$SNR = \frac{A_{signal}}{\sigma_{noise}} \quad (4.1)$$

Where A_{signal} denotes the peak amplitude of the shear stress and σ_{noise} denotes the standard deviation of the noise, which has to be calculated from a part of the trace, where no reflections or backscatters are present. In Figure 4.4, the SNR calculation is illustrated schematically.

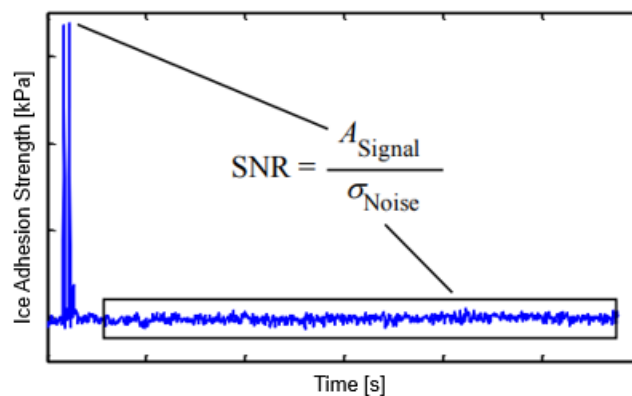


Figure 4.4 – Signal to noise ratio (SNR) calculation based on measurement data [86].

An $SNR \geq 3$ is considered a reliable threshold for distinguishing signal from background noise [87].

The signal-to-noise ratio study for the different tests of the Wearlon coating are presented in Table 4.3. Of the eight tests carried out for the Wearlon coating, only four had the SNR greater than 3, therefore only these values were considered for the calculation of the average ice adhesion strength (consult Annex D).

Table 4.3 – Signal-to-noise ratio calculation for the different tests of the Wearlon coating.

	A_{signal}	σ_{noise}	SNR	
Test A	6.00	2.39	2.52	< 3
Test B	40.81	2.81	14.53	> 3
Test C	21.86	3.45	6.33	> 3
Test D	6.42	2.25	2.85	< 3
Test E	6.30	2.35	2.68	< 3
Test F	29.53	2.45	12.05	> 3
Test G	5.97	2.26	2.65	< 3
Test H	14.45	2.44	5.93	> 3

However, even for these graphics it is not possible to guarantee that the peaks of the shear stress are the values corresponding to the adhesion between the ice and the substrate. As it was not possible to remove the mold from the cube, these peaks can correspond to the adhesion of the mold itself to the substrate. Even though the ice adhesion has not been measured with accurate values, due to the sensitivity of the measuring instrument and the fact that the mold was not removed, it is possible to conclude that its ice adhesion strength average is at a low level, less than 27 kPa and the ARF is at least 30. As discussed previously this might result from the proper level of roughness that produces a Cassie-Baxter wetting state even at low temperatures.

Regarding the standard deviations, although the uncoated sample has the highest value (117 kPa), with regard to the relative standard deviation, the sample with the greatest dispersion in relation to the mean is the Wearlon coating, with a RSD of 37%. The particular reason for this is, as it is a sample with a very small ice adhesion strength, the measuring equipment was not able to quantify the precise values. An alternative would be to repeat more tests, to get a larger sample of results, or to measure the shear stress on an equipment with greater sensitivity. The remaining coatings have adequate relative standard deviation values. For more details, see Annex E.

The superhydrophobic coating, HIREC 300-W, is the one that after the uncoated sample shows the highest measured value. This coating partly loses its superhydrophobic character near -10°C , enhancing ice adhesion on their surfaces. This is explained by the vapour condensation in the cavities of the solid

because when the temperature drops down to -10°C , the humidity in the air fills the surface cavities and acts as a precursor for initiating the ice adhesion to the surface. This leads to a so-called Cassie-Wenzel regime transition, resulting in an increase in the contact area and, as a result, an increase in the shear stress value. This confirms that a more hydrophobic surface does not imply a higher icephobicity.

So, further analysis can be made by comparing the ice adhesion strengths of these surfaces and their wetting properties. Figure 4.5 gives the graphic trends showing the contact angles of the surfaces plotted with the shear stress recorded.

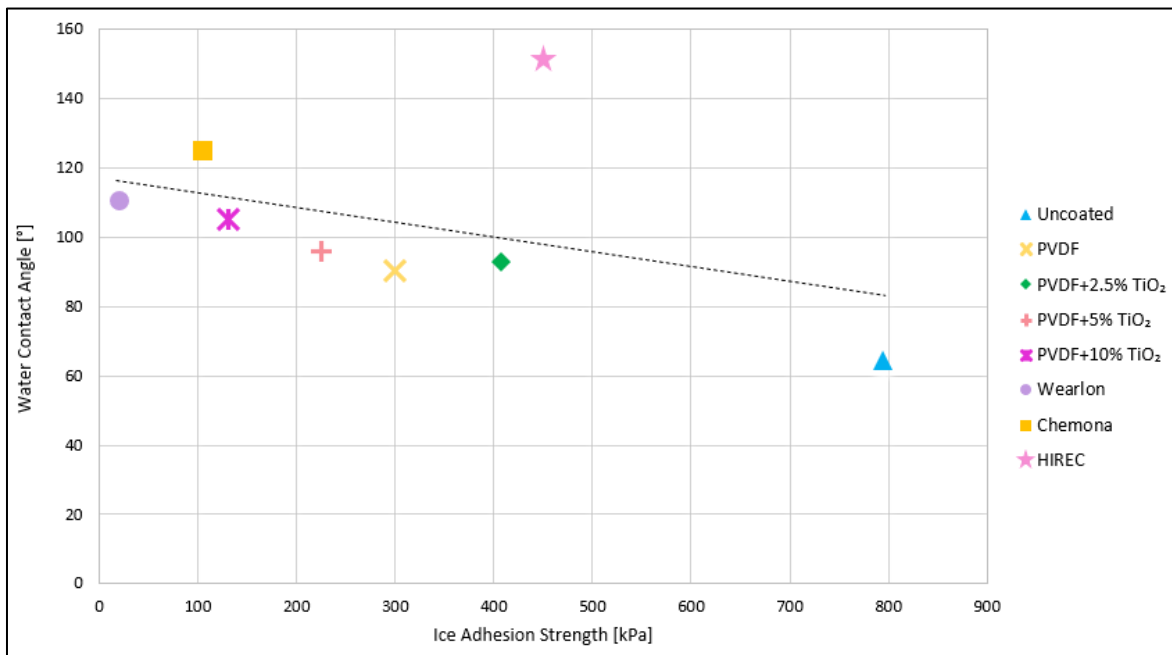


Figure 4.5 – Comparison of the contact angle and ice adhesion strength.

It can be seen that, although, with the increase of the CA the overall trend line shows a little decrease in shear stress, there are inconsistencies in data, reinforcing that that water contact angle has no obvious correlation with ice adhesion strength of the coatings. This is because the water contact angle only reflects the surface chemistry and topography, while ice adhesion strength is determined by various parameters, such as surface chemistry and topography, elastic modulus, the type of ice, temperature of the icing condition, and others. Generally, the increase in contact angle and the decrease of surface energy are favourable to the reduction of ice adhesion strength, but they are not decisive factors.

An example that does not follow this trend, is the superhydrophobic coating HIREC, which has a very high contact angle ($>150^{\circ}$), but a low adhesion reduction. This result is easily understood as a consequence of increased surface areas and asperities at the ice–surface interface, these asperities act to reinforce interfacial ice and increase adhesion. However, one of the keys to avoid the formation of ice

using superhydrophobic surfaces would be to avoid the primary formation of water droplets on the blades, and, in this case, as the water has extremely little adhesion, its implementation could be a possibility.

Another example that corroborates with the fact that the ice adhesion does not vary linearly with the CA is the introduction of 2.5% of TiO₂ nanoparticles to PVDF when compared to the sample with only PVDF. As mentioned earlier, this correlation is believed to be associated with the roughness of the surface. Additionally, the Wearlon coating, which presented the lowest force to de-bond the ice from the substrate, does not present the highest CA, also confirming that the strength does not depend solely on wettability.

On the other hand, interestingly, the remaining coatings exhibit a certain correlation between the decrease in ice adhesion strength with the increase in the water contact angle. It can be deduced that the samples were able to remain in the Cassie-Baxter state even at negative temperatures.

The obtained results emphasize the fact that the ability of superhydrophobic and hydrophobic surfaces to reduce ice adhesion derives from their ability to maintain a robust Cassie state, which is not necessarily correlated with the contact angle. Since, when they move to a Wenzel state, these surfaces will have even more adhesion. Despite this, in an overview, all tested materials could assist the manual de-icing since each of them exhibit a lower ice adhesion strength than the uncoated blade sample.

To simplify the measurement process, the ice adhesion test method comes with a set of assumptions, so some additional sources of error present in the experiments reported must be mentioned. As a complex physicochemical process, ice adhesion is not easy to quantify or compare since it depends on process parameters. Examples of these include ice density, ice formation conditions, substrate nature, and surface profile. Therefore, ice adhesion comparative tests should be performed using the same conditions throughout the evaluation process.

However, the ice adhesion tests were performed ex-situ and the ice samples and tested surfaces were moved from the freezer to the testing apparatus. As the adhesion strength is affected by the environment's temperature at which the test was performed, a temperature control would be necessary to ensure repeatability. Another factor influencing temperature is the heat transfer between the fixed platform and the ice cube, as it is a good thermal conductor, part of the heat will be transferred to the ice cube during the test. Also, removing the mold can inadvertently push or pull on the ice if done incorrectly or too forcefully, affecting the adhesion of the ice, the bonding with the surface, or even causing the ice to melt. This is especially true for low ice adhesion surfaces.

Another factor to take into account is the type of ice. The nature of ice is such that its mechanical properties vary according to the manner that it is made. The literature on ice adhesion testing often

differentiates between static ice (nonimpact ice) and impact ice. Static ice is typically formed gradually by pouring water into a mold and allowing it to freeze in a specific structure or geometry [88].

By contrast, in real-life scenarios, ice accumulation doesn't occur in the form of a single stationary cube frozen over the course of several hours, instead, the impact ice is essentially formed by water droplets that impact the surface of the wind turbine blades at high speed and freeze in unpredictable patterns and circumstances [9]. This involves high droplet inertia and often a high stress due to wind, so that water droplets may penetrate and freeze into the porous structure of the material. Consequently, if the ice anchor between the surface roughness peaks, the adhesion strength of bulk-formed ice on textured surfaces may increase.

Although impact ice is more representative of the accumulation of ice in the blades, it adds a layer of complexity to the analysis. Contrary, the static ice results in a uniform ice layer with constant cross-section enabling fracture mechanics calculations. In addition, the mechanical properties of statically grown ice have already been well studied and characterized, thus allowing an introduction of a fracture mechanics framework as a first step towards providing a mechanical understanding of the shedding of ice from microtextured substrates.

Typically, the closer an ice adhesion test is to reality, the higher the cost and complexity of the setup. Additionally, the testing rate of different surfaces and the number of repeated tests on a surface are generally reduced as the conditions and loading become more realistic. Despite static ice testing methods do not directly mimic the real-life accumulation of ice on surfaces, they do offer a much more simplified and straightforward methods to determine the ice adhesion strength of a surface in an idealized laboratory setting.

Regardless of the potential problems associated with the vertical shear test, relevant information can be retrieved from these studies, that will provide a point of reference for future studies.

4.3. NUMERICAL ANALYSIS

In this chapter are presented the results of the stress distribution and the influence of the aerodynamic forces obtained through ANSYS and COMSOL, respectively.

4.3.1. STRESS DISTRIBUTION

A finite element model of the adhesion strength experiment was used to quantify the stress distribution at the ice-substrate interface. The numerical analysis shows the presence of both normal and shear stresses (mixed) as opposed to only shear stress in the ideal case. Figure 4.6 and Figure 4.7 describes the shear stress and normal distribution, respectively, at the ice-substrate interface.

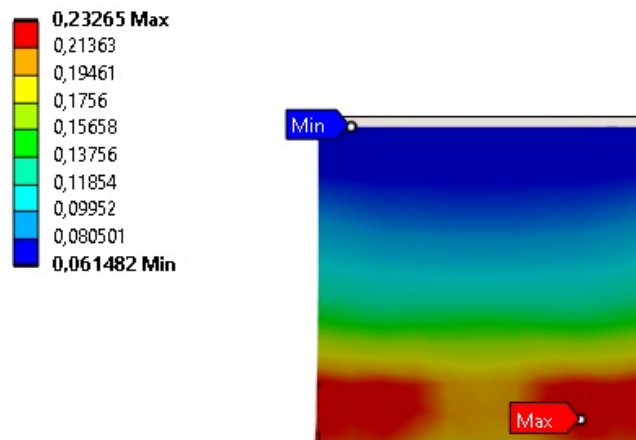


Figure 4.6 – Shear stress values and distribution at the ice-substrate interface.

The figure above points out that the maximum shear stress (red) is at the bottom of the interface, for the particular reason that this is where the contact between the platform and the ice cube takes place, it is the area where the force is received.

Although the platform was placed as close as possible to the substrate to minimize the effect of torque, a pure shear stress condition cannot be generated. Figure 4.7 indicates the normal stress distribution contours, where it is possible to confirm the effect of the moment, with the existence of tension (red) in the inferior part of the ice cube face and compression in the superior part (blue).

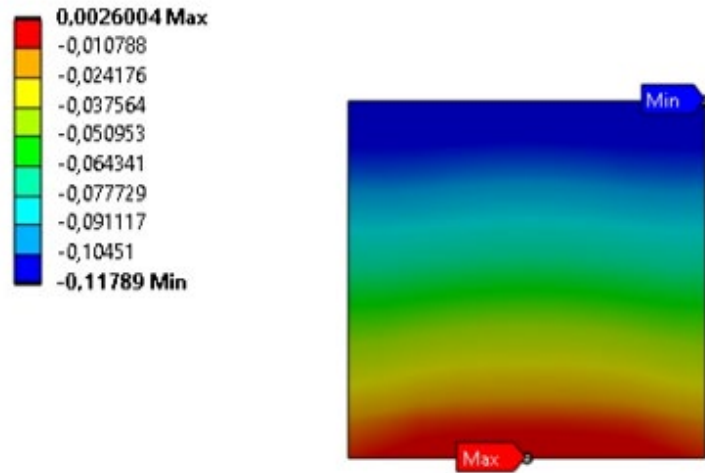


Figure 4.7 – Normal stress values and distribution at the ice-substrate interface.

Through the results obtained it is possible to affirm that the detachment of the ice from the substrate is not done solely through shear stress, it is always verified the existence of normal stresses due to torque (Figure 4.8).

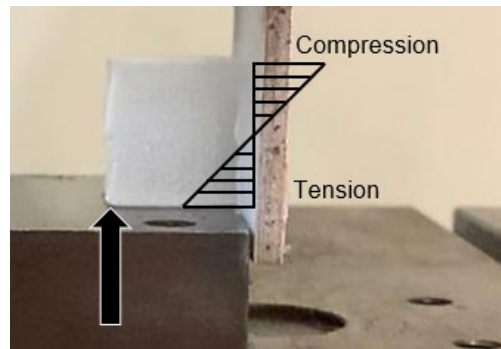


Figure 4.8 – Torque effect leading to compression at the top and tension at the bottom.

Even so, it is the shear stress that predominates since the values of the normal stress are much lower, validating the obtained experimental results.

4.3.2. AEROMECHANICAL FORCE ANALYSIS

To analyse whether the use of only icephobic coatings would be a reliable option, it is necessary to verify whether the shear stress at the interface between the ice and the substrate generated by external forces is higher than the adhesive shear stress of the ice, to allow the ice to fall off the substrate.

For this, a numerical analysis of the shear stress was carried out in two different ice geometries with three dimensions in four different positions and velocities. Below is an example of the images taken from the COMSOL software, for each geometry, Figure 4.9 and Figure 4.10 respectively. The remaining images for the various parameters are detailed in the Annex F.

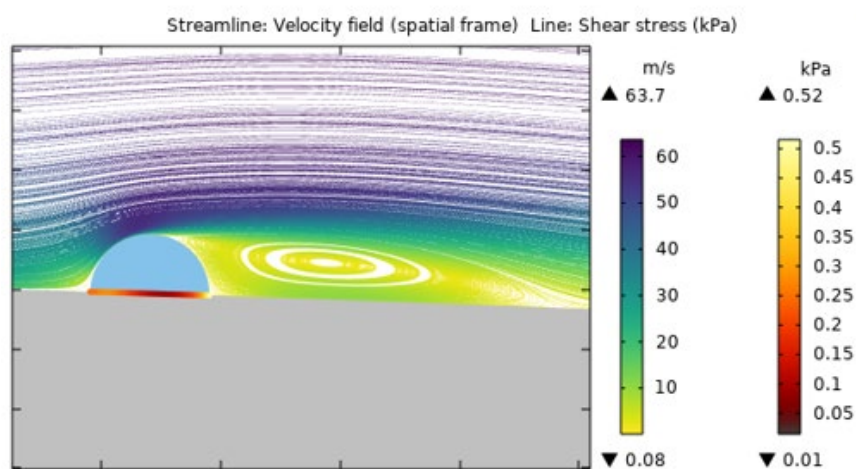


Figure 4.9 – Image obtained from the COMSOL software for the circular geometry.

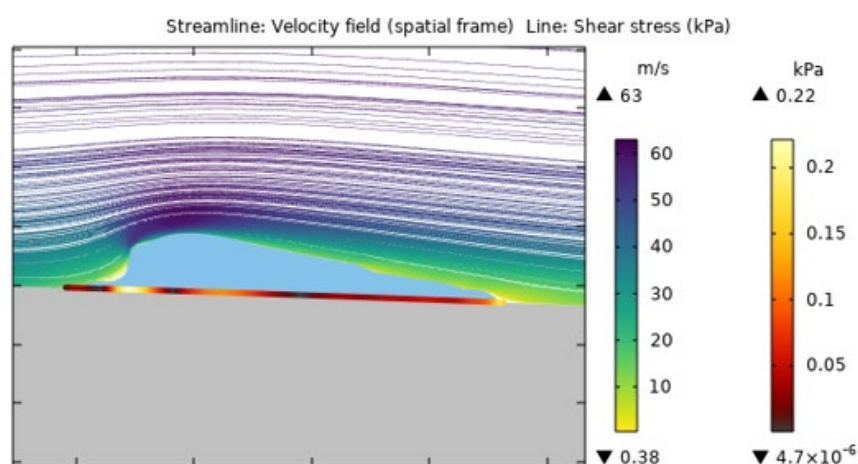


Figure 4.10 – Image obtained from the COMSOL software for the runback ice geometry.

From the images obtained it is possible to verify the presence of vortices, created due to the pressure difference when wind passes around the ice. Through the streamline it can be conclude that the velocity in the upper part of the airfoil is higher than in the lower one, this is due to Bernoulli's Principle

in which the velocity is inversely proportional to the pressure. In addition, it is also observed that the velocity profile is less altered in the second image, because this geometry it is much more aerodynamic than the circular one.

The different results of the shear stress at the ice-airfoil interface, essential for the answer to the initial problem, are shown in the tables in the Annex G, each one corresponding to the different geometries and dimensions. For a better interpretation of the data and its variation, column graphs were created for the different situations, that relate the maximum shear stress with the geometry, dimension and position of the ice and the wind speed (from Figure 4.11 to Figure 4.16).

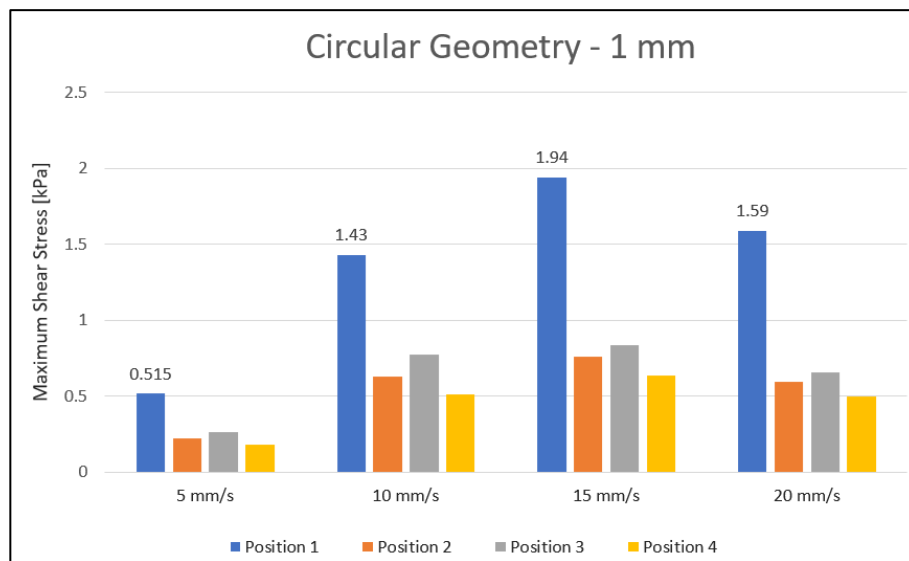


Figure 4.11 – Variation of the shear stress for the circular geometry with a radius of 1 mm.

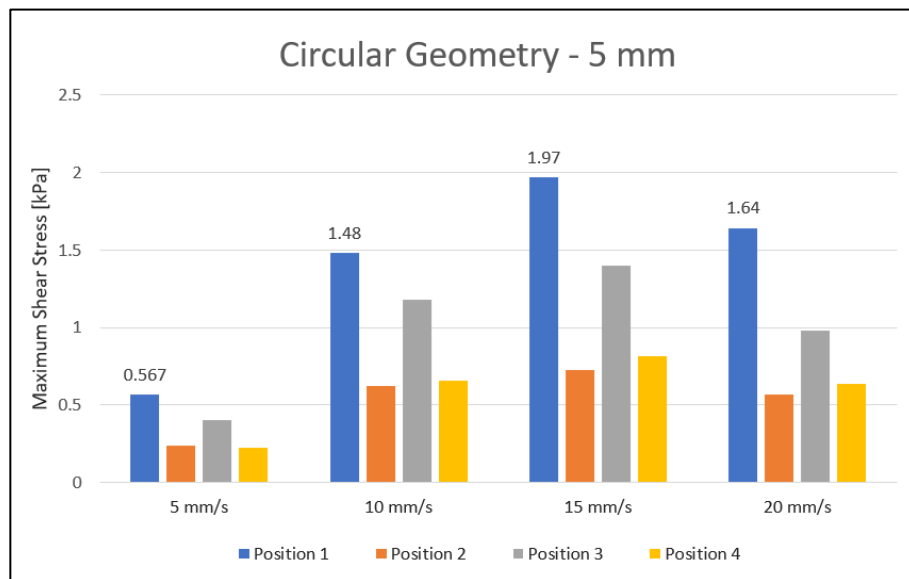


Figure 4.12 – Variation of the shear stress for the circular geometry with a radius of 5 mm.

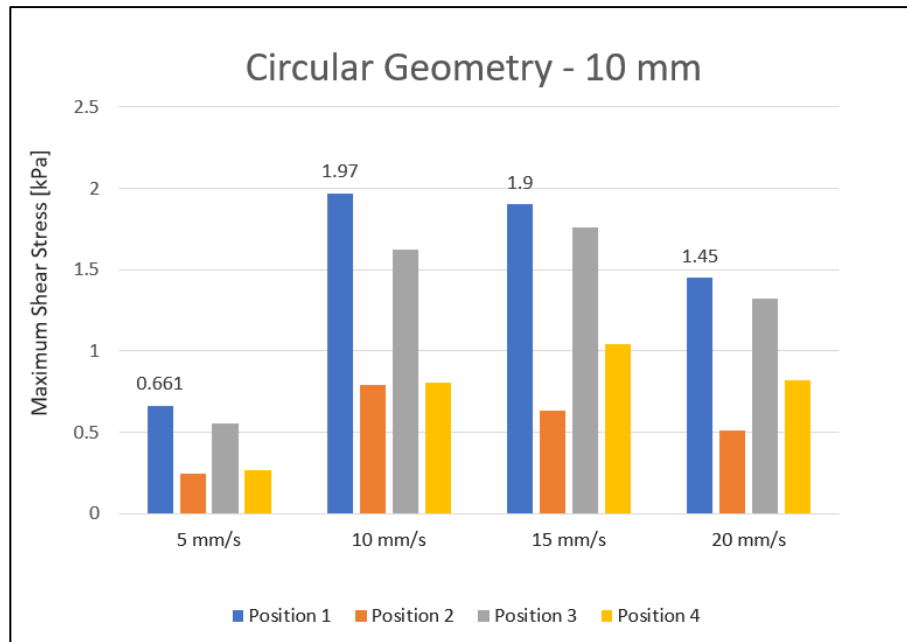


Figure 4.13 – Variation of the shear stress for the circular geometry with a radius of 10 mm.

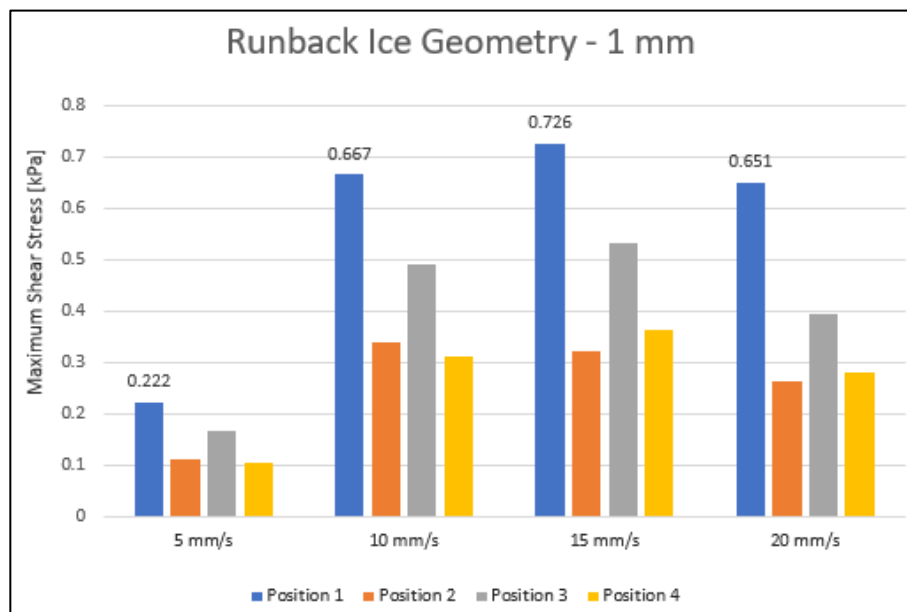


Figure 4.14 – Variation of the shear stress for the runback ice geometry with a height of 1 mm.

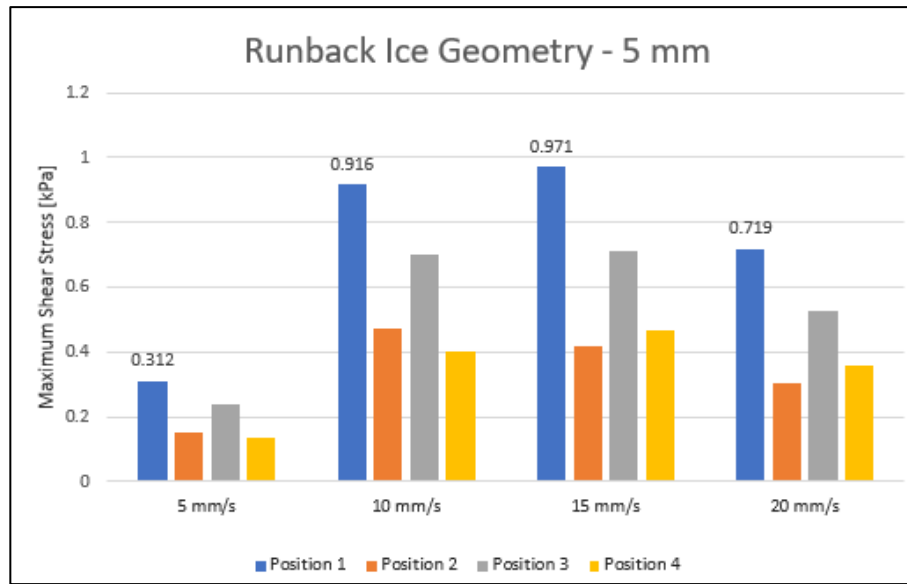


Figure 4.15 – Variation of the shear stress for the runback ice geometry with a height of 5 mm.

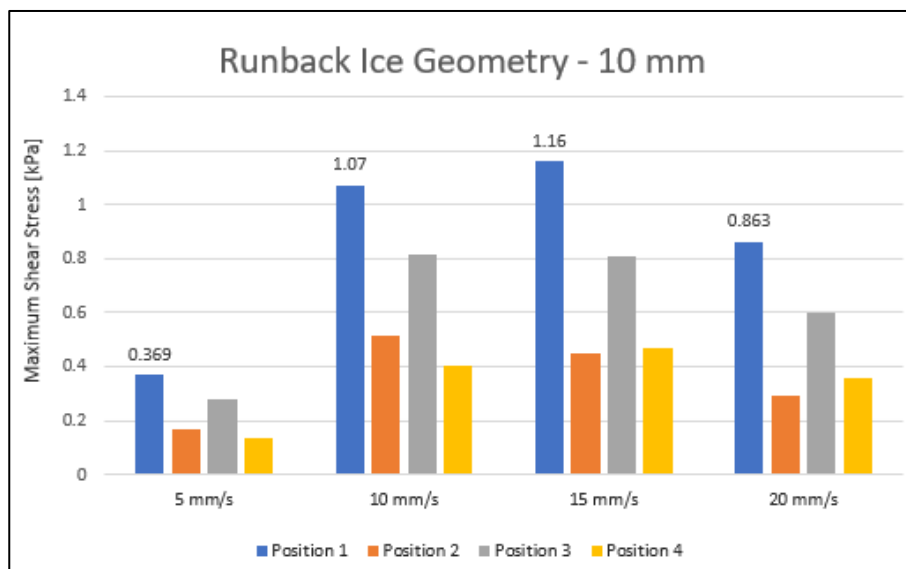


Figure 4.16 – Variation of the shear stress for the runback ice geometry with a height of 10 mm.

For the comparison between the results above and the maximum shear stress values taken from ANSYS of the different coatings, the graph with the best-case scenario was considered, circular geometry with a radius of 10 mm (Figure 4.13), where the shear stress caused by aerodynamic forces is the greatest (aerodynamic forces are stronger). The comparison of the results is presented in the graph of the Figure 4.17.

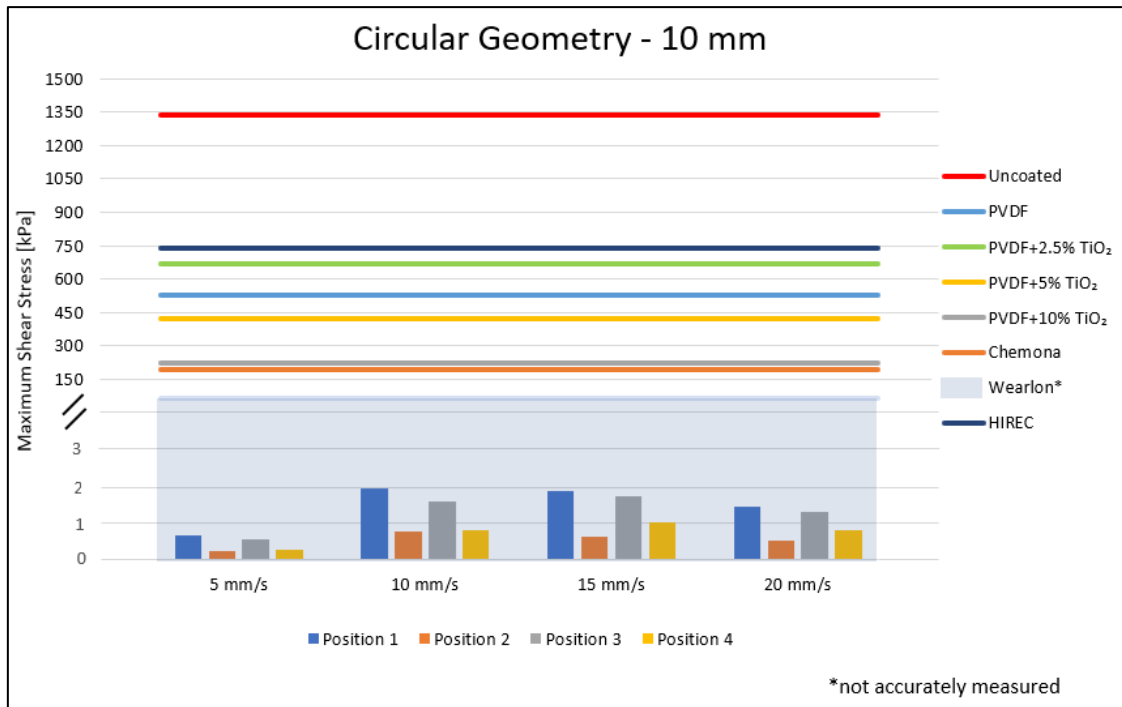


Figure 4.17 – Comparison between the shear stress results taken from the COMSOL software (when the forces are higher) and the results obtained in the ANSYS software.

From the results, it is possible to conclude that even for this case, the values of the shear stress caused by aerodynamic forces are much lower than the ones measured in the simulation of the stress distribution. However, as the ice adhesion strength of the Wearlon coating couldn't be measure with accuracy, since it was a very low value for the measuring device resolution, its shear stress could possibly be lower than the stresses caused by external forces, being this surface the most promising.

Having said that, it is plausible to state that the implementation of simply icephobic coatings, even the Wearlon coating, may not be efficient in combating ice accumulation on wind turbine blades. A more realistic alternative would be, as previously mentioned, a hybrid system, in which the use of these coatings would complement the existing ice mitigation systems.

Once again, these simulations were performed on a very simplistic model and with several assumptions, namely the proprieties of the materials and the geometric shape and type of the ice. To obtain more accurate data, the ideal would be to carry out aerodynamic wind tunnel tests of representative full-scale runback ice shapes on a sectioned full-scale blade.

5. CONCLUSIONS AND FUTURE WORK

This chapter describes the main findings of this dissertation and also includes the recommendations for the future work.

5.1. MAIN CONCLUSIONS

The present study was aimed at understanding the effectiveness of a coating strategy to mitigate ice formation on wind turbine blades exposed to icing conditions.

To achieve the primary objective, the ice adhesion strength of eight different surfaces was evaluated through a vertical shear testing facility. The various surfaces characterized include one uncoated sample, four lab-made and three commercial coatings. The lab coatings were prepared by varying the ratio of TiO_2 nanoparticles in the PVDF solution. To further characterize the variation in the ice adhesion strength for different materials, correlation studies were conducted. The contact angle measurements show the surface wettability nature of the test surfaces, from hydrophilic to superhydrophobic.

The results of the water contact angle revealed that the uncoated sample is the one with the highest wettability, with an average angle of 64.3° . The evaluation of the effect of the nanoparticle's concentration was made through the samples of PVDF with 0%, 2.5%, 5% and 10% of TiO_2 . The increase in the percentage of TiO_2 led to an increase in the contact angle value. The enhance of the surface roughness resulted in a lotus effect. Both commercial coatings, Wearlon and Chemona, exhibit hydrophobic behaviour. The highest measured value was the HIREC surface, which has proved to be superhydrophobic, with a contact angle above 150° .

The ice adhesion strength measurements demonstrated that the material with the most significant icephobic behaviour was the commercial Wearlon coating with an outstanding adhesion reduction factor value of at least 30 compared to the uncoated sample. As this last coating exhibits such low adhesion, the measuring equipment did not have sufficient resolution to measure the values accurately. The second coating with the lowest shear stress value was Chemona, which showed an average ARF of 7.5. On the other hand, surprisingly, the superhydrophobic HIREC coating, showed a poor performance as icephobic material, presenting a reduction of only 1.8 in the force required to detach the ice cube.

Overall, increasing the weight of titanium dioxide led to a decrease in adhesion strength, except in the case of the percentage of only 2.5%, where the value was higher than the PVDF sample without any particles. The cause of this was the same as for the HIREC coating, which is the transition from the

Cassie-Baxter state to the Wenzel state, where the ice penetrated the surface asperities, increasing ice adhesion strength. Despite this, all the coatings studied showed a reduction in shear stress in relation to the reference sample.

The correlation graphic provided compelling evidence that ice adhesion strength does not always vary linearly with water contact angle. Although water repellency may directly affect icephobicity, strictly speaking, these characteristics are not direct measures of the icephobic capacity of a surface, this is because the mechanics of ice and water adhesion on the surface are different, therefore, mechanical forces acting on both the liquid droplet and ice are also dissimilar.

For the application of hydrophobic surfaces for ice mitigation, they must have the capability to retain a Cassie-Baxter wetting state at subfreezing temperatures. The example that best confirms that hydrophobicity does not automatically lead to icephobicity is the superhydrophobic coating, HIREC, which, after the uncoated sample, is the one with the highest adhesion strength value. An alternative approach considered in this paper is the idea of using superhydrophobic coatings to take advantage of water repellency and low adhesion of drops in a liquid state to reduce liquid water accumulation on the surface before water can freeze.

Another important feature of this study is the numerical model of the ice adhesion experiment to evaluate the stress state at the ice-substrate interface and qualitatively compare it with the experimental ice adhesion measurements. The numerical parametric study showed that the debonding of the ice from the surface did not occur entirely through shear stress, but also through normal stress, a consequence of the torque effect. However, its influence is not significant.

From the numerical analysis it was also possible to visualize that the aerodynamic forces that an airfoil is subject are not enough to remove the ice from the surface with the majority of the coatings studied. The only one that could possibly be sufficient to allow the removal of ice with the presence of only external forces would be the Wearlon, but without guarantees, since its value has not been accurately measured. Implying that the application of these coatings alone is likely to be insufficient against ice build-up, showing promises as a supplementary passive strategy to diminish the energy consumption of the typical active systems.

In short, considering all the data presented in this study, most of the coatings analysed could be credible materials for icephobic applications, since compared to the uncoated blade, the ice adhesion strength was decreased. Suggesting, at the end, that a coating strategy may be implemented in combination with an active system to make ice removal more effective in wind turbine blades.

5.2. FUTURE WORK

Although the work completed in this thesis has shown that there is a great deal of promise for using icephobic coatings on wind turbine blades, these systems are still in their infancy and there are multiple challenges that must be overcome to put them into service.

As of yet, there is no model to accurately describe ice adhesion strength. The method used is simplified and considers a set of assumptions which means that can be improved in several ways. One of its fallibilities is how the ice is formed, slowly and static, considering only one geometric shape, so the interaction with the surface is different from the ice formed from the impact. Also, ice adhesion critically depends on the temperature at which the test was performed. Further investigations on these effects are necessary to obtain a comprehensive understanding of ice adhesion and more efforts are needed in order to achieve a standardization of ice adhesion strength testing methods.

Icing wind tunnels, on the other hand, can create a wide spectrum of atmospheric icing scenarios. Performing dynamic wind tunnel testing to determine how ice builds up on icephobic surfaces at different temperatures and with different types and shapes of ice, would allow a more viable study of their effectiveness in combating ice accumulation. Furthermore, it would be possible to examine the freezing process on a rotating blade and test the ice adhesion strength taking centrifugal force also into account.

For a more detailed characterization of the morphology and surface roughness, analysis with an atomic force microscope (AFM) or a profilometer would be indicated. In this way, it would be possible to obtain high-resolution images that could provide information on the influence of roughness on ice adhesion strength. Also, another consideration that could be added to this analysis is a weighted score reflecting the ease of application. Introducing a new material into the blades like a coating could be easily done if the method does not require multiple layers or pre-treatments.

Another significant factor that could be integrated within the evaluation process throughout this procedure is the evaluation of the coatings' mechanical resistance and durability to erosive and corrosive conditions. As the target application is the blades of wind turbines, the surfaces of these components are subjected to several inclement conditions that can undermine the integrity of the coating and significantly reduce its efficiency. Therefore, icephobic surfaces must pass rigorous durability testing, to see if they are able to withstand erosion, wear, and other weathering conditions, before being considered for any real application.

In a further future, the most promising materials could be assessed in a full-scale trial and integrated into the existing mitigation systems with an actual operational setup, to validate the laboratory and numerical results. This testing should focus on identifying the vulnerabilities of the coating's performance in the context of an actual wind turbine operation.

To sum up everything that has been stated so far, although ice adhesion strength is an important parameter for icephobic surfaces, there is no standard method to evaluate it. The chosen method benefits from its simplicity and economical set-up and although it contains some errors, the closer the test becomes to the real application, the more expensive and difficult it becomes to interpret the data.

Ice adhesion measurement as a research topic does not appear to be slowing down in the least. Collaborations between research labs often result in the fitting of an existing facility with an ice adhesion rig of another but using lessons learned from the first to improve upon it. In this way, the results of this work could be used for screening purposes to adequately select the most promising materials prior to performing an extended evaluation.

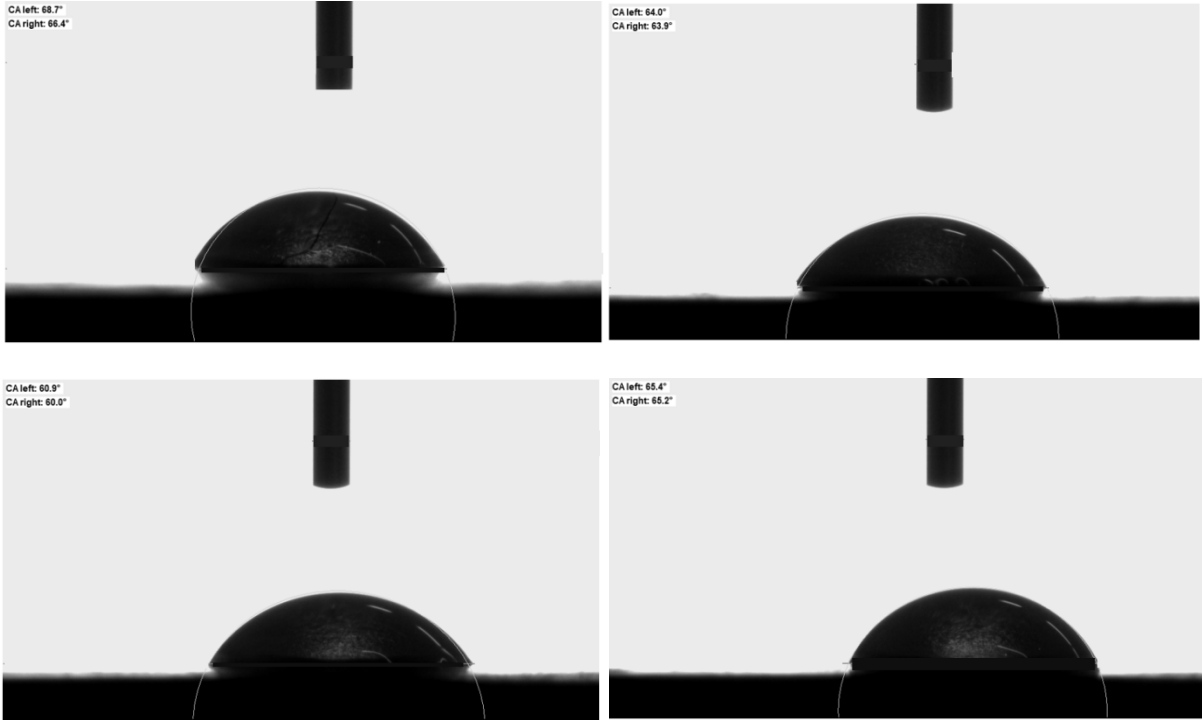
ANNEX A: SUMMARY OF ICE MITIGATION METHODS

ADIS	Method	Description	Advantages	Disadvantages
Passive De-icing Systems	Flexible Blades	Blade flexing helps to shed the ice	Low cost	Not be efficient at breaking up thin layers of ice Compromise the aerodynamic properties of the blade
	Active Pitching	Orient iced blades into the sun	Work in light icing environments	Not scientifically verified and may damage wind turbines
	Mechanical	Directly smashes the ice layer on the blade by machinery or manual	Used for all turbine types	Consumes a lot of time and efforts Safety issues Cannot be utilized if the weather conditions are too harsh
Passive Anti-icing Systems	Black Paint	Allows blade heating during daylight, causing the ice to melt	Significant improvement in performance Decrease the number of birds victims	Only works well in areas with high winter solar intensity May overheat the blades and impact their mechanical properties
	Chemicals	Lower the water's freezing temperature	Low cost	Pollutant, requires special application and higher maintenance Incapable of remaining on the blade surface for a long period
	Operational Stops	Stopping the wind turbine as soon as the icing event begins	Simple and requires no investment	The benefits are close to zero
	Icephobic Coating	Special coatings prevent ice from sticking to the surface because of their anti-adherent property	Low cost, easy application and maintenance No need for special lighting protection Reduction of the energy consumption and the sensitivity to dirt and insects	Coating can become porous after a short time and may lose its ability to repel ice

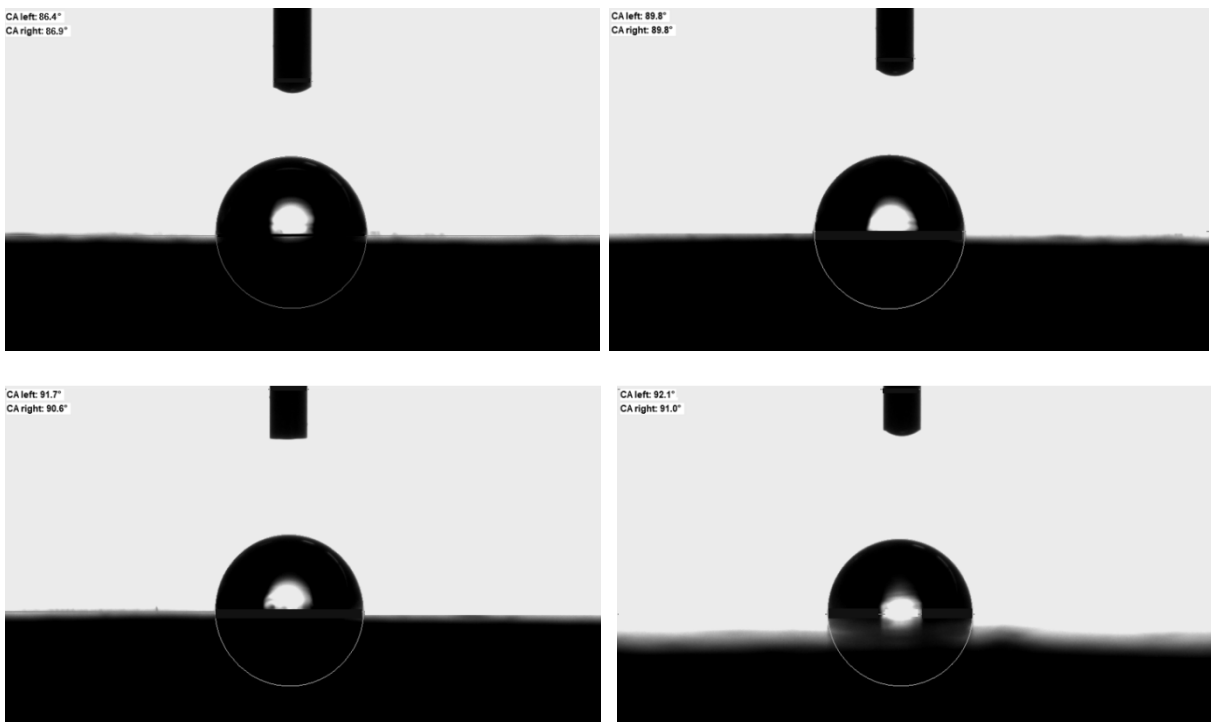
ADIS	Method	Description	Advantages	Disadvantages
Active De-icing Systems	Electro-thermal Heating	Electrical heating element creates a water film between ice and blade surface and centrifugal forces throw the ice away	Higher thermal efficiency, close to 100% because of direct heating Requires quite small heating energy during rime accretion Energy demand doesn't increase with the size of the blade	Power consumption Risk for lightning strikes Runback ice
	Hot Air Injection	Blow warm air into the rotor blade with special tubes to keep the blade free of ice	No negative effect on the lightning protection system or aerodynamics	Low thermal efficiency The heat source is located typically at the blade root while the highest heat fluxes are needed at the blade's tip
	Pneumatic Boots	Inflate with compressed air to break ice	Consumes low energy	Affects aerodynamics by increasing drag and cause more noise Requires intensive maintenance
	Electro Impulsive/Expulsive	Electromagnetically induced vibration pulses flex a metal abrasion shield and crack the ice	Environmentally friendly, efficient, consumes low energy and easily automated	Not yet been tested on wind turbines Ice expulsion is a potential problem
	Ultrasonic	The piezoelectric transducer excited the propagation of the ultrasonic waves and induces the shear stress over the layered ice-material structure	Energy-saving, low running costs, good applicability and environmental conservation	Needs to be adapted The delamination risk must be taken care of
Active Anti-icing Systems	Hot Air Injection	Ducting of hot air into the adjacent surface to the icing area	Very effective	High cost and medium-high energy consumption
	Electro-thermal Heating	Electrical heating element on the leading edge creates a water film between ice and blade surface	Higher thermal efficiency, close to 100% because of direct heating Energy demand doesn't increase with the size of the blade	Power consumption Risk for lightning strikes Runback ice
	Microwave Heating	Generates heat with microwaves to prevent ice formation on blade surface	Even heat distribution, consumes less energy, easy to maintain and not subject to lightning	Safety issues
	Air Layer	Pushed through small holes near the blades' leading and trailing edges to generate a layer of air around the blade surface	Deflect the majority of water droplets in the air and melt few droplets that managed to hit the surface	Little published information

ANNEX B: WATER CONTACT ANGLE RESULTS

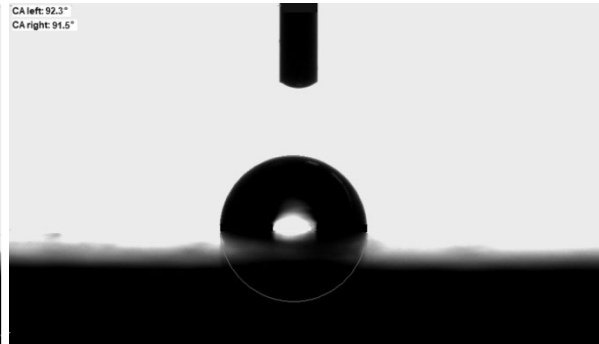
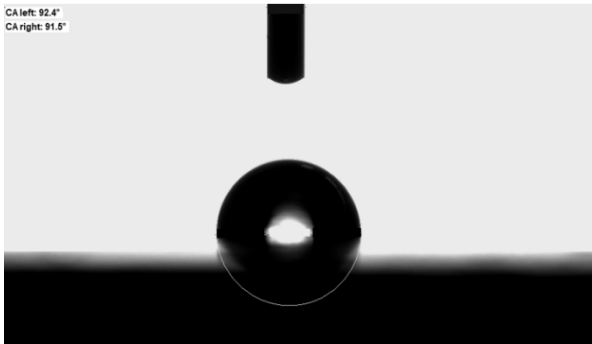
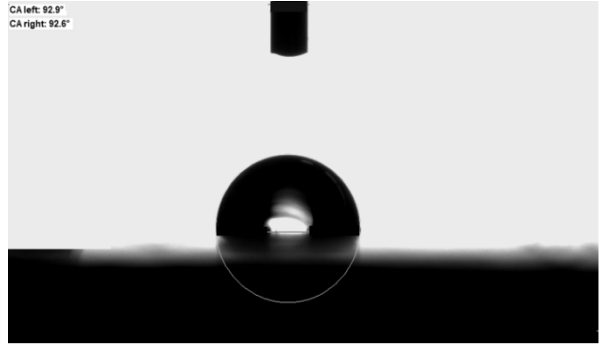
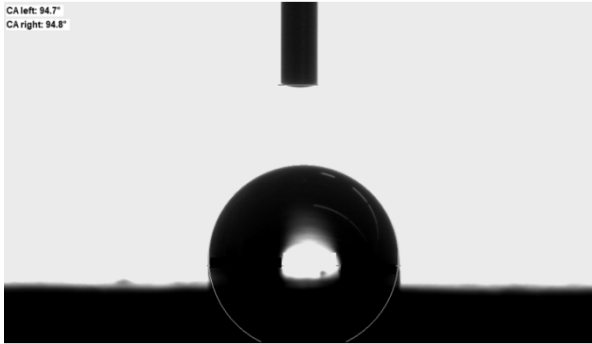
Uncoated Sample



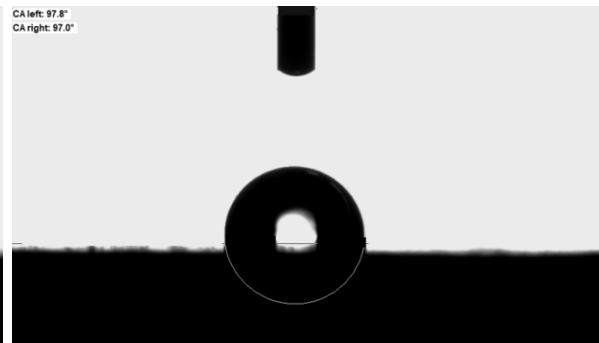
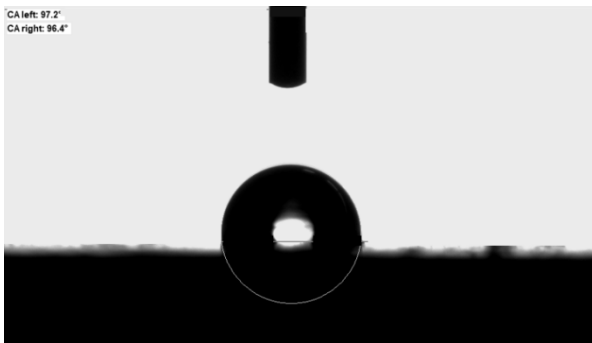
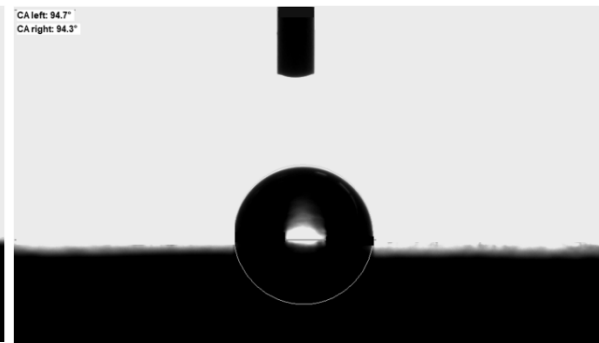
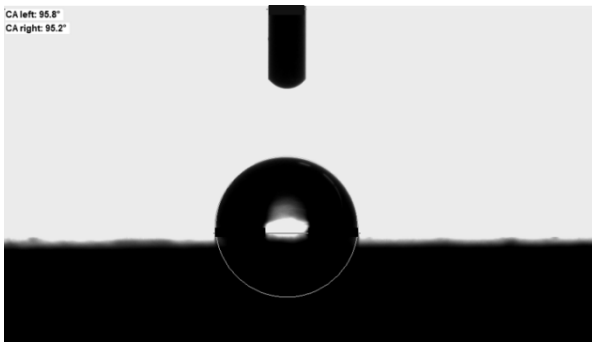
PVDF Sample



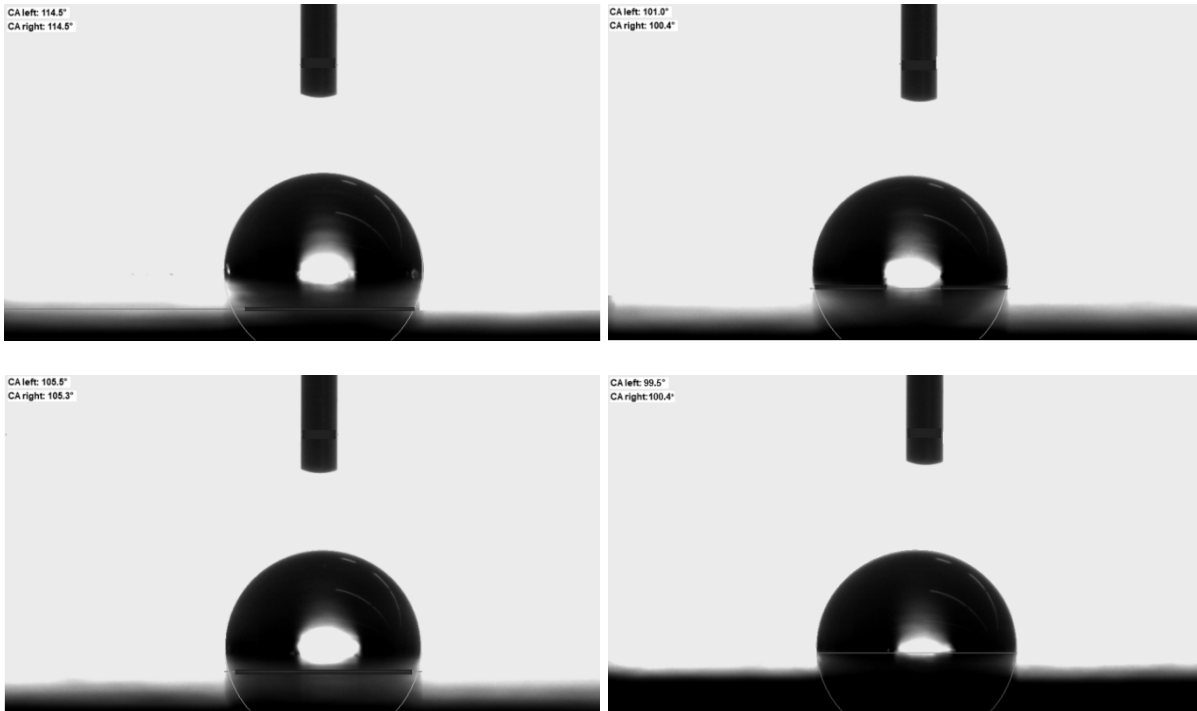
PVDF + 2.5% Sample



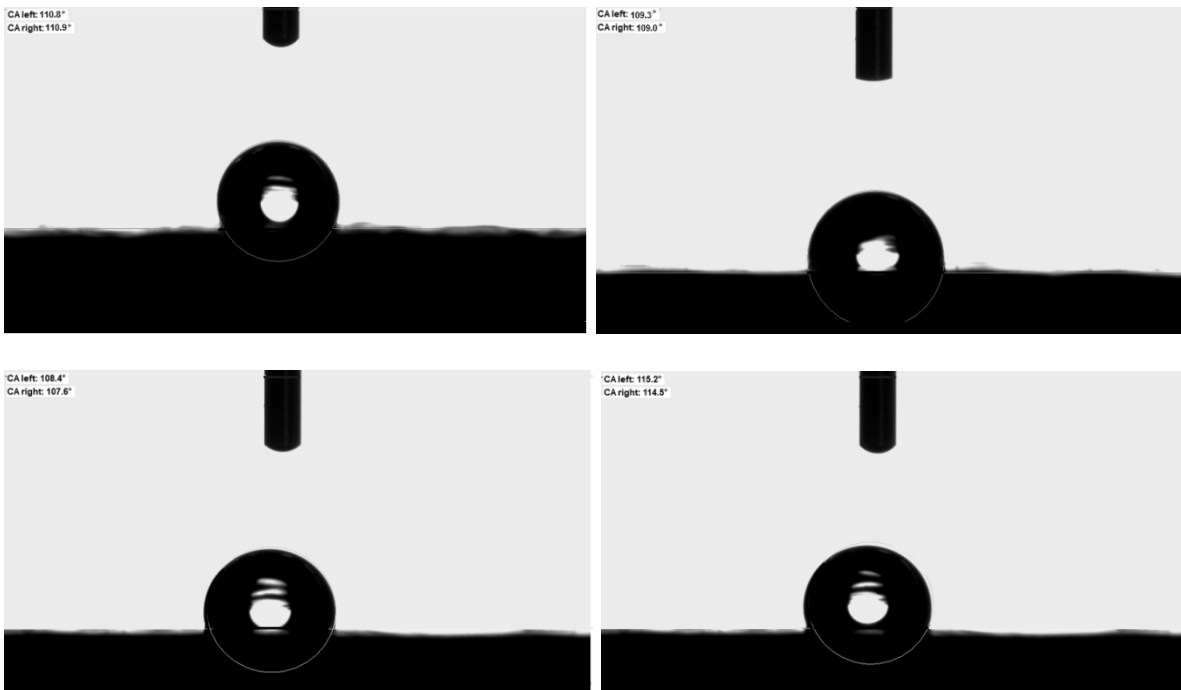
PVDF + 5% Sample



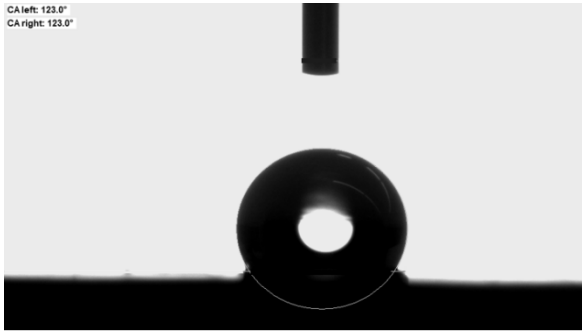
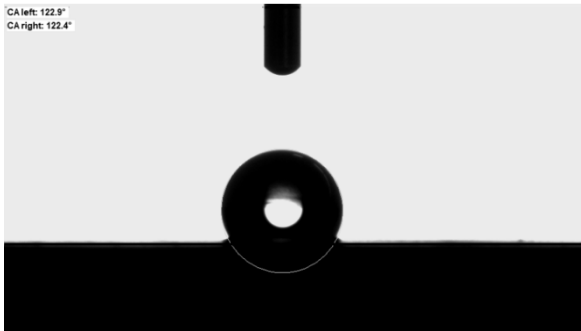
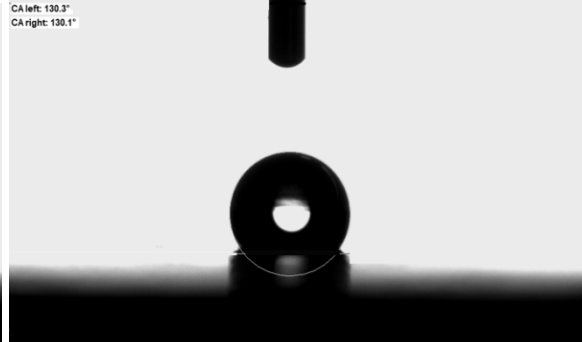
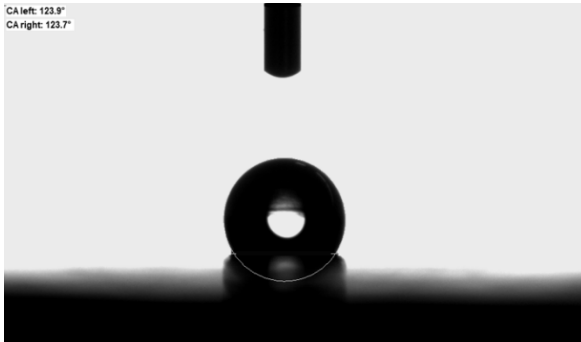
PVDF + 10% Sample



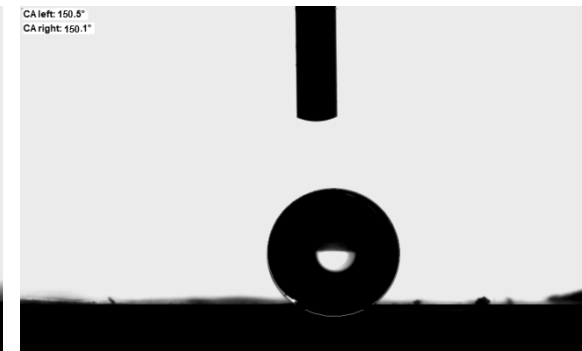
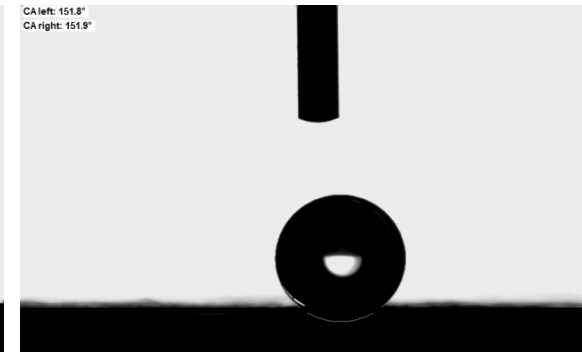
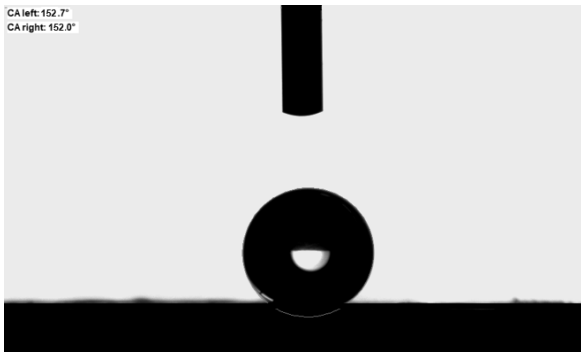
Wearlon



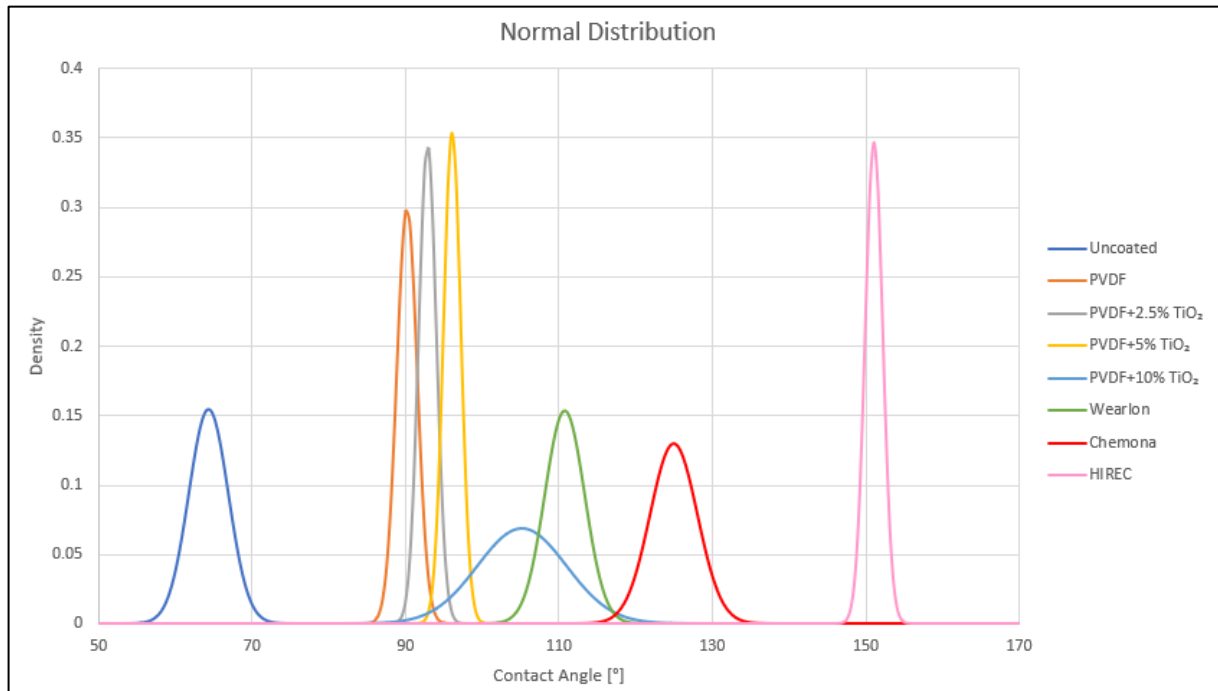
Chemona



HIREC

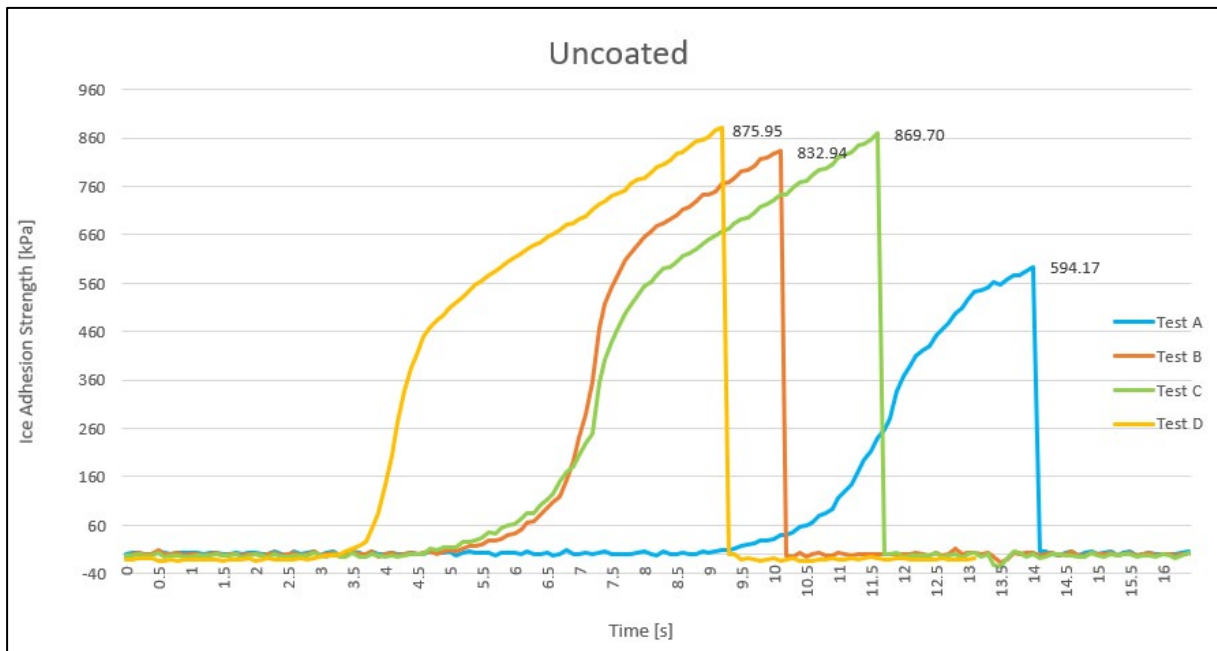
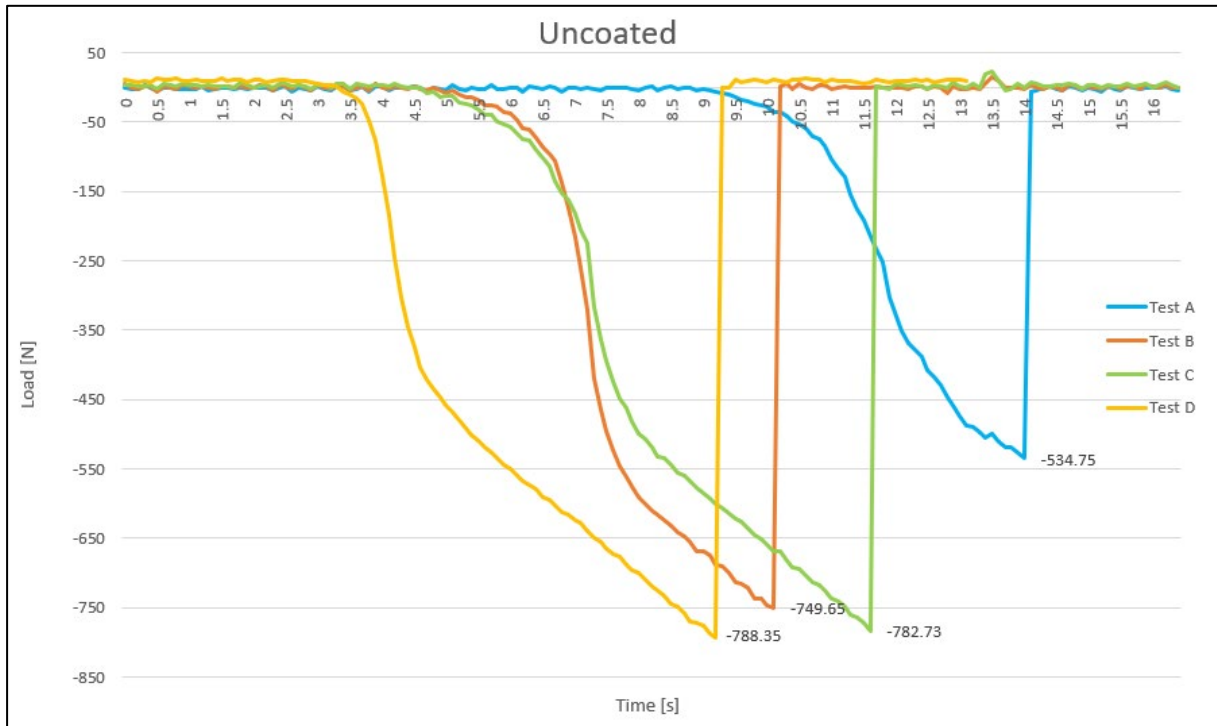


ANNEX C: WATER CONTACT ANGLE NORMAL DISTRIBUTION

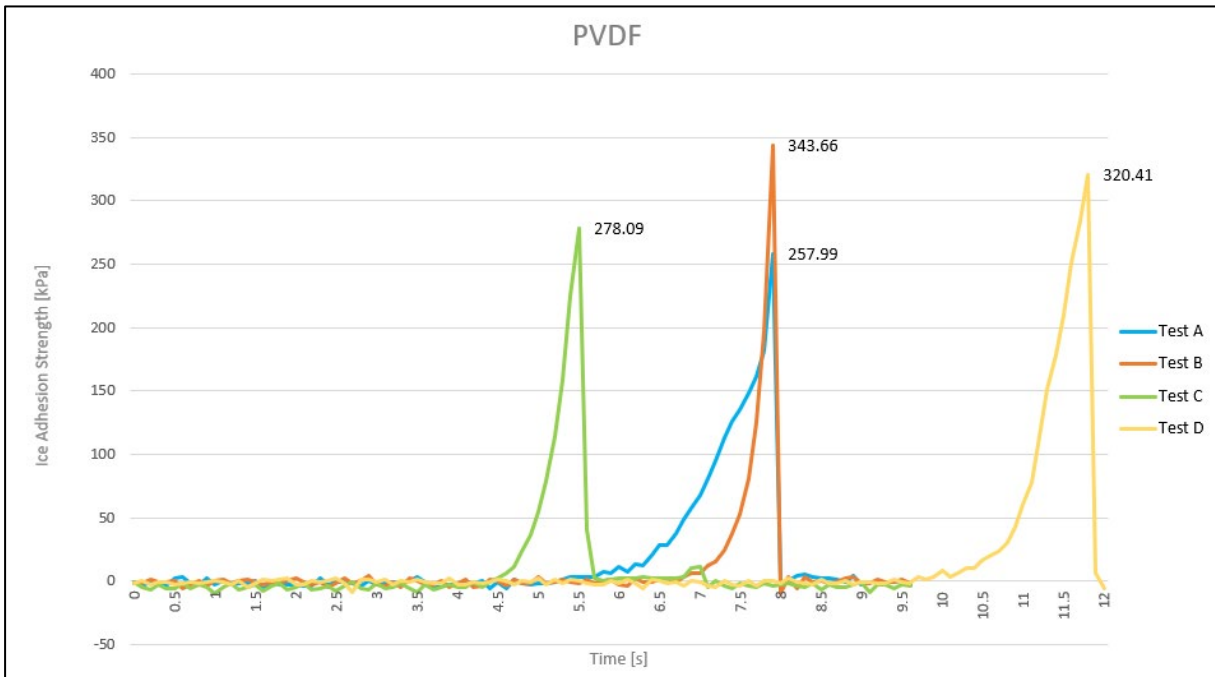
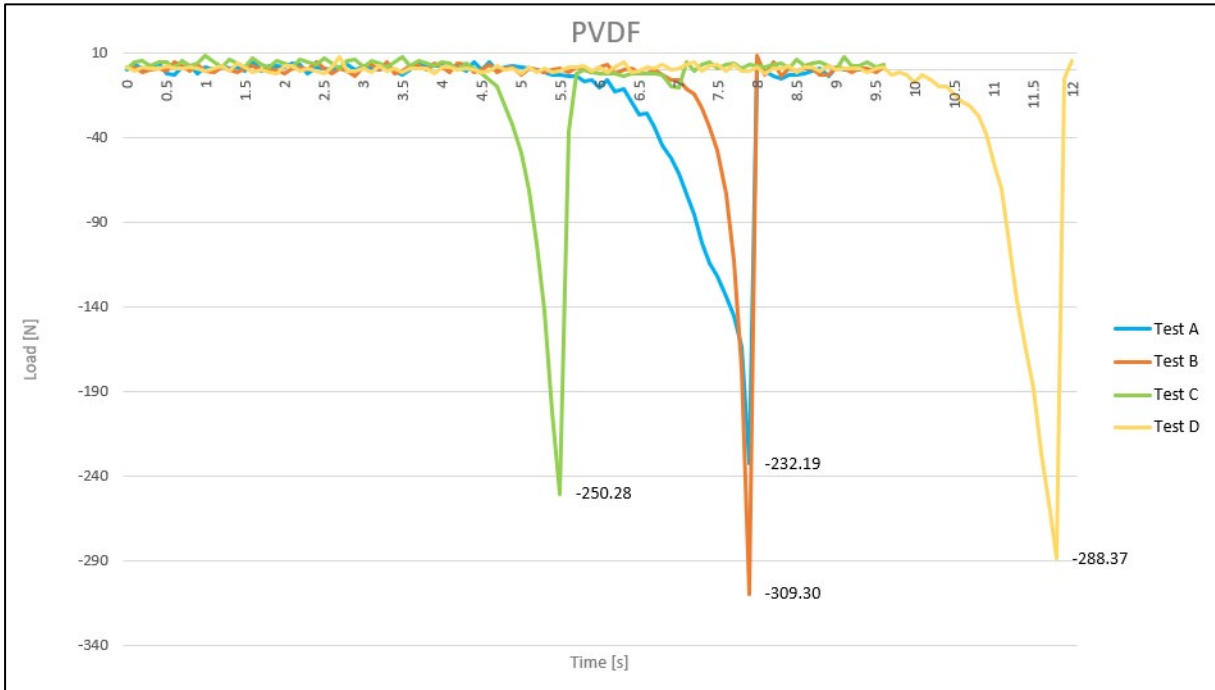


ANNEX D: ICE ADHESION STRENGTH RESULTS

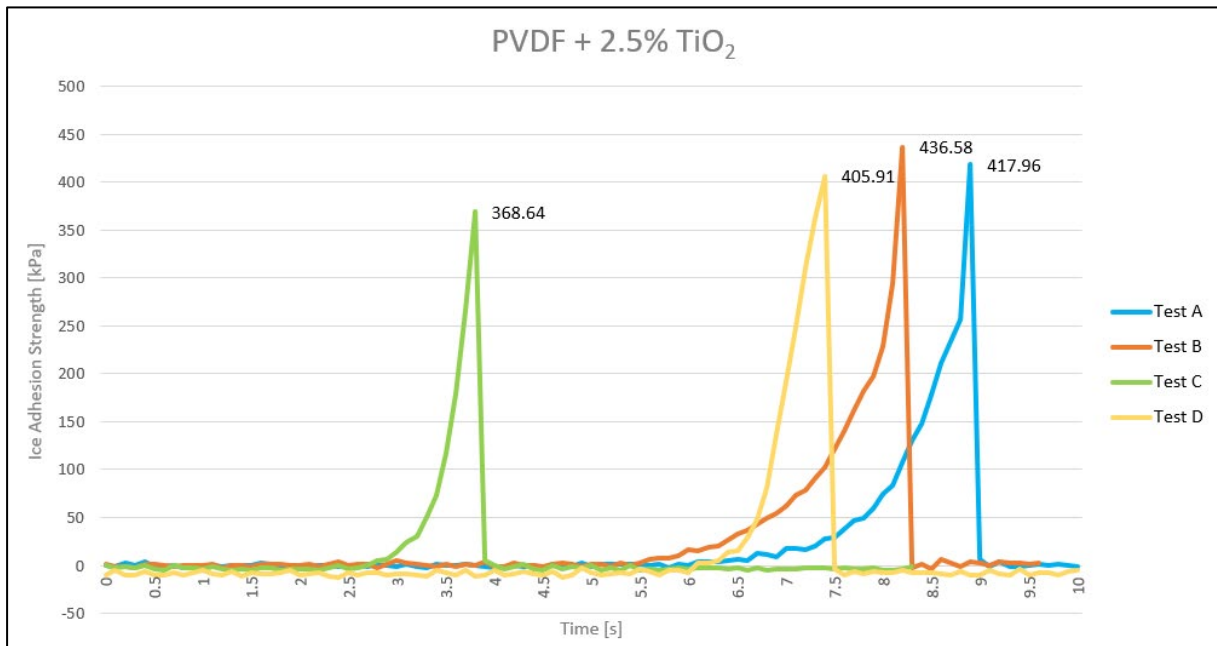
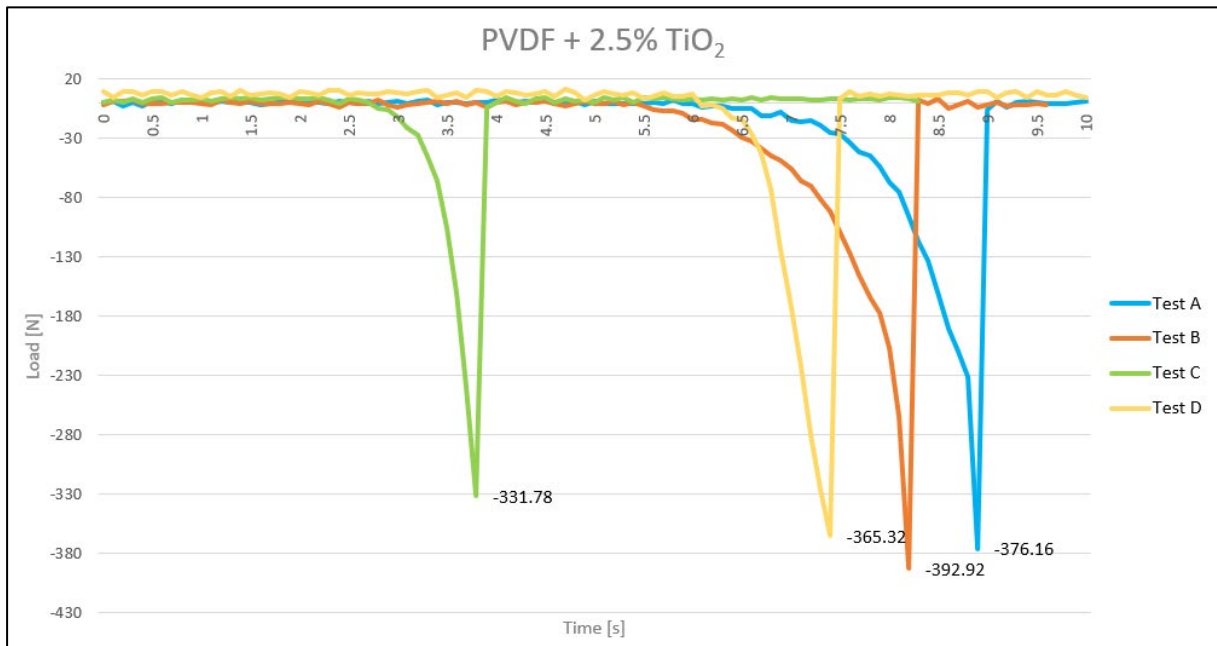
Uncoated Sample



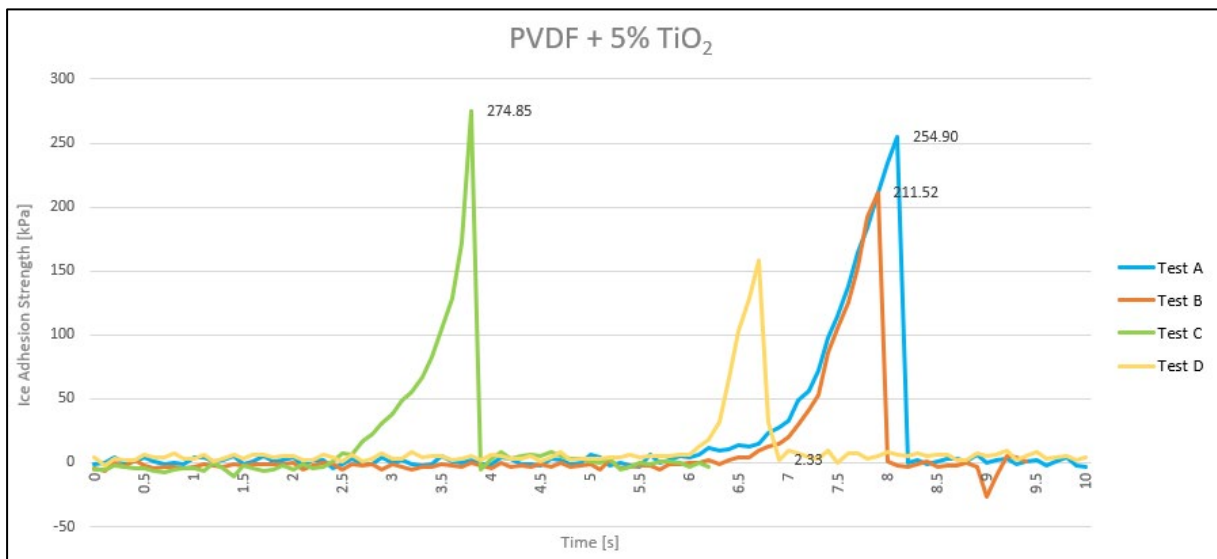
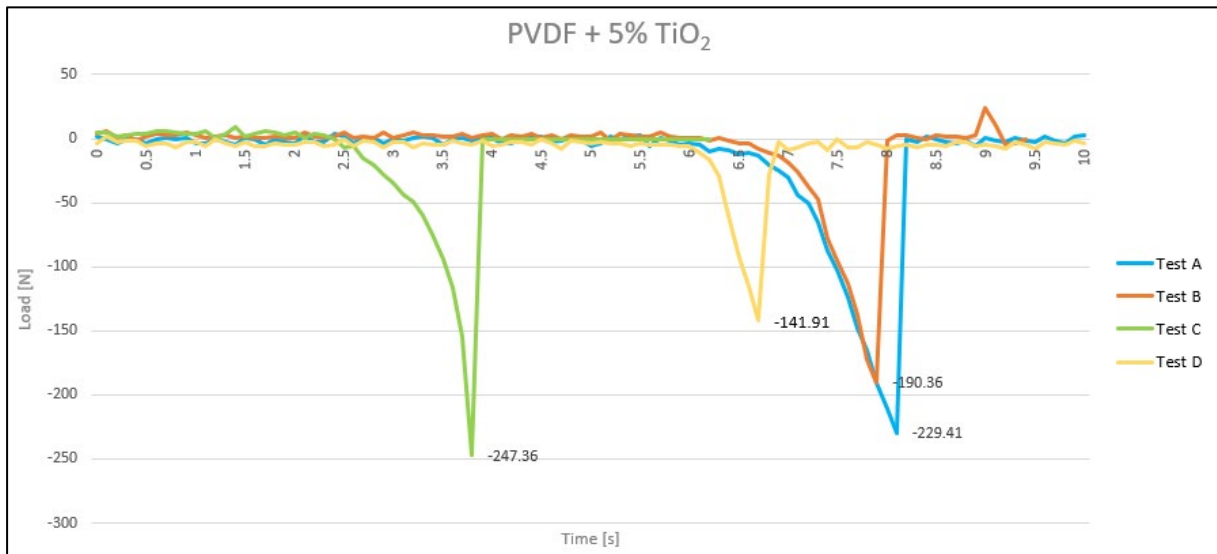
PVDF Sample



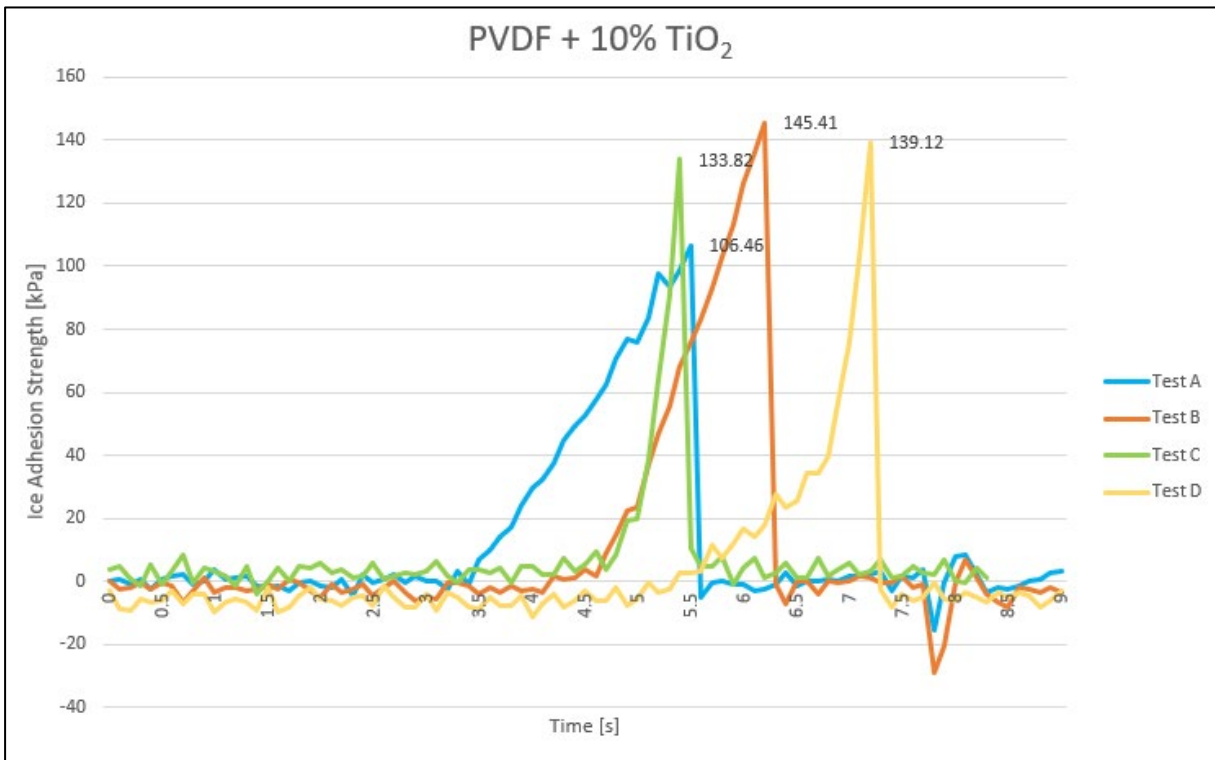
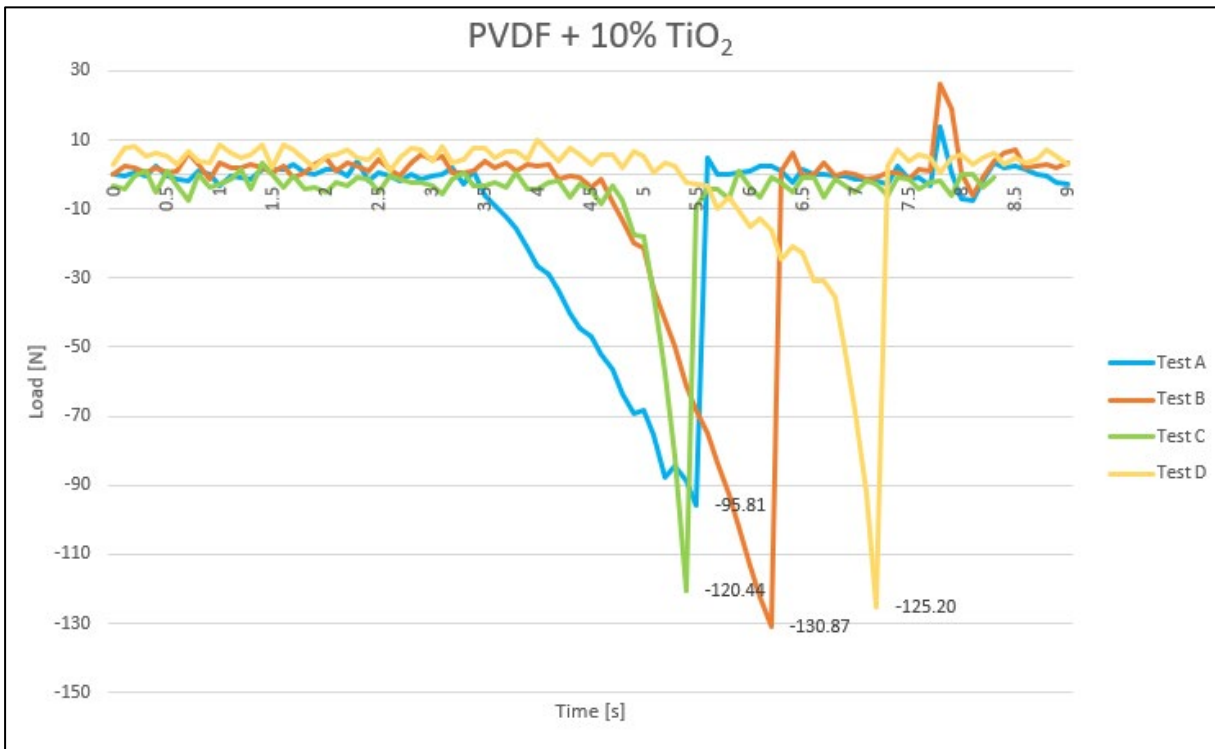
PVDF + 2.5% Sample



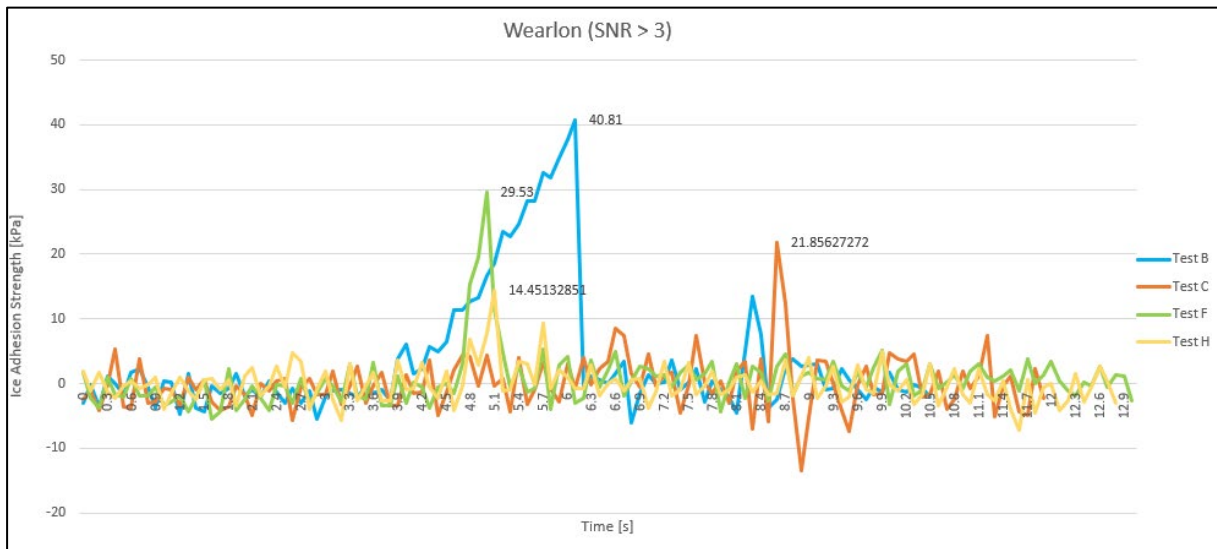
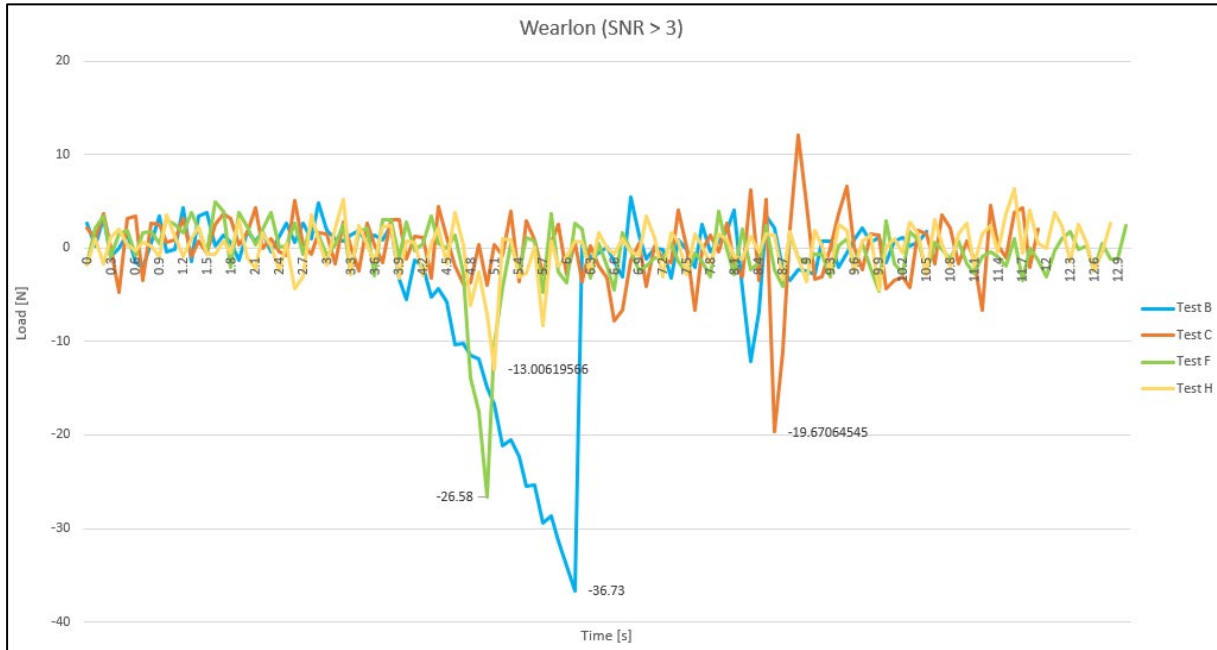
PVDF + 5% Sample



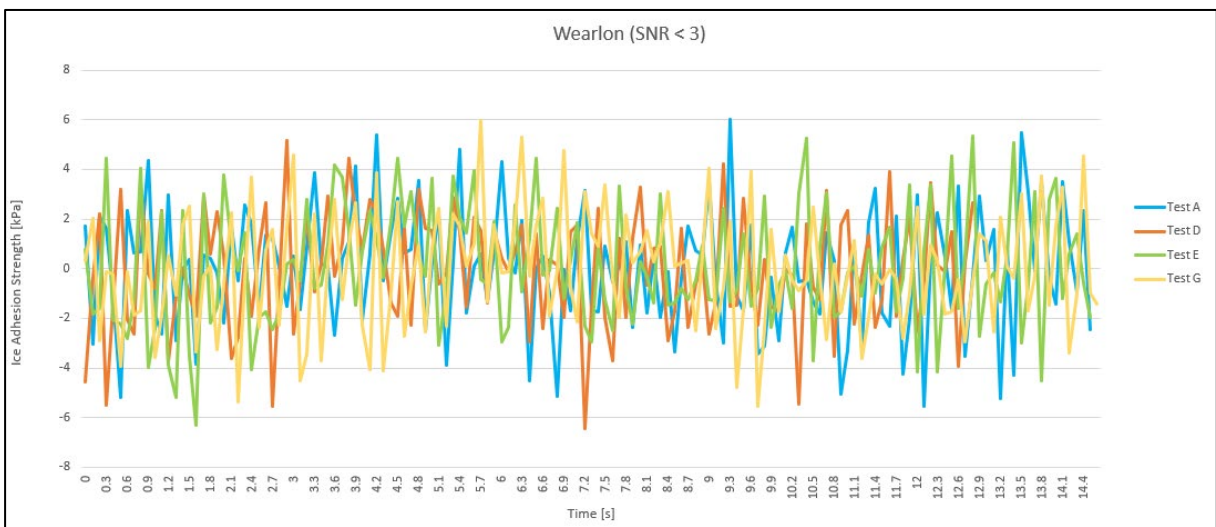
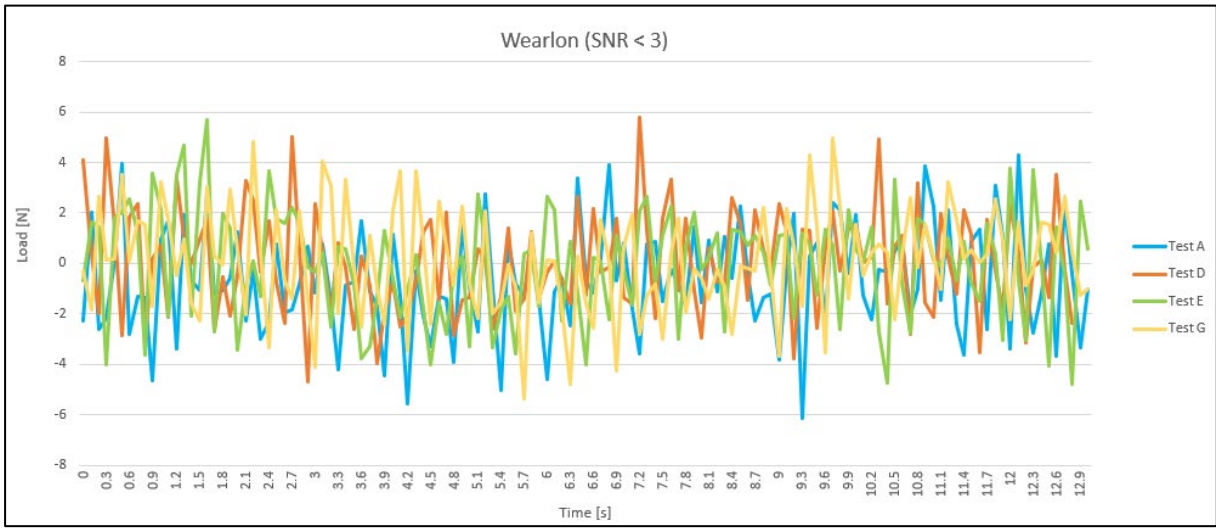
PVDF + 10% Sample



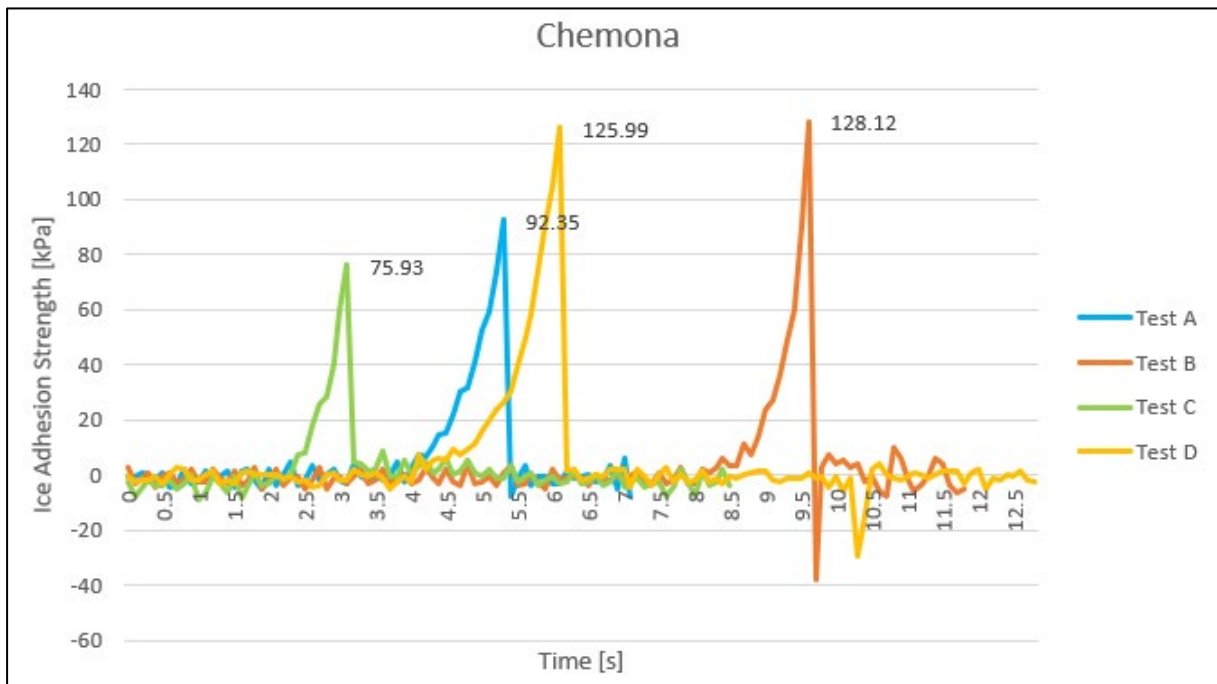
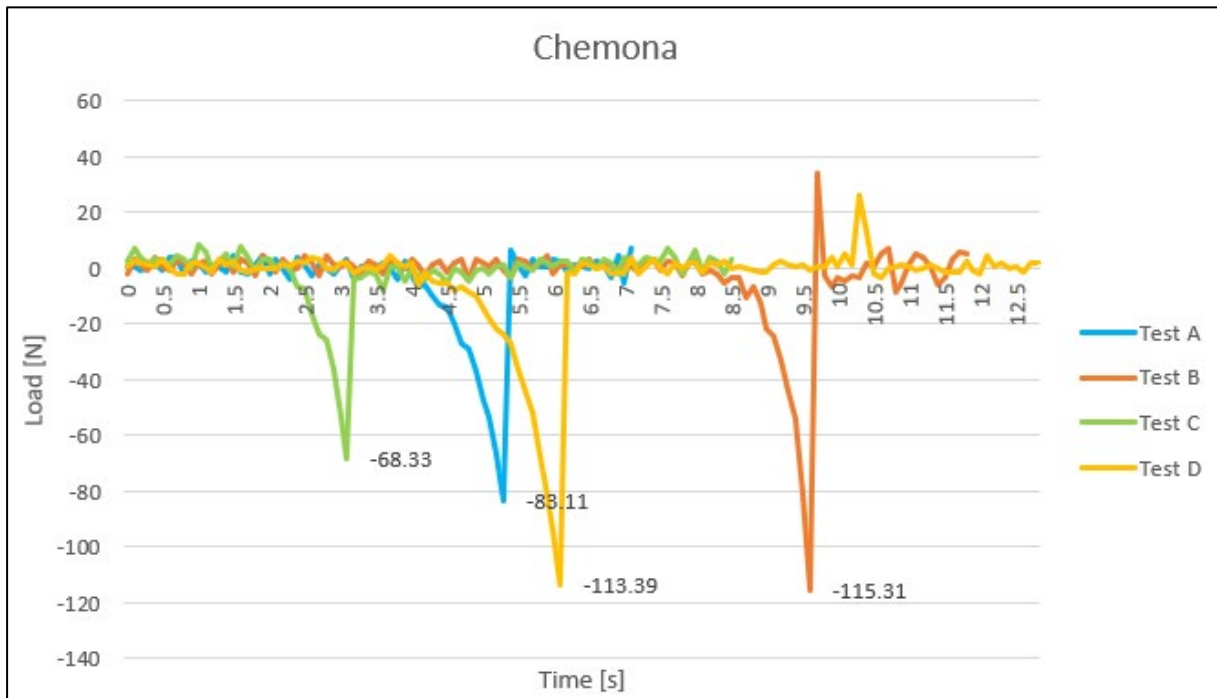
Wearlon (SNR > 3)



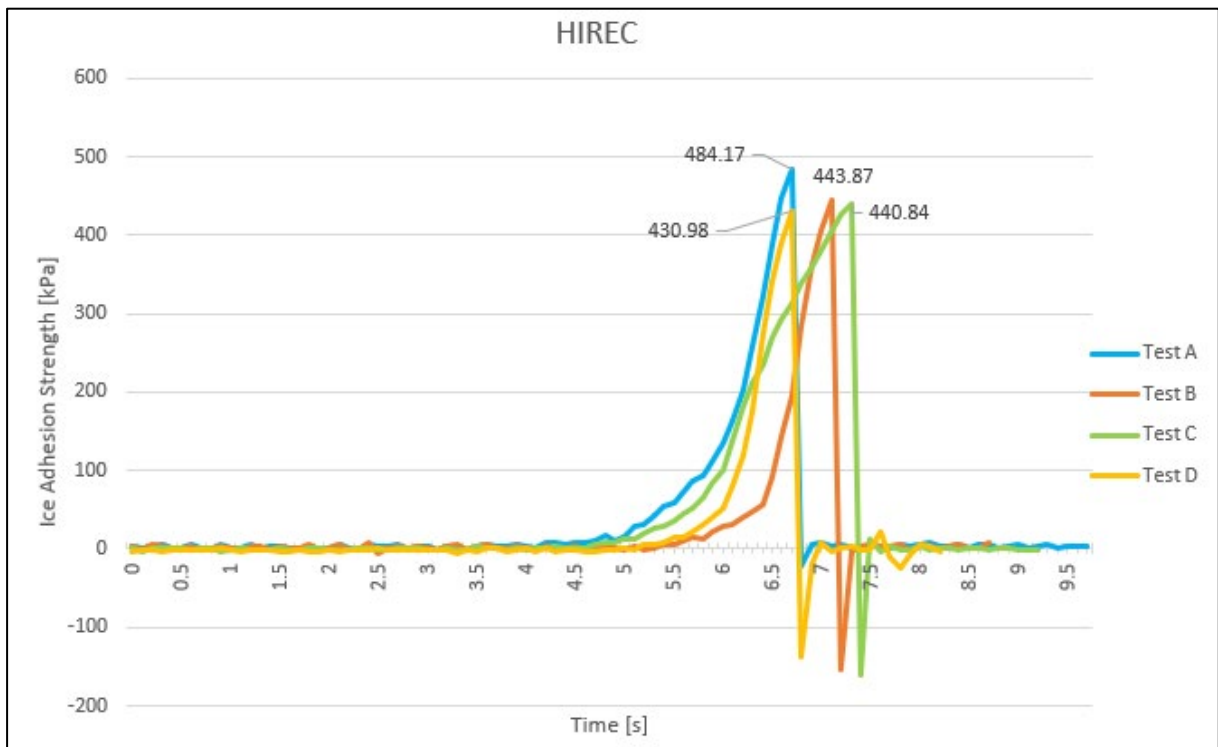
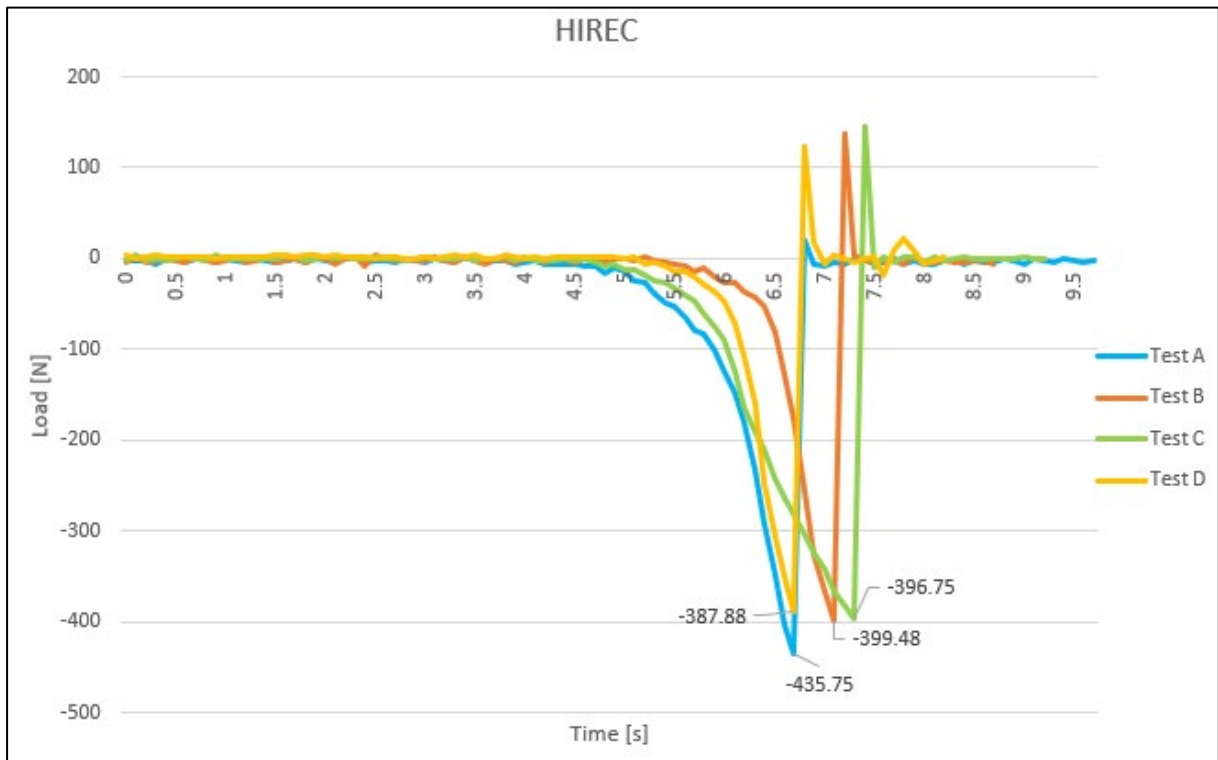
Wearlon (SNR < 3)



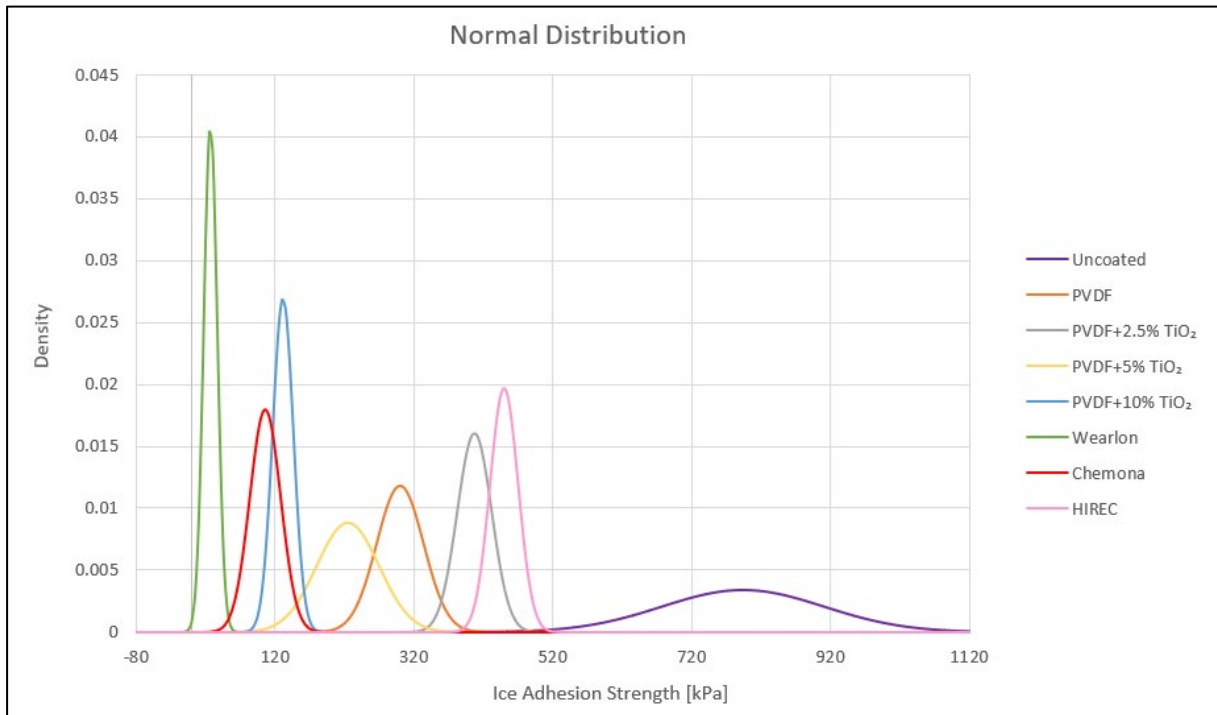
Chemona



HIREC

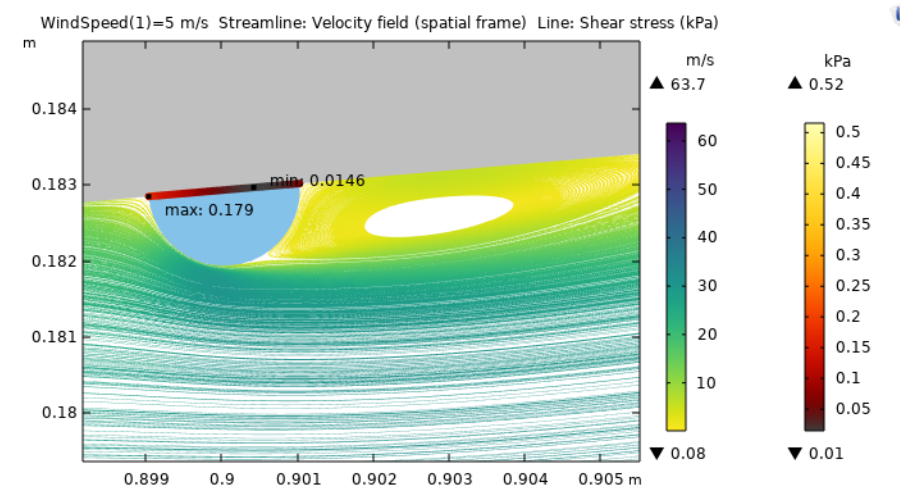
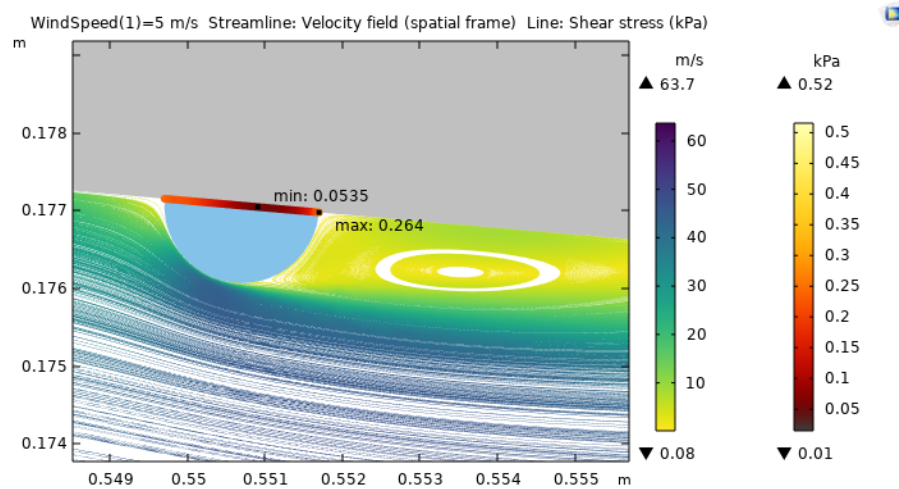
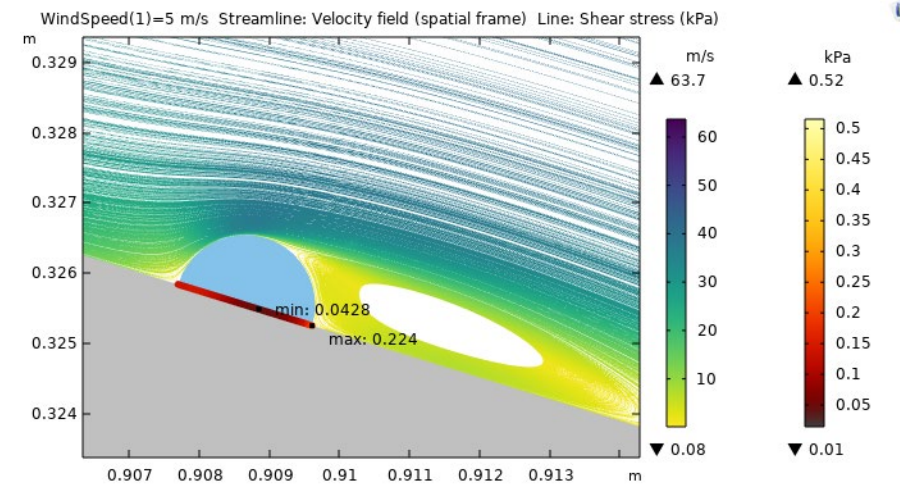
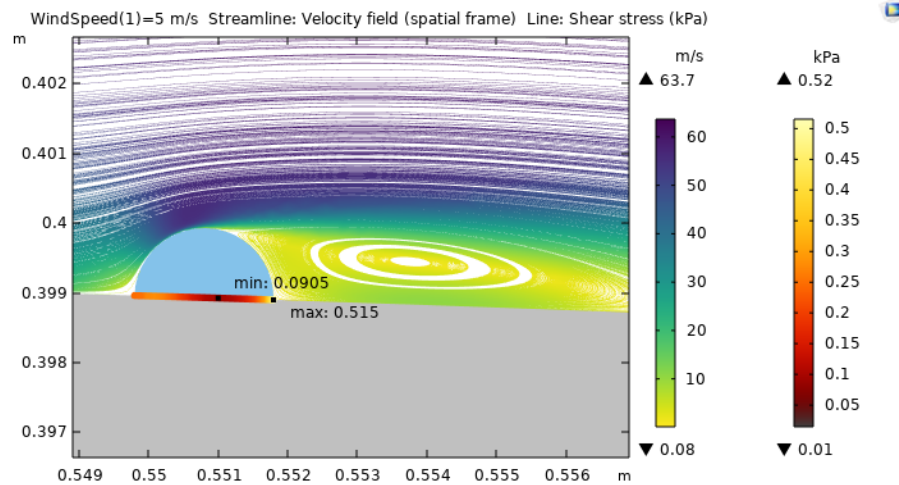


ANNEX E: ICE ADHESION STRENGTH NORMAL DISTRIBUTION

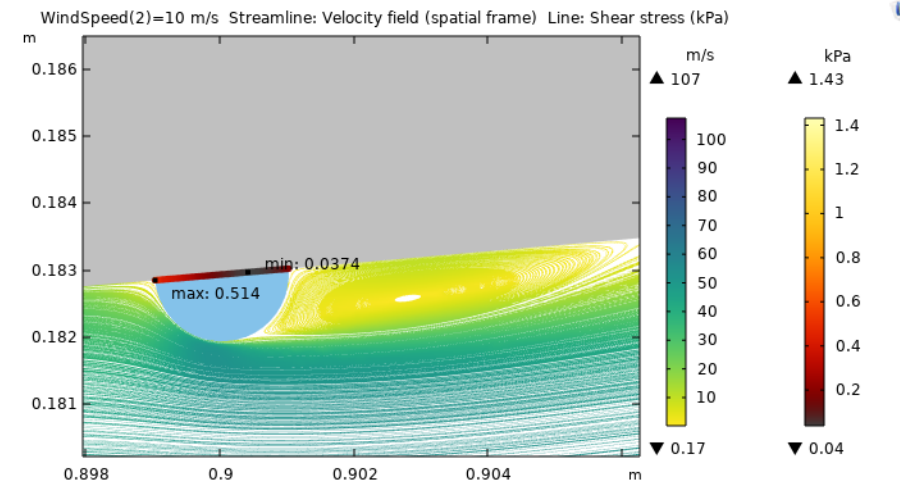
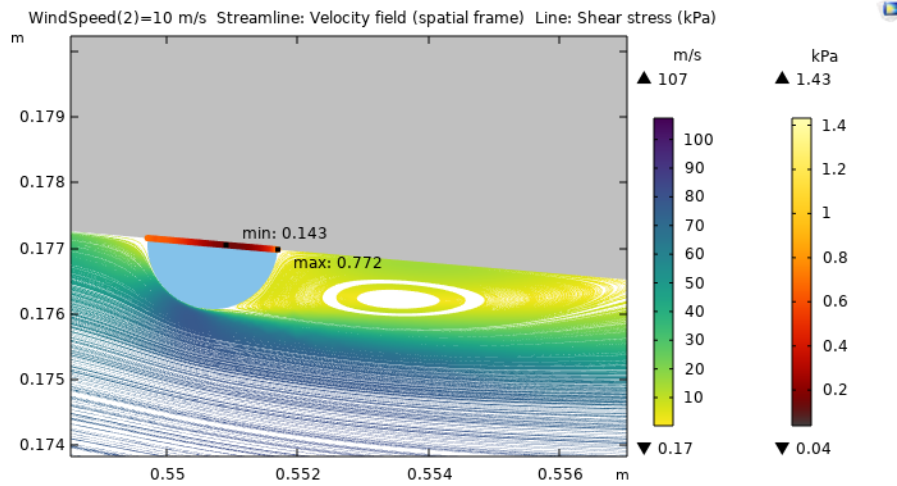
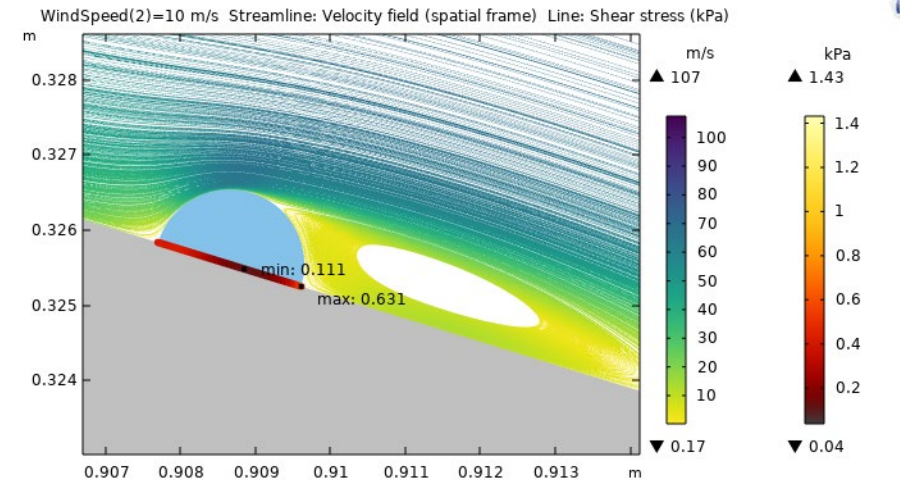
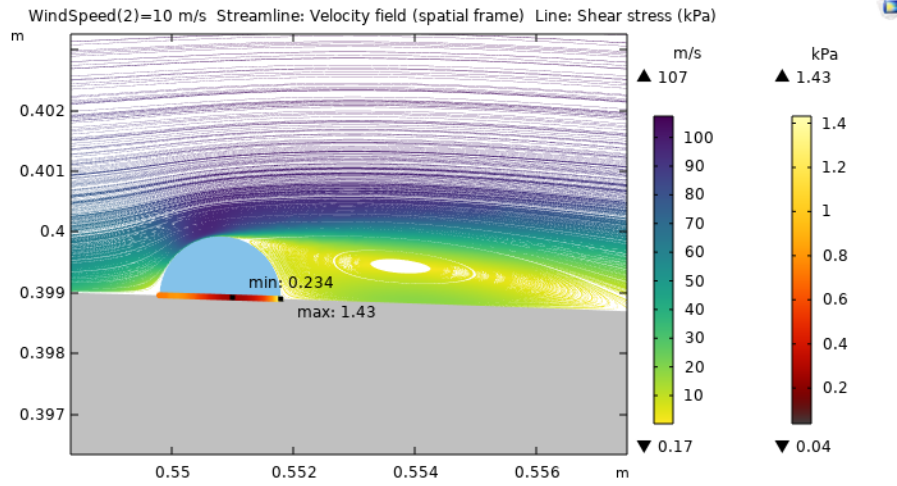


ANNEX F: COMSOL IMAGE RESULTS

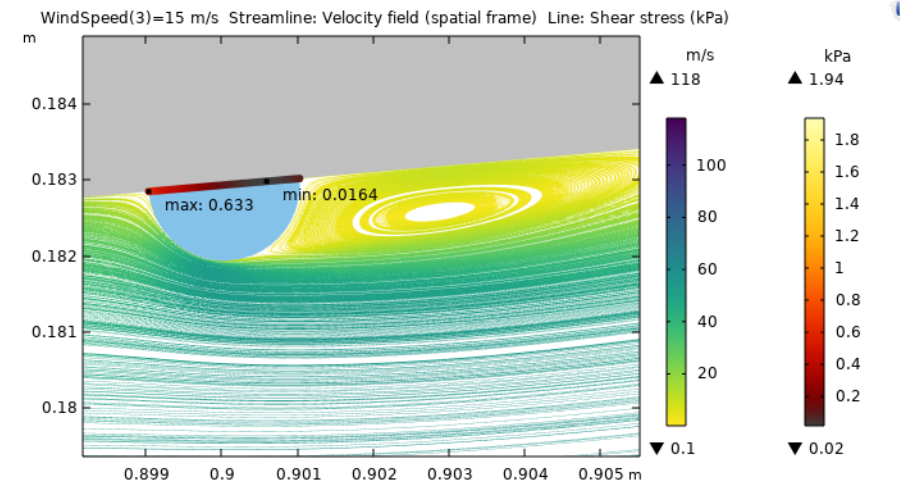
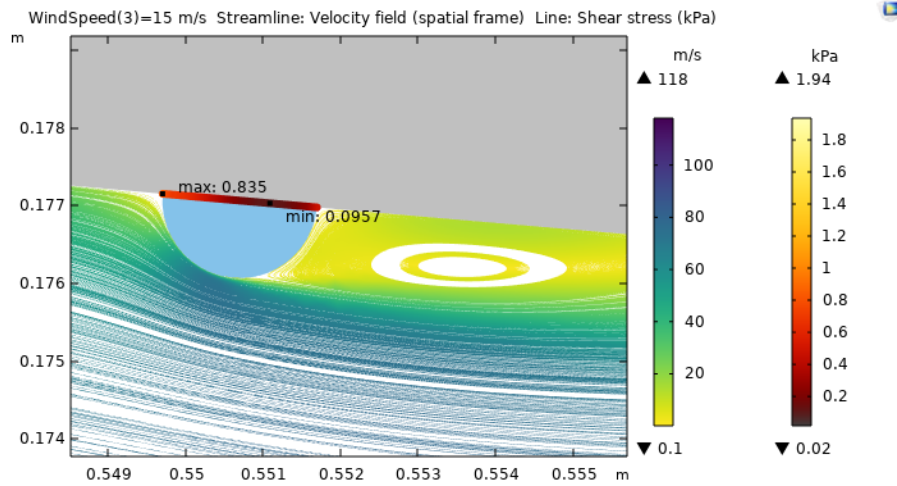
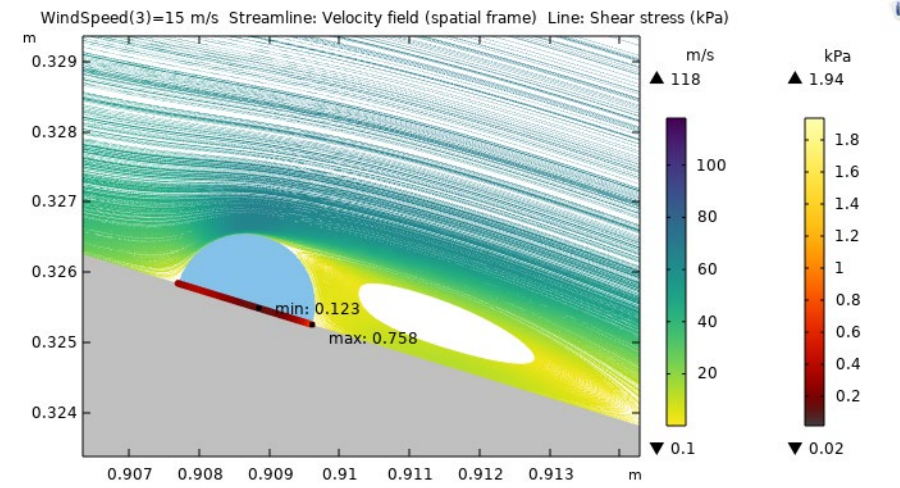
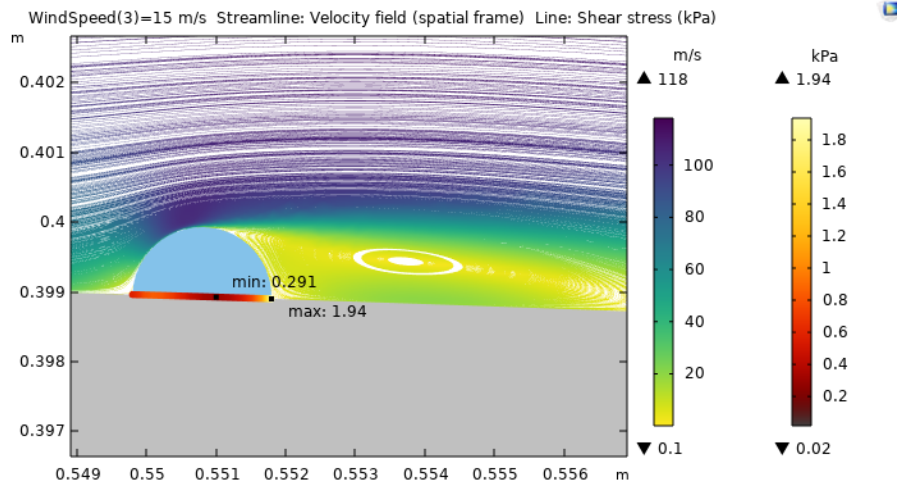
Geometry = Circle; Radius = 1 mm; Wind Speed = 5 mm/s



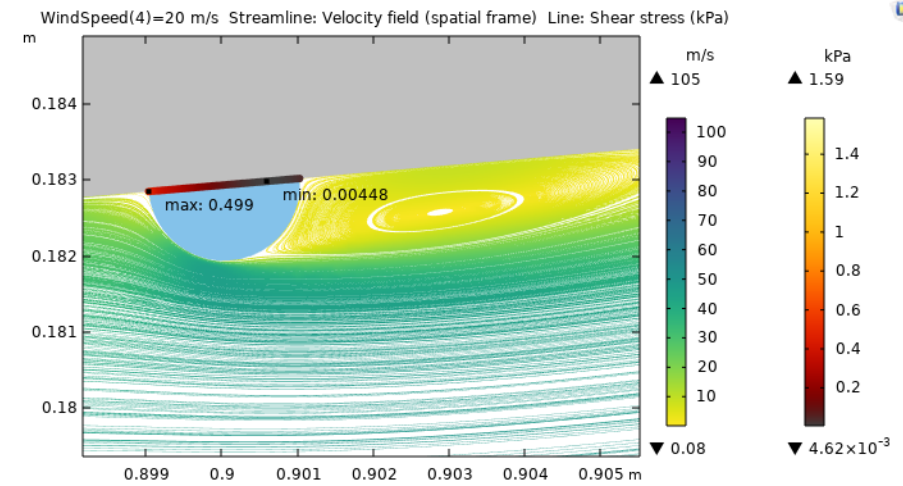
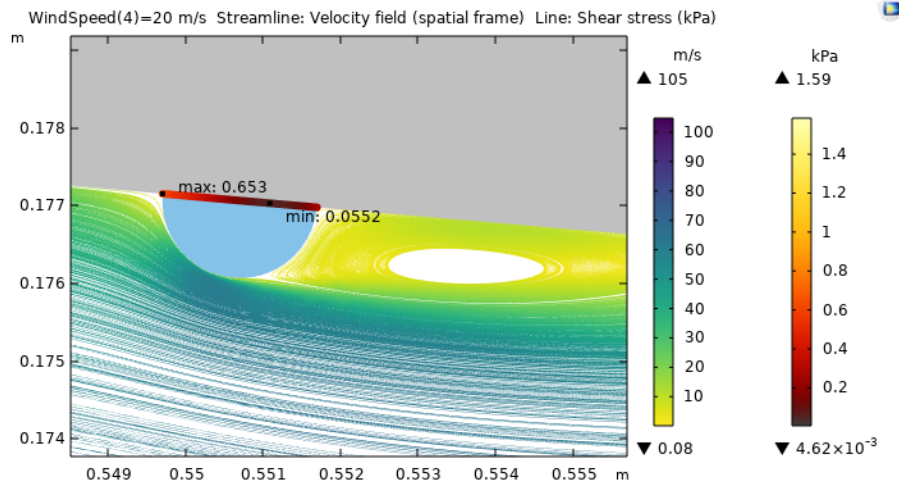
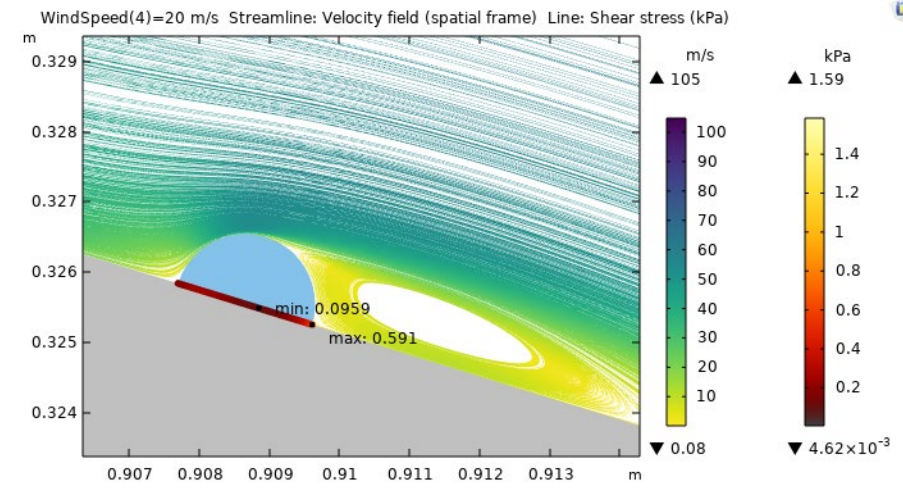
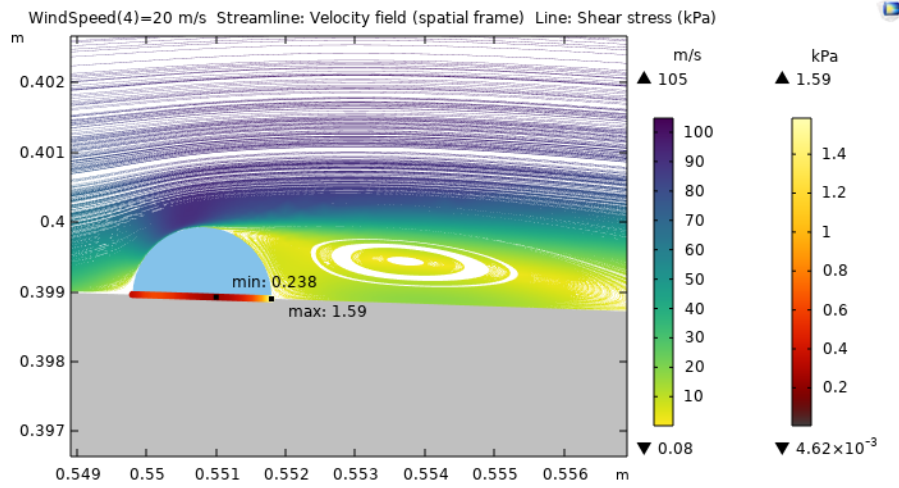
Geometry = Circle; Radius = 1 mm; Wind Speed = 10 mm/s



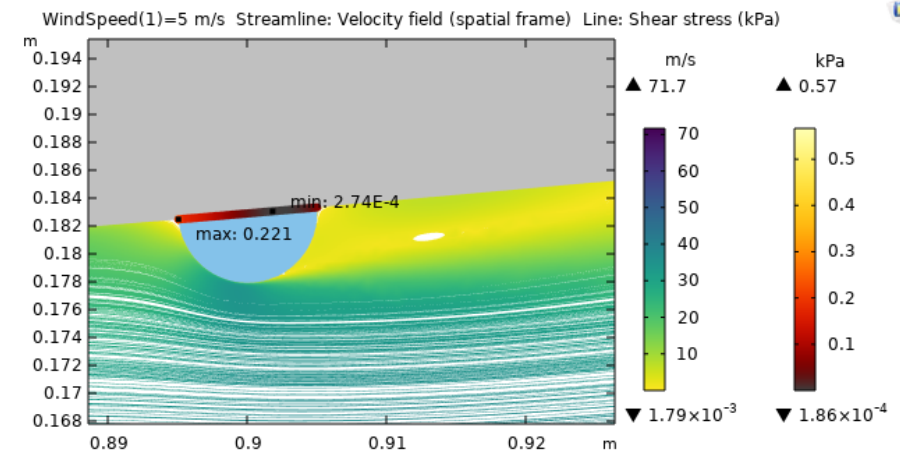
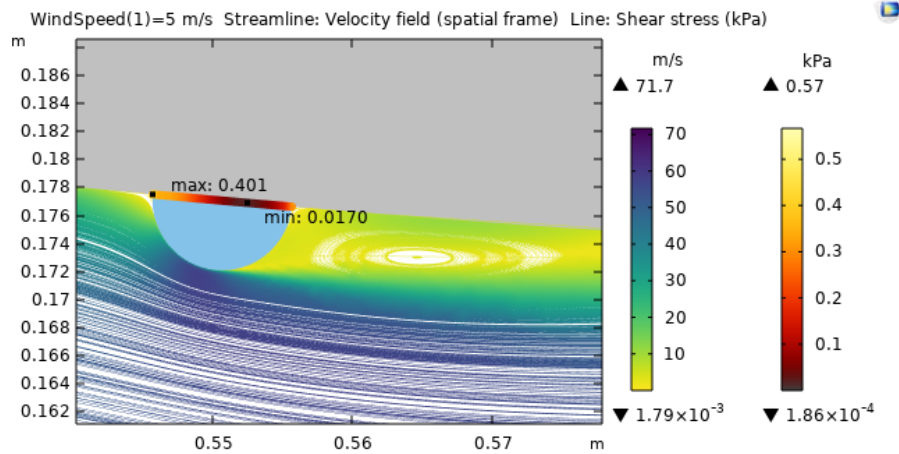
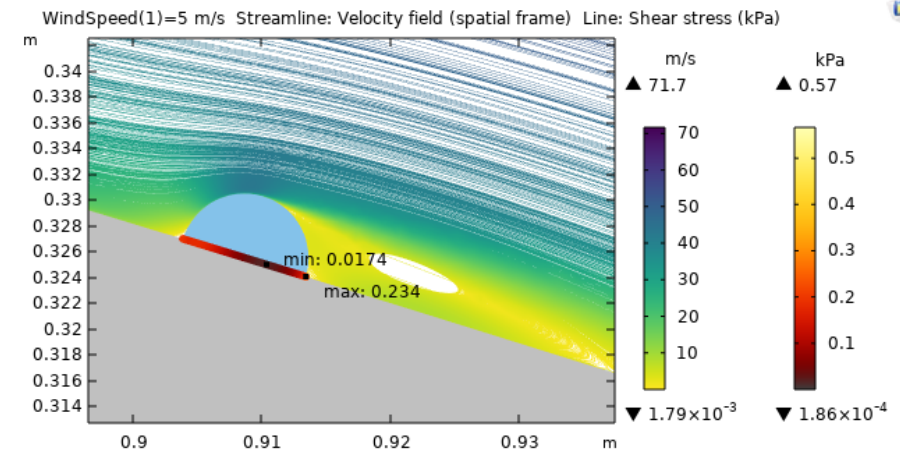
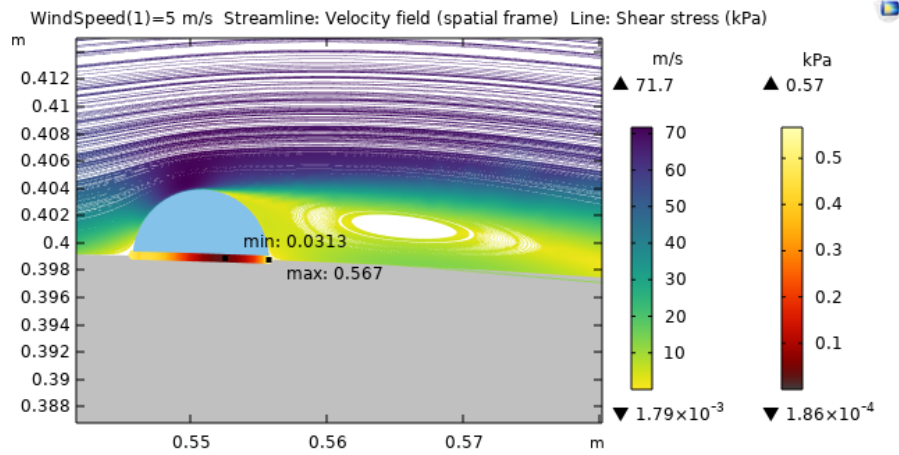
Geometry = Circle; Radius = 1 mm; Wind Speed = 15 mm/s



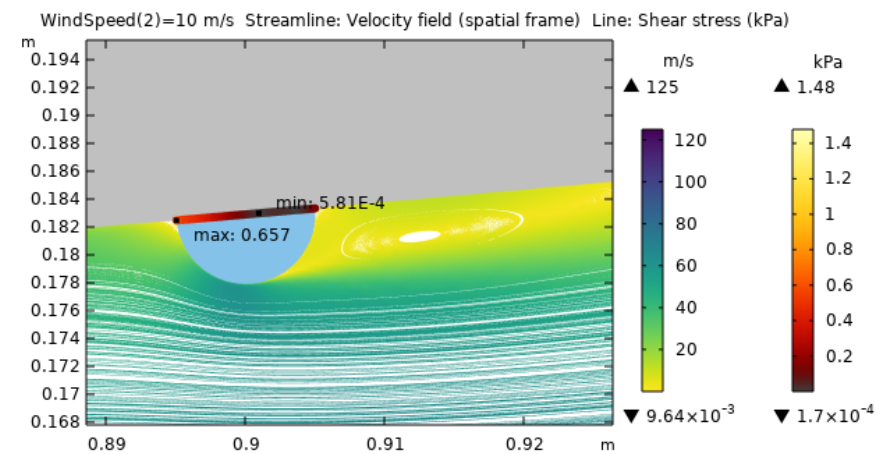
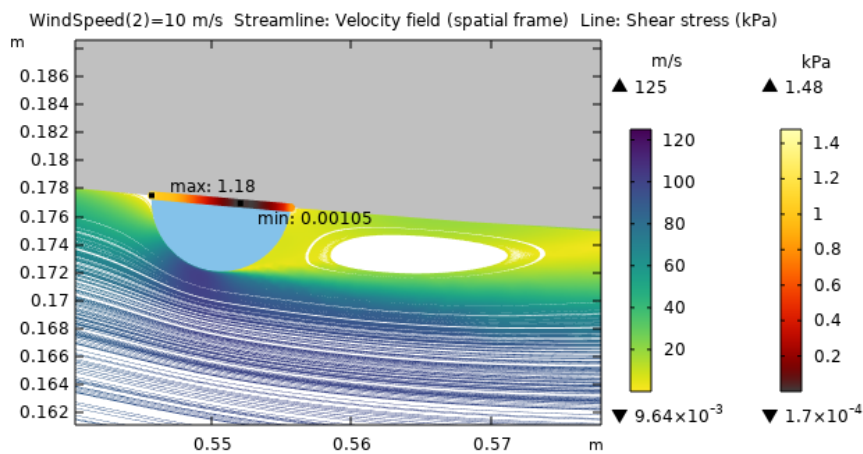
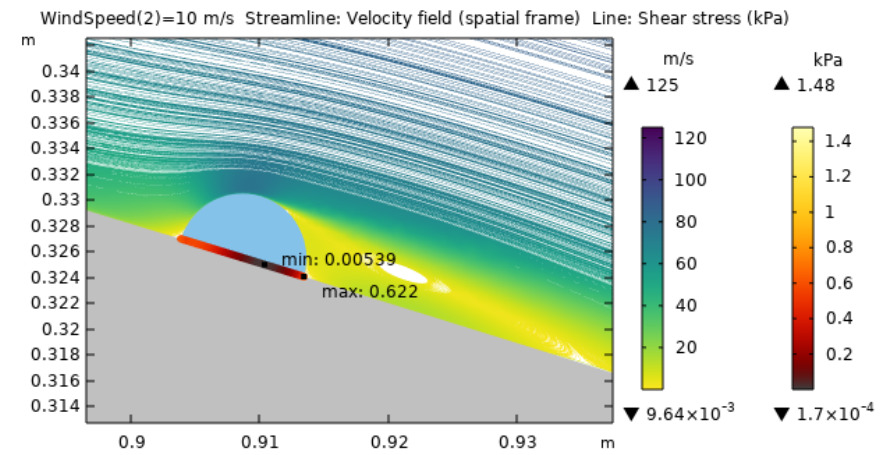
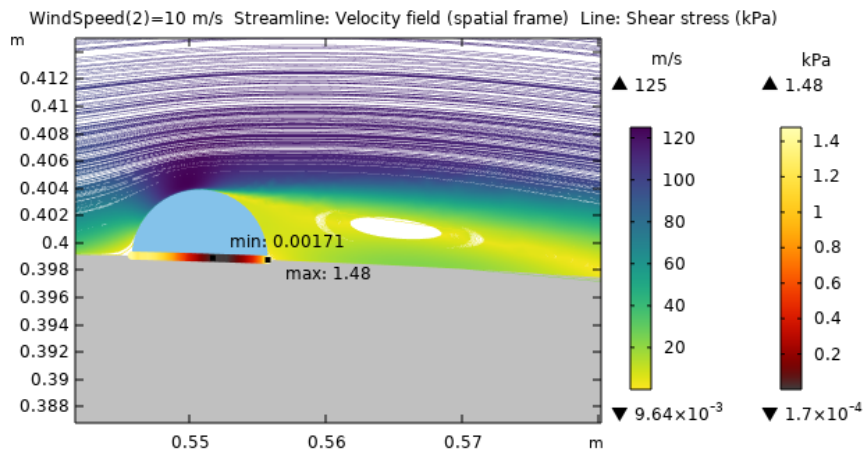
Geometry = Circle; Radius = 1 mm; Wind Speed = 20 mm/s



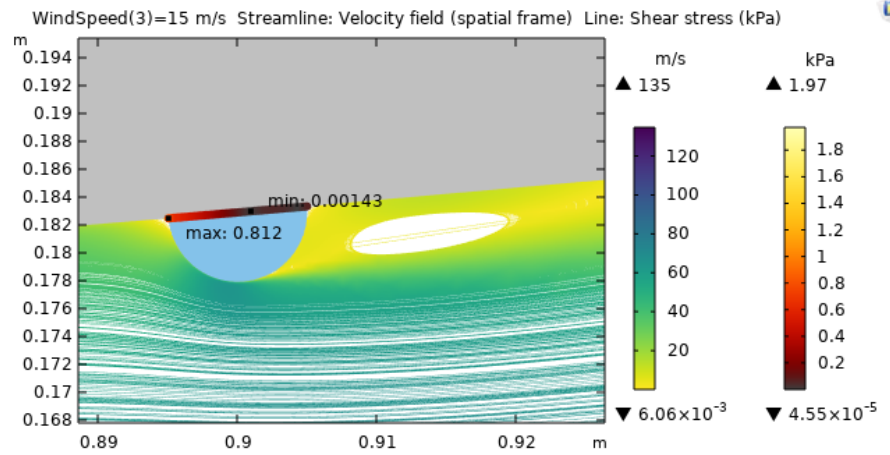
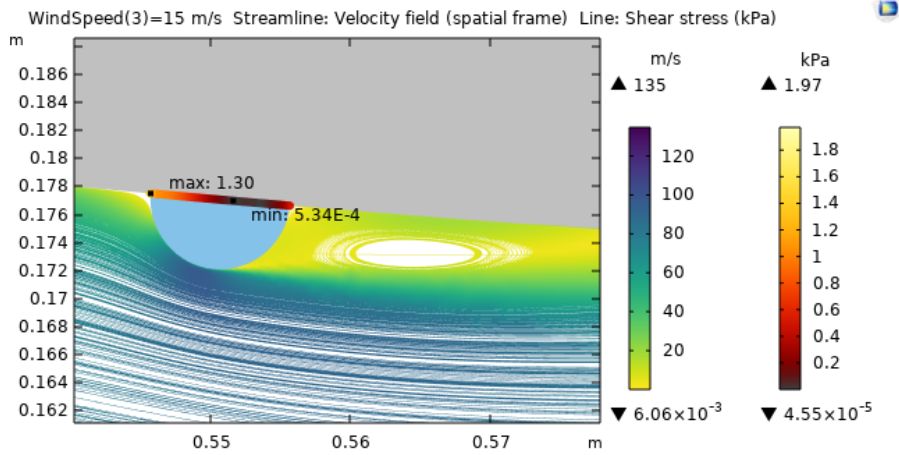
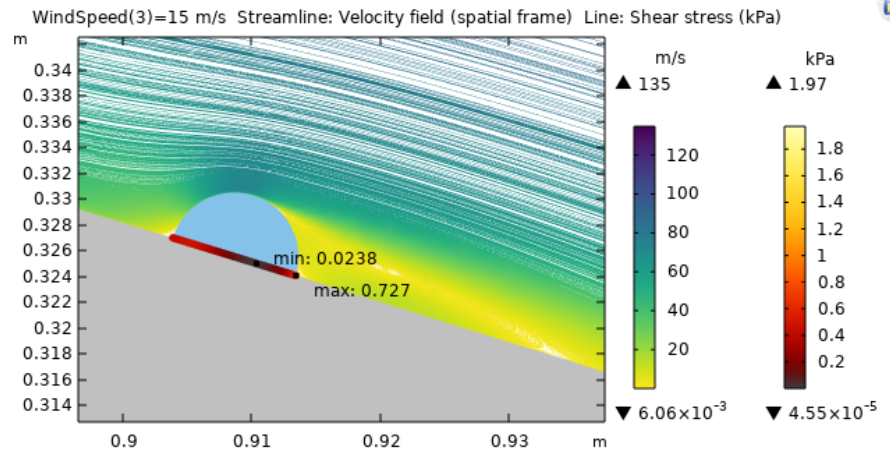
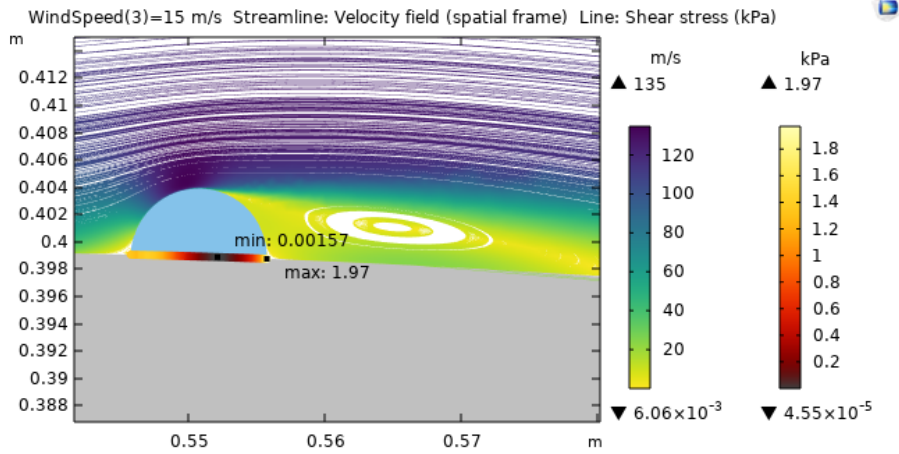
Geometry = Circle; Radius = 5 mm; Wind Speed = 5 mm/s



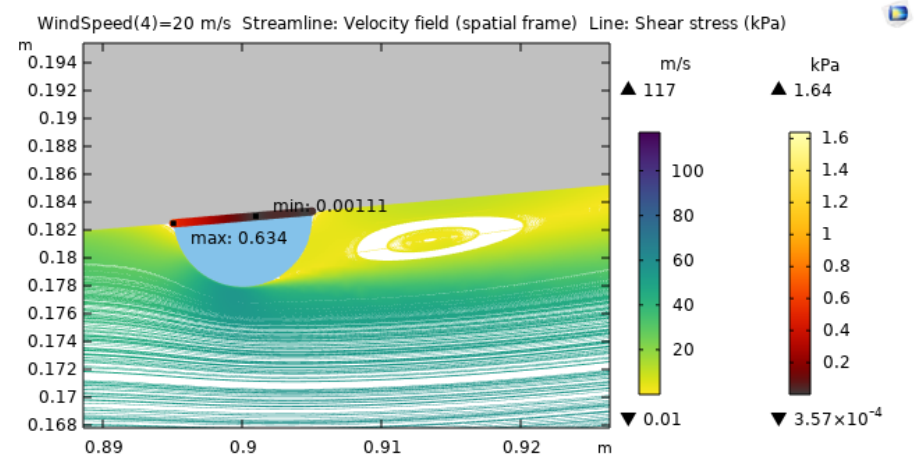
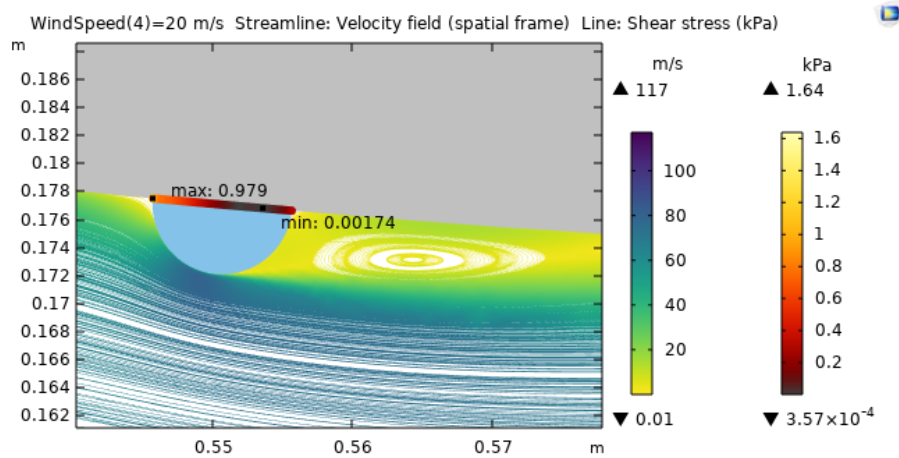
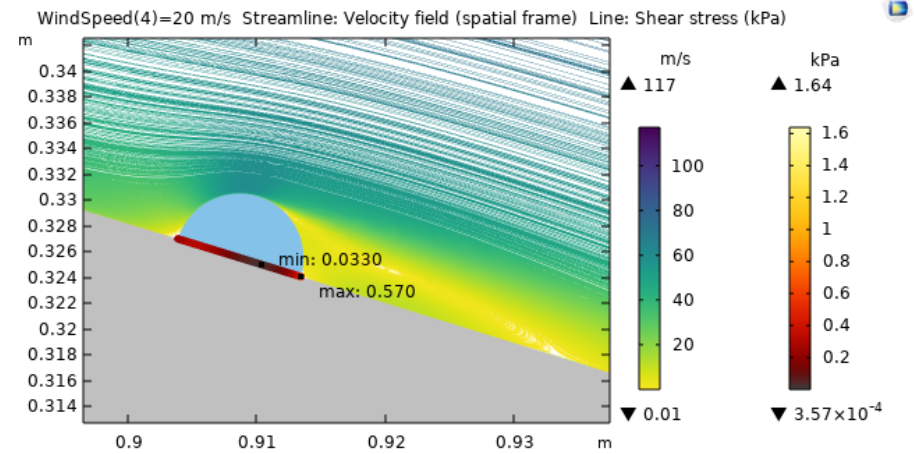
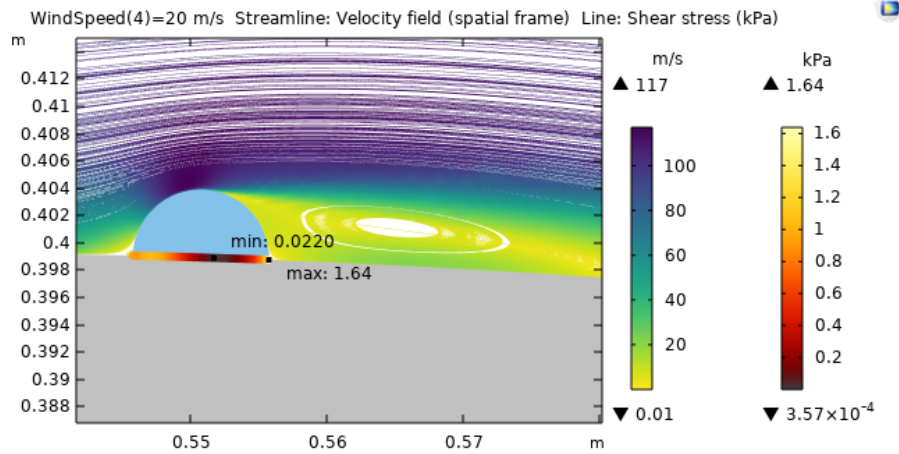
Geometry = Circle; Radius = 5 mm; Wind Speed = 10 mm/s



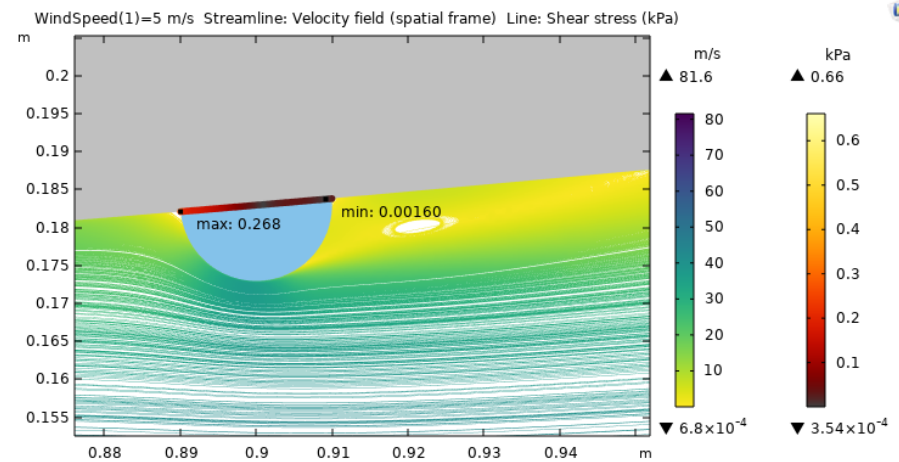
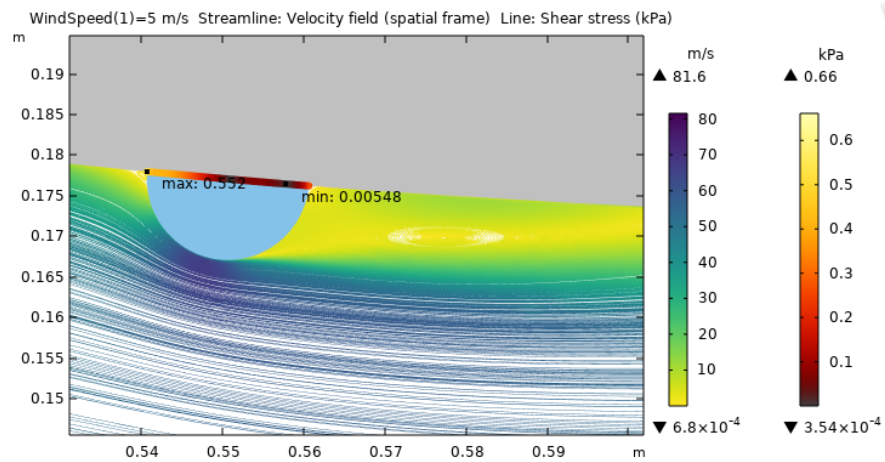
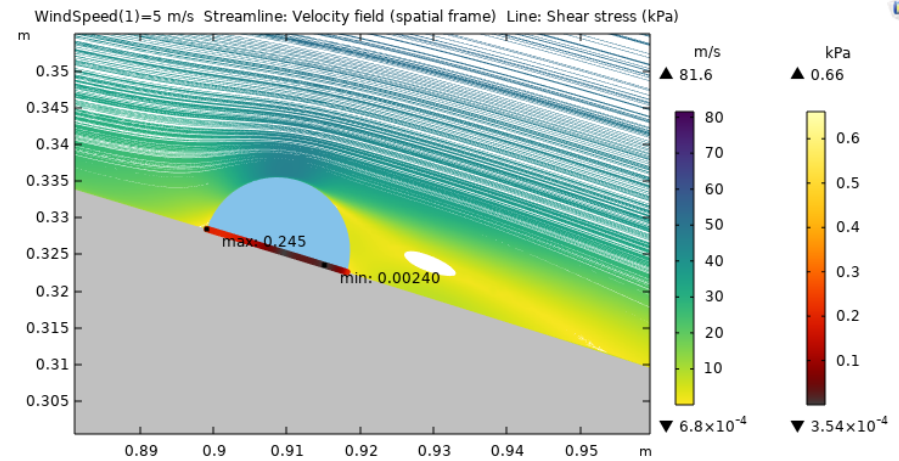
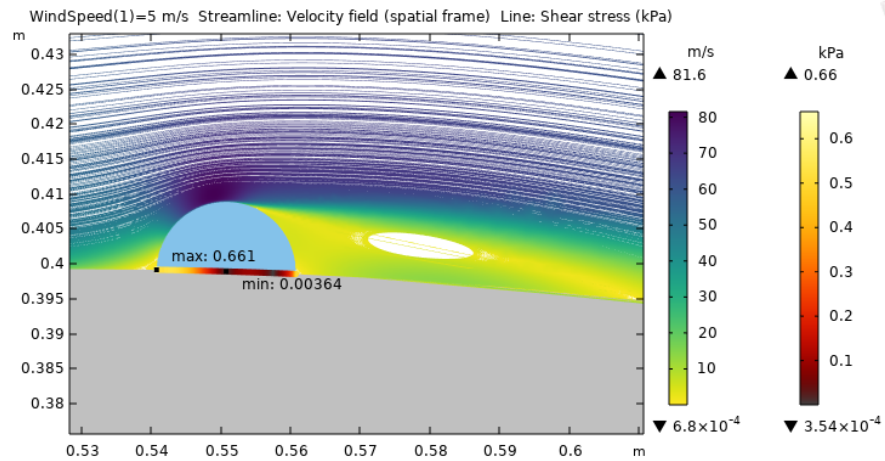
Geometry = Circle; Radius = 5 mm; Wind Speed = 15 mm/s



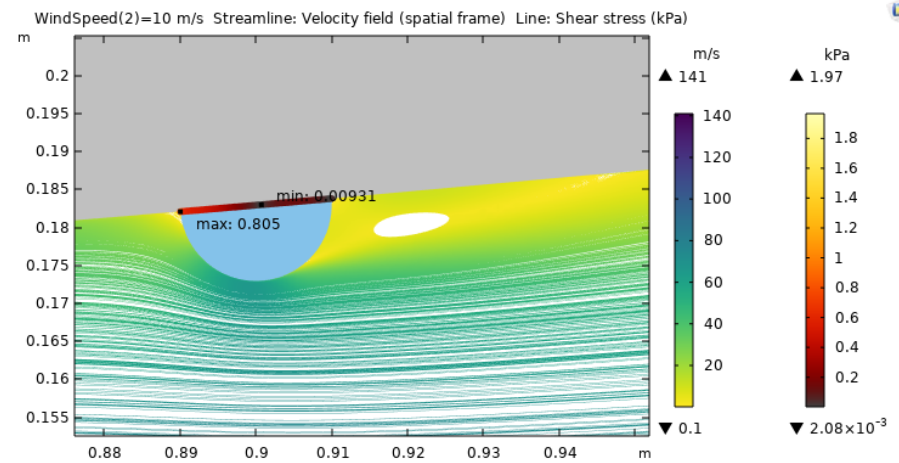
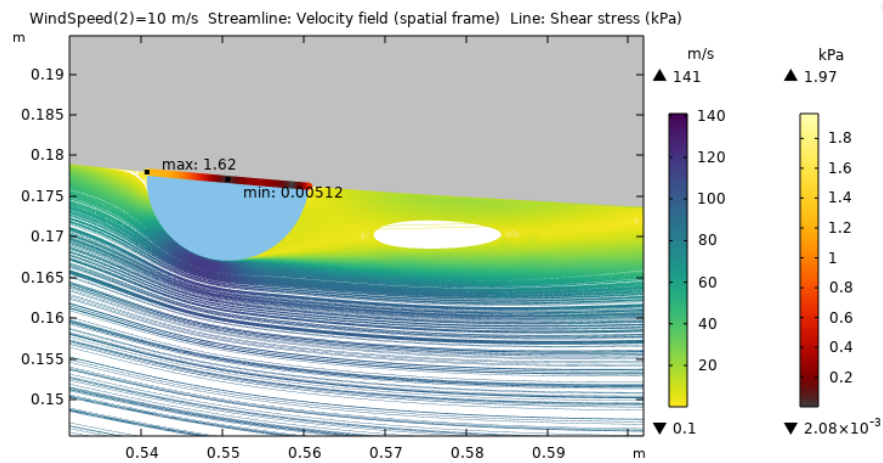
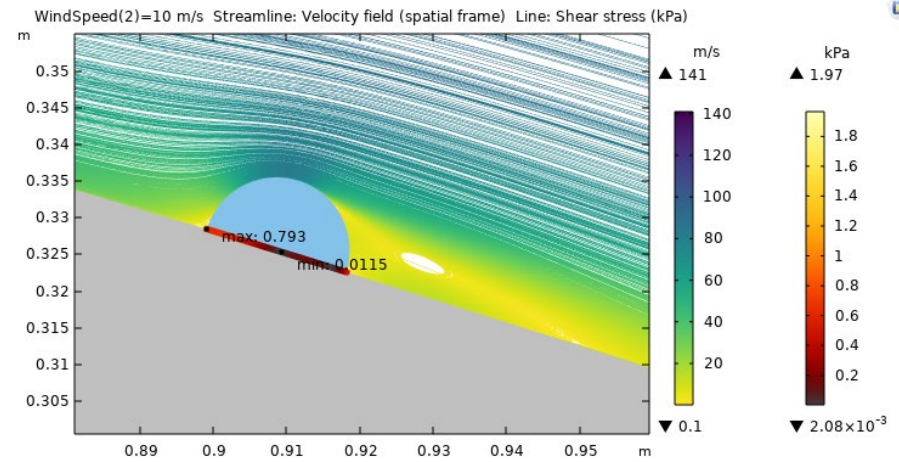
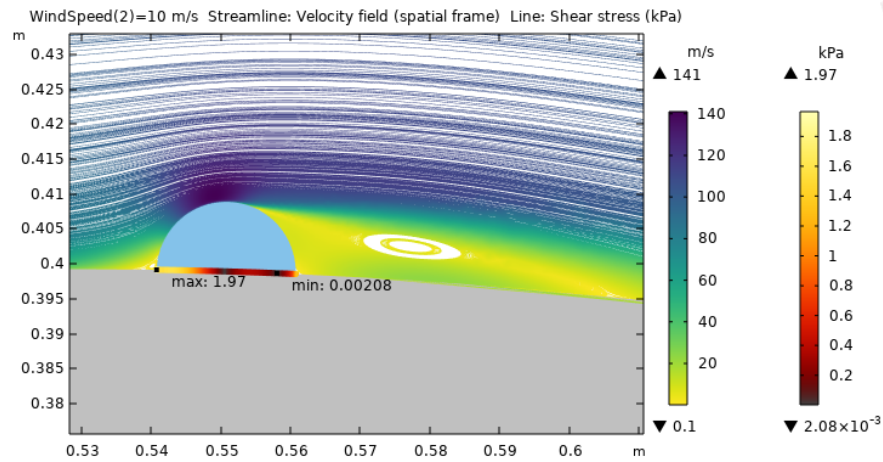
Geometry = Circle; Radius = 5 mm; Wind Speed = 20 mm/s



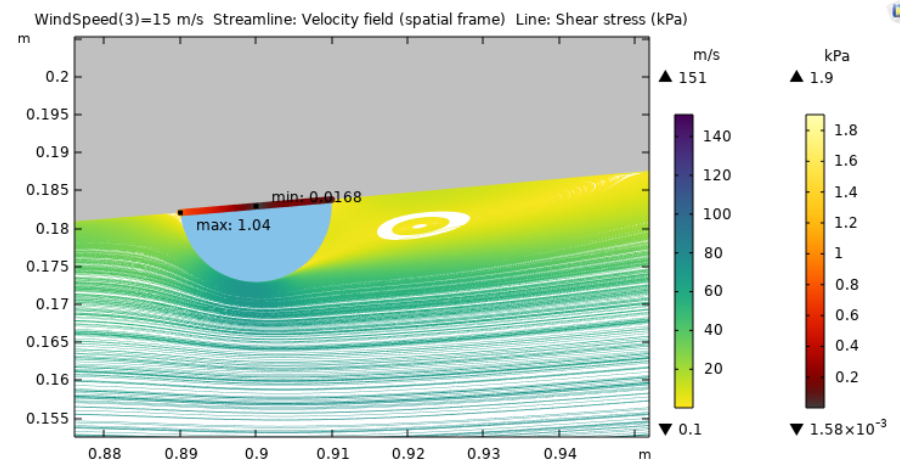
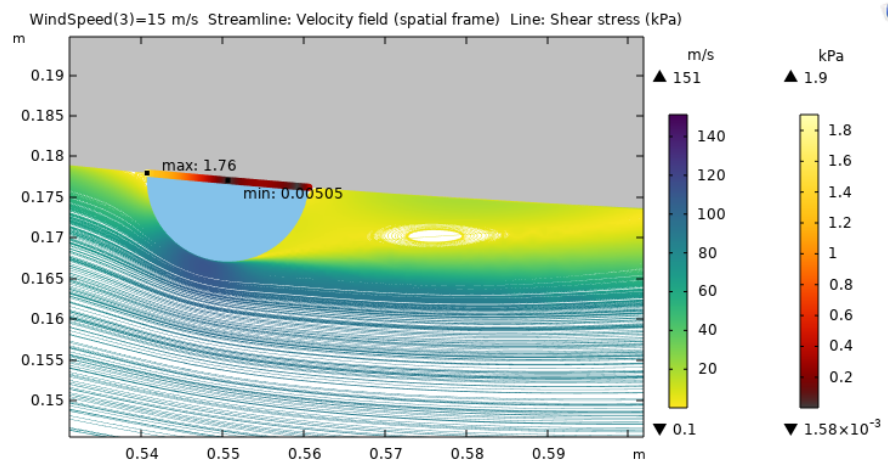
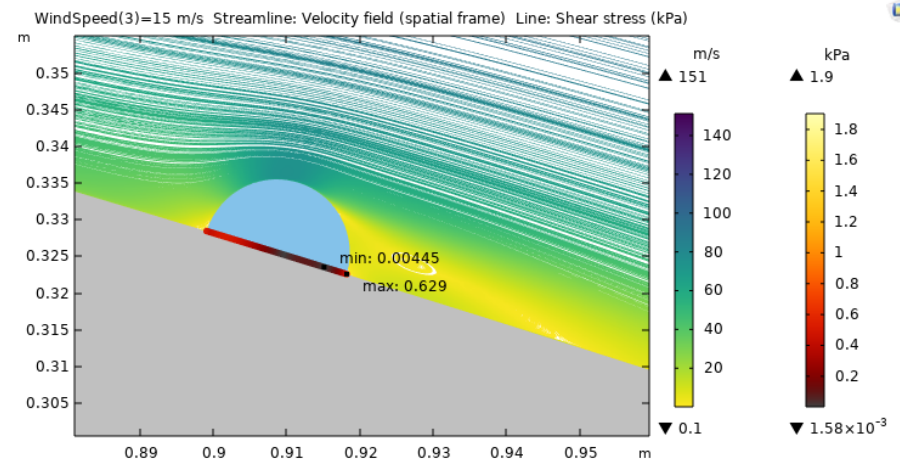
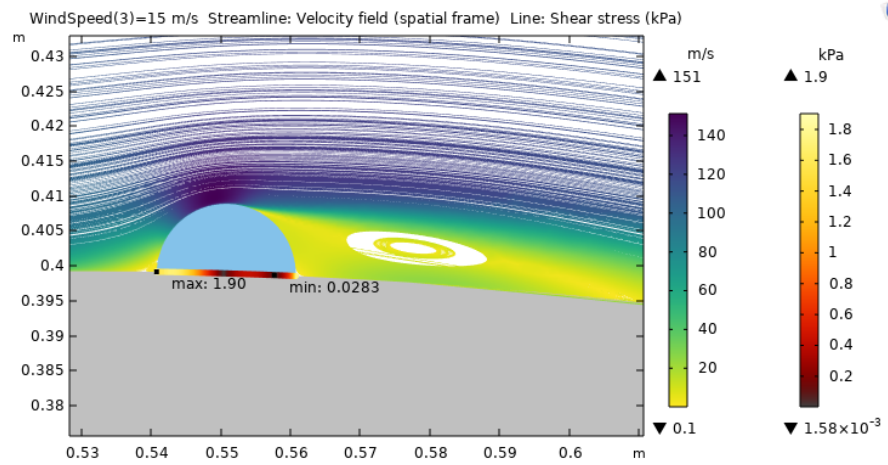
Geometry = Circle; Radius = 10 mm; Wind Speed = 5 mm/s



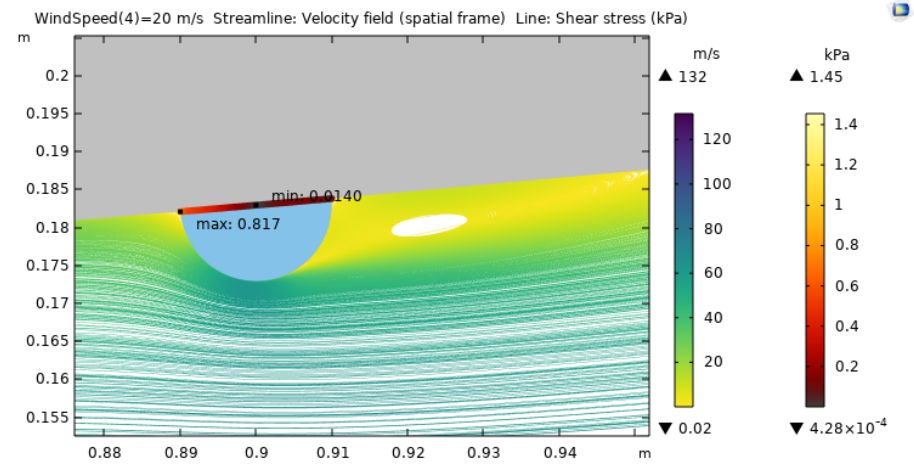
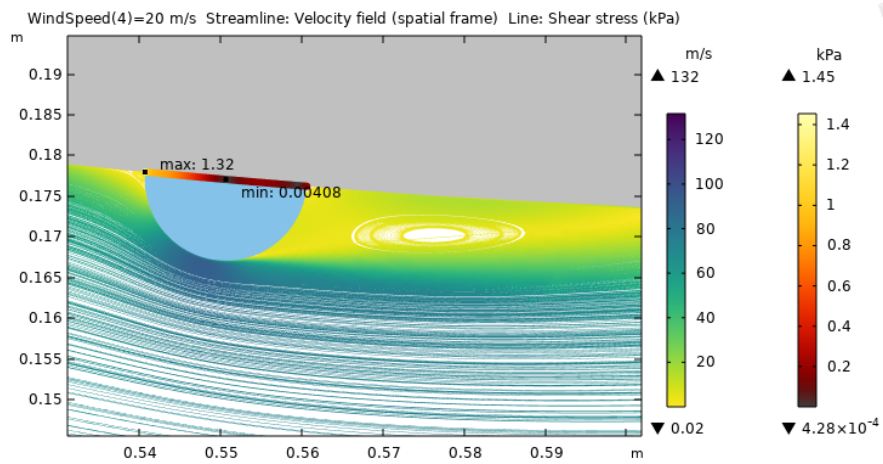
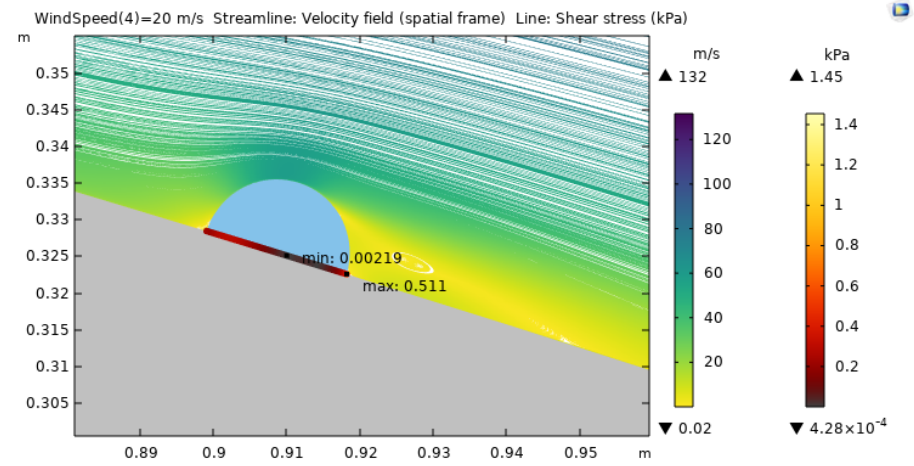
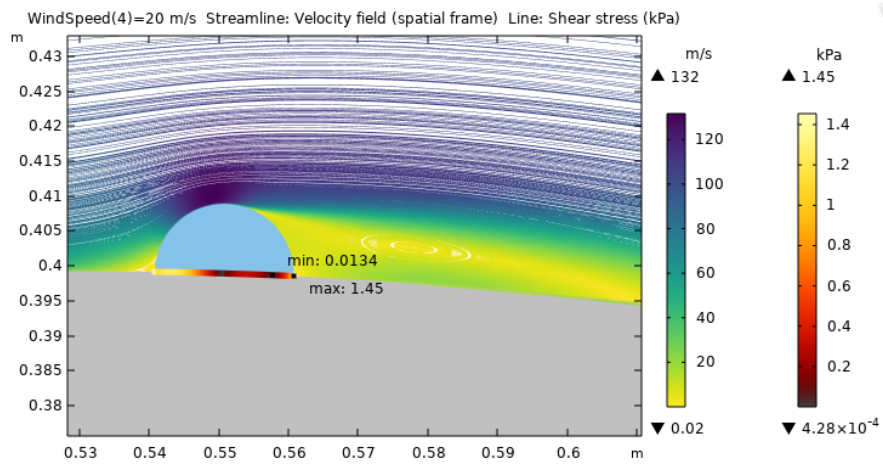
Geometry = Circle; Radius = 10 mm; Wind Speed = 10 mm/s



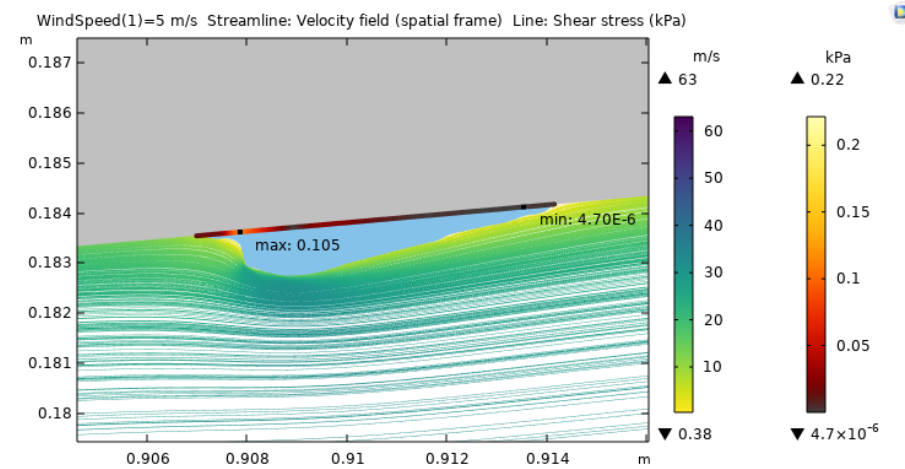
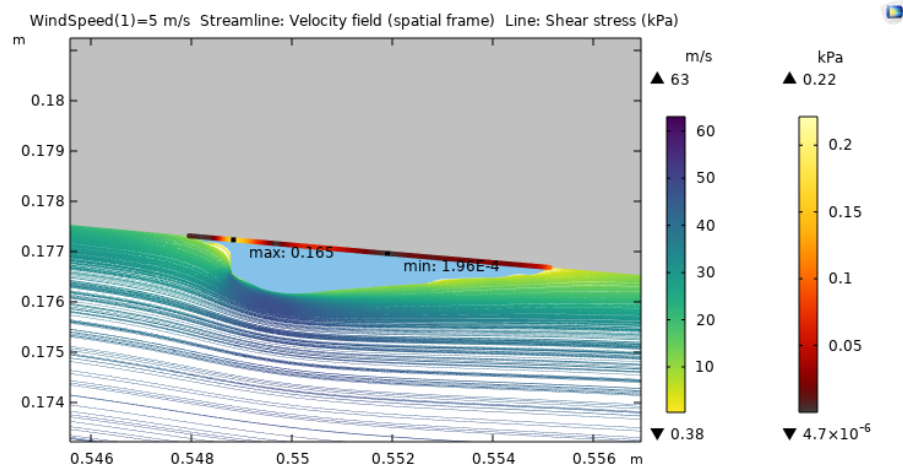
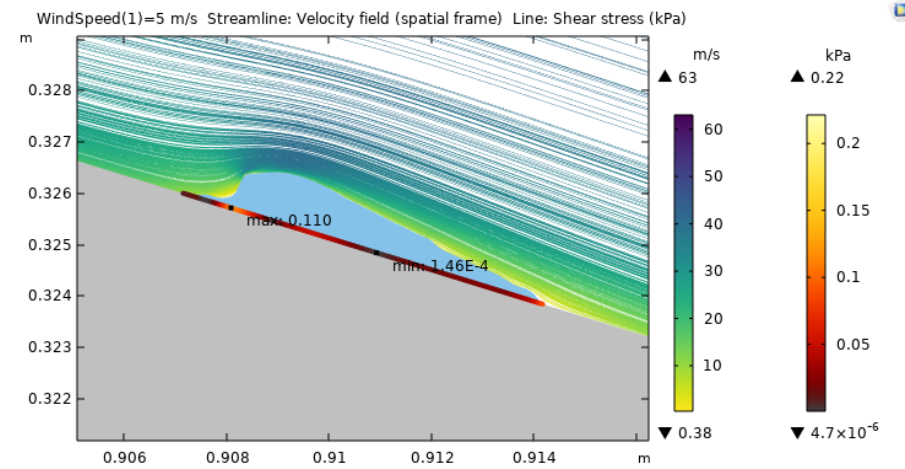
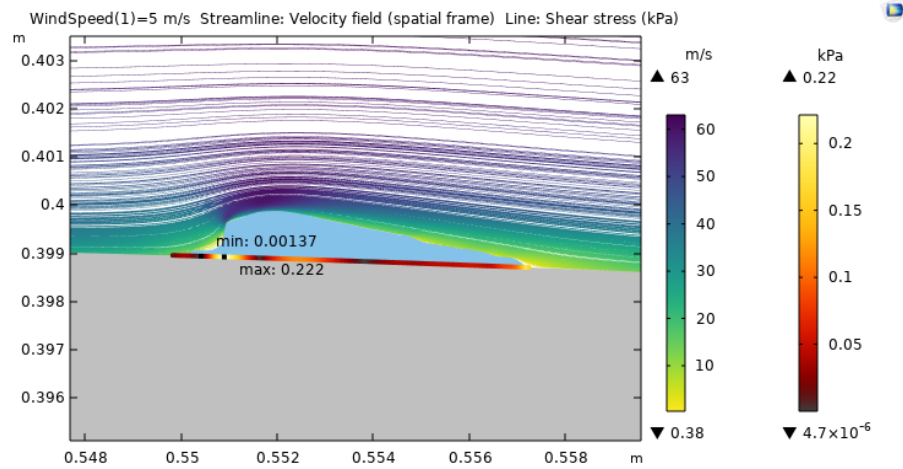
Geometry = Circle; Radius = 10 mm; Wind Speed = 15 m/s



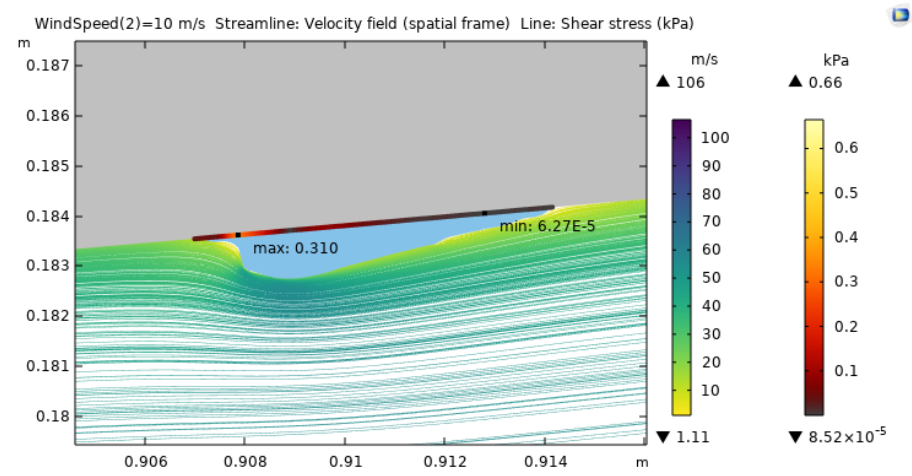
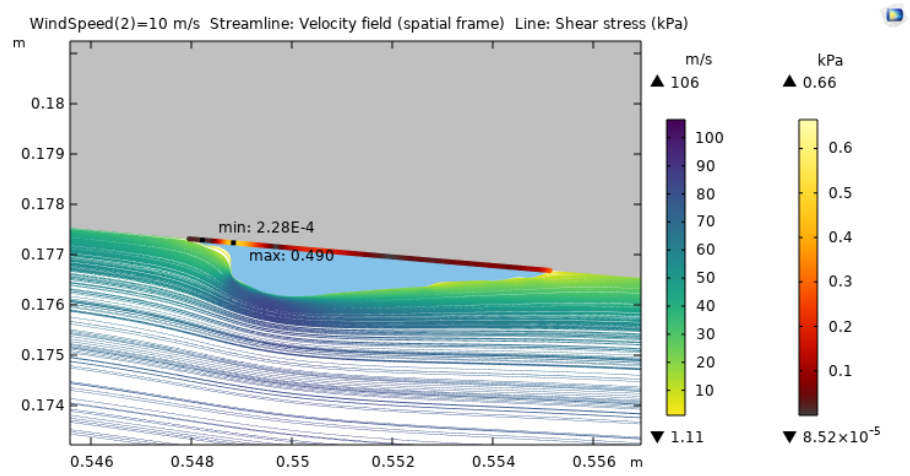
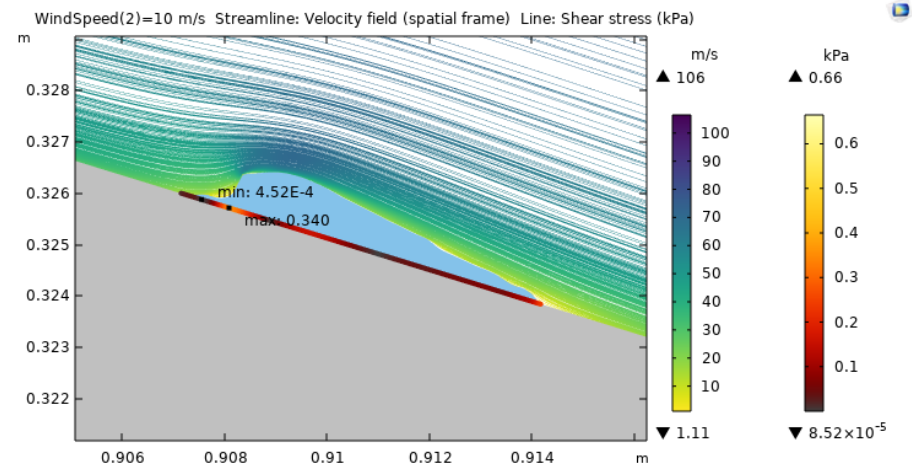
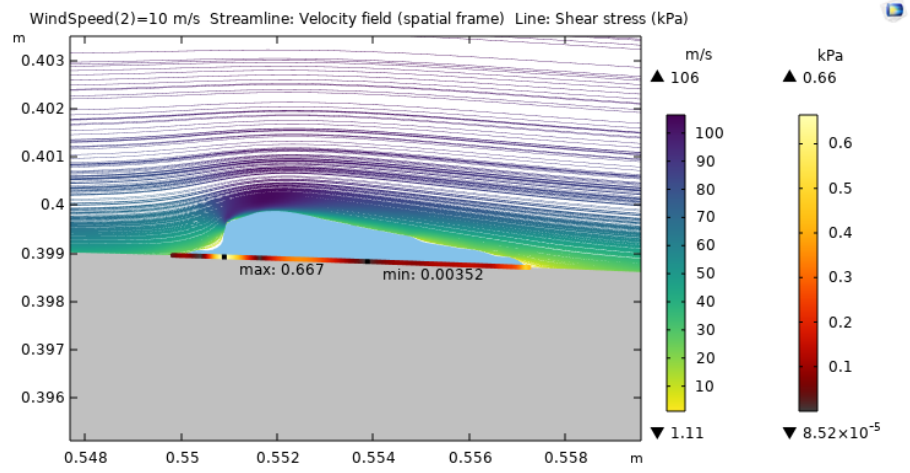
Geometry = Circle; Radius = 10 mm; Wind Speed = 20 mm/s



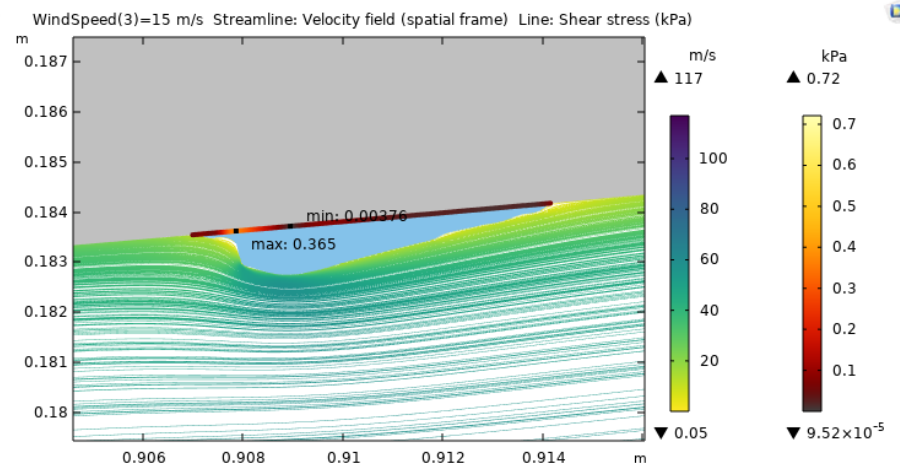
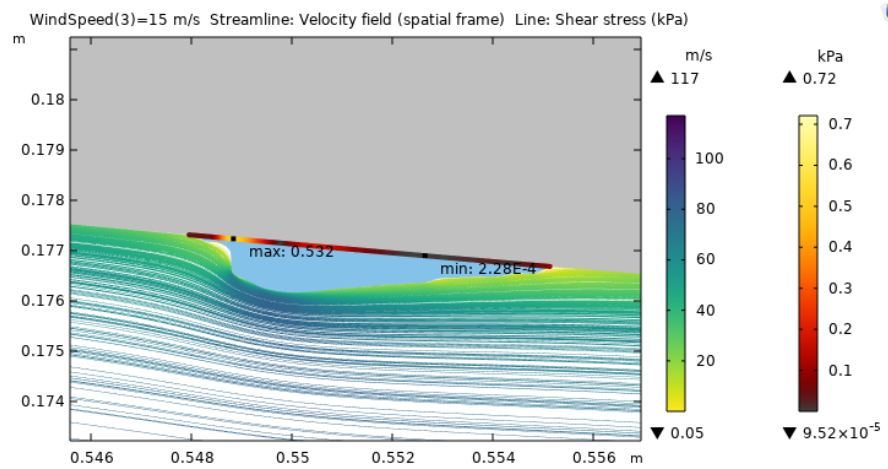
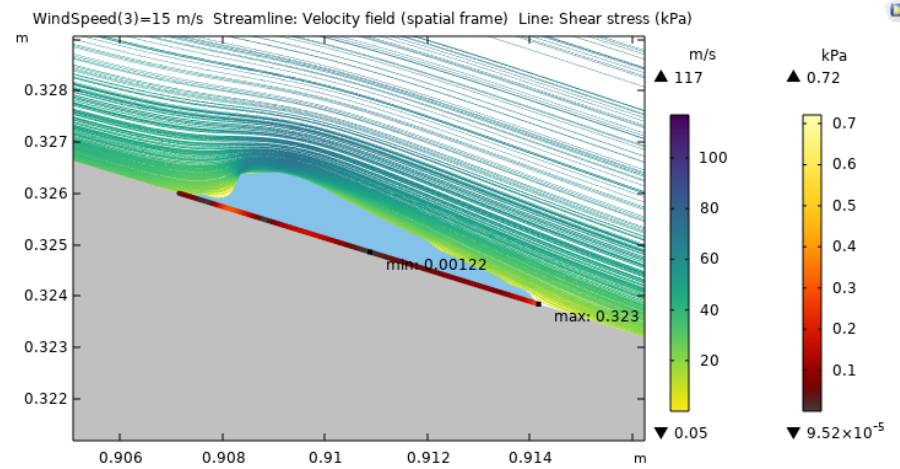
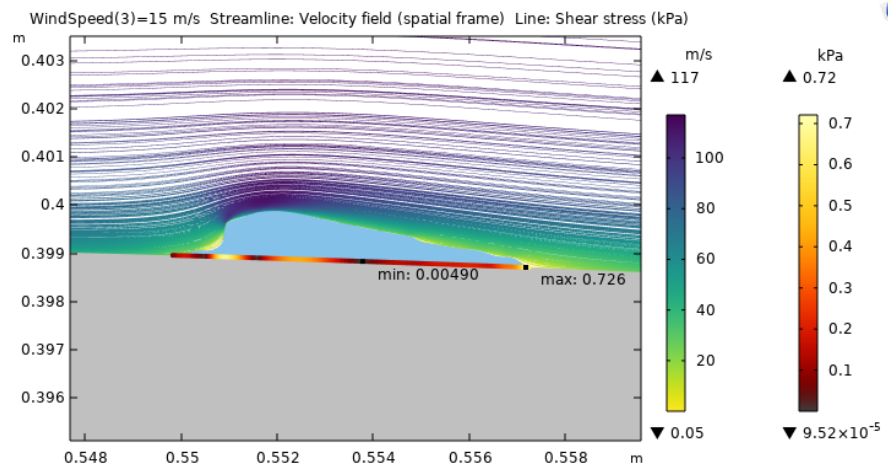
Geometry = Runback Ice; Height = 1 mm; Wind Speed = 5 mm/s



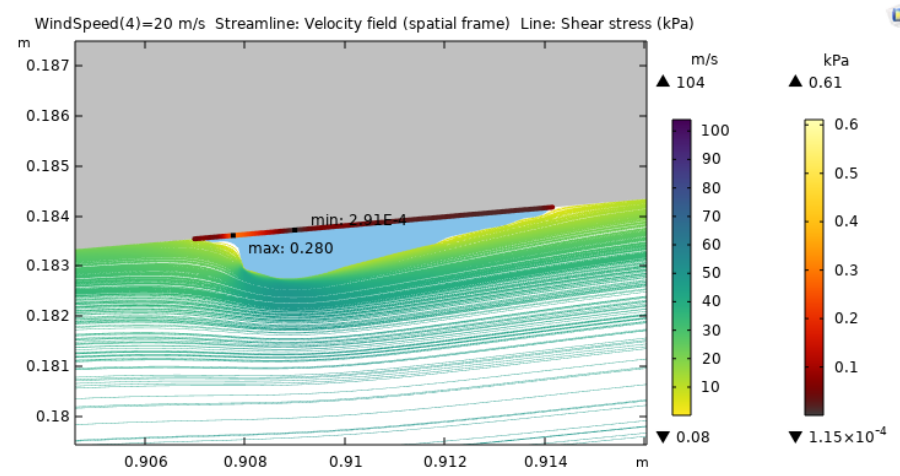
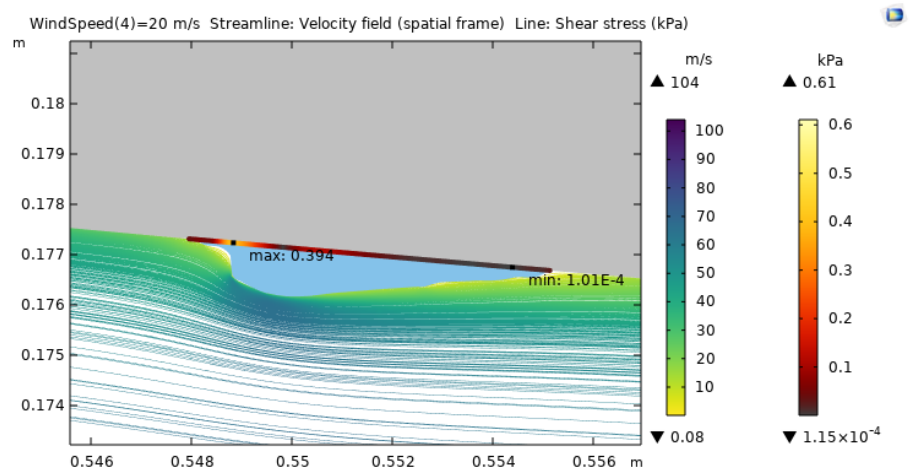
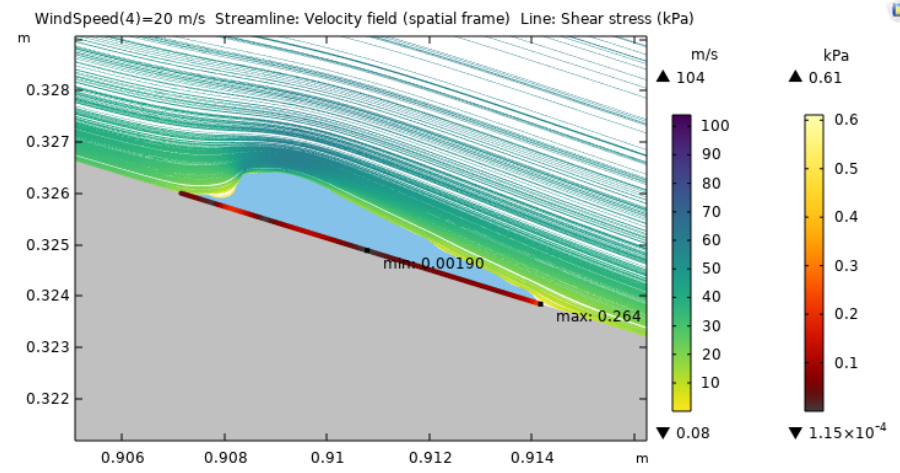
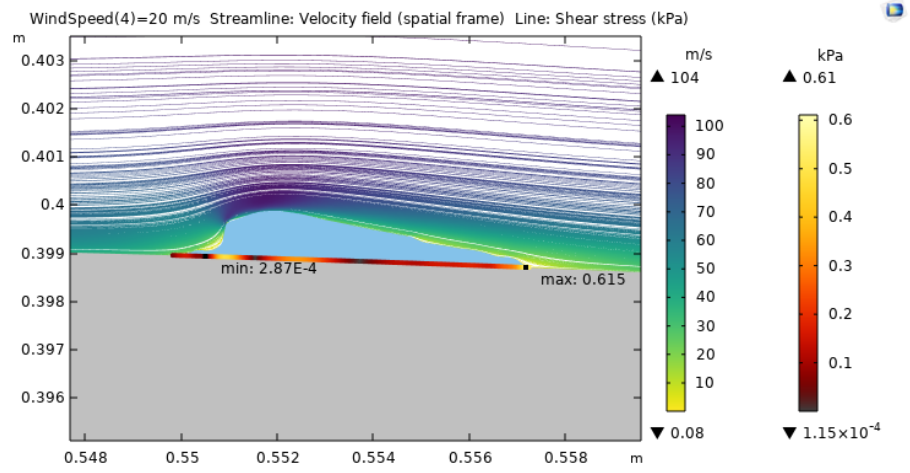
Geometry = Runback Ice; Height = 1 mm; Wind Speed = 10 mm/s



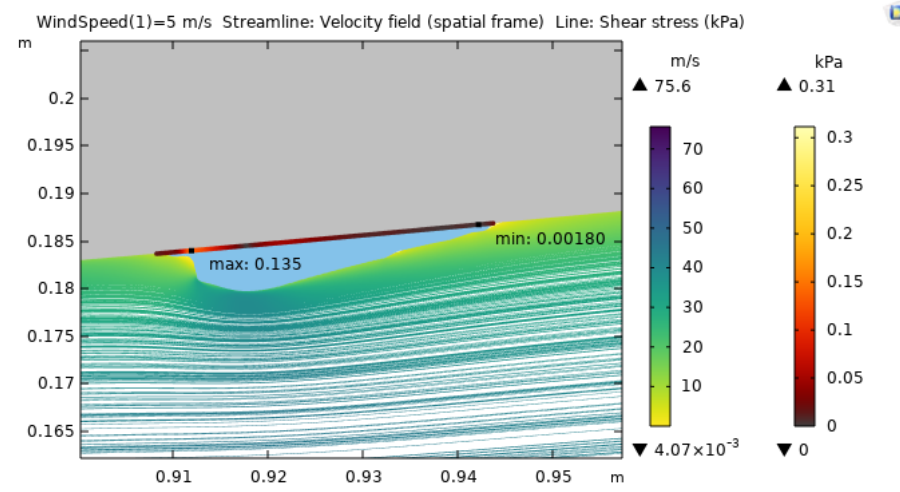
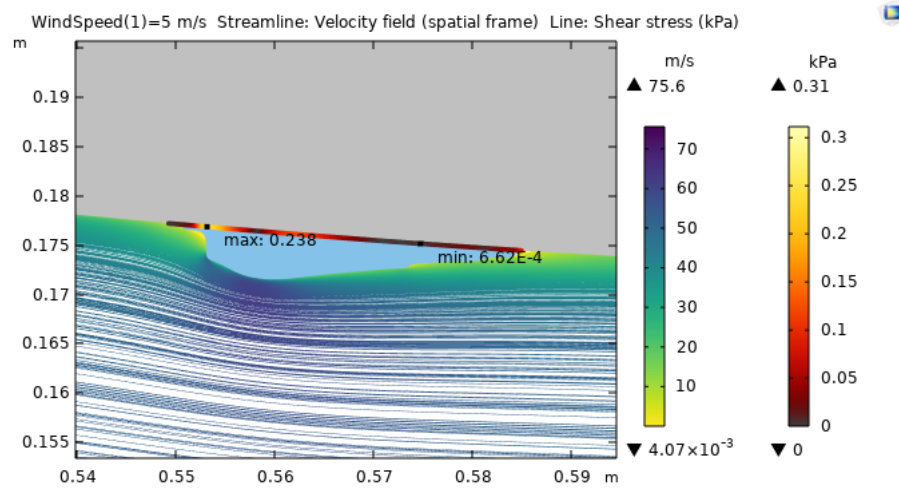
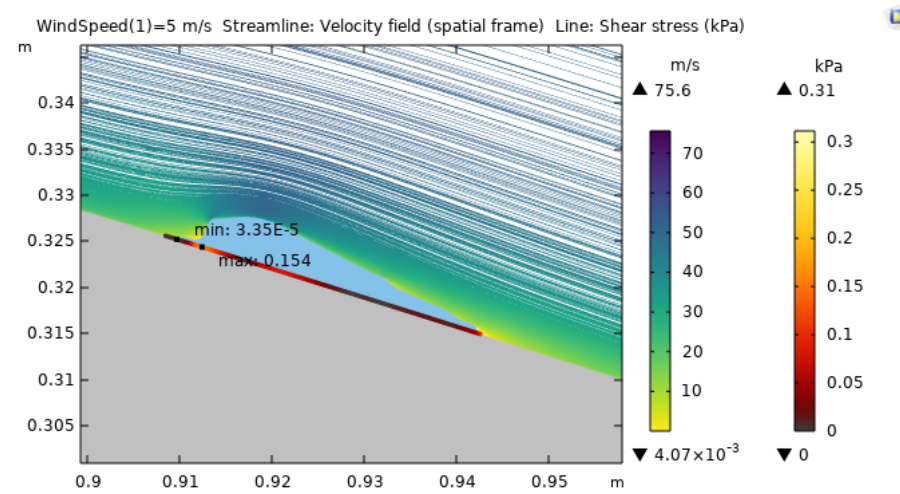
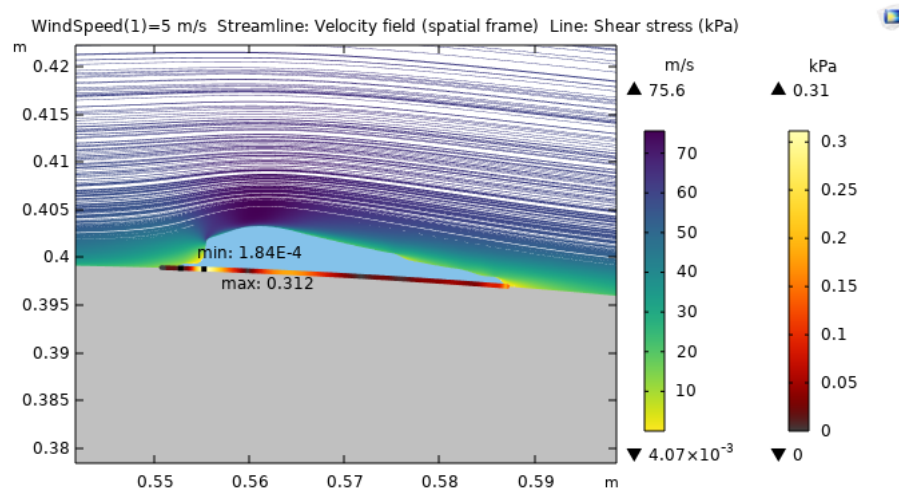
Geometry = Runback Ice; Height = 1 mm; Wind Speed = 15 m/s



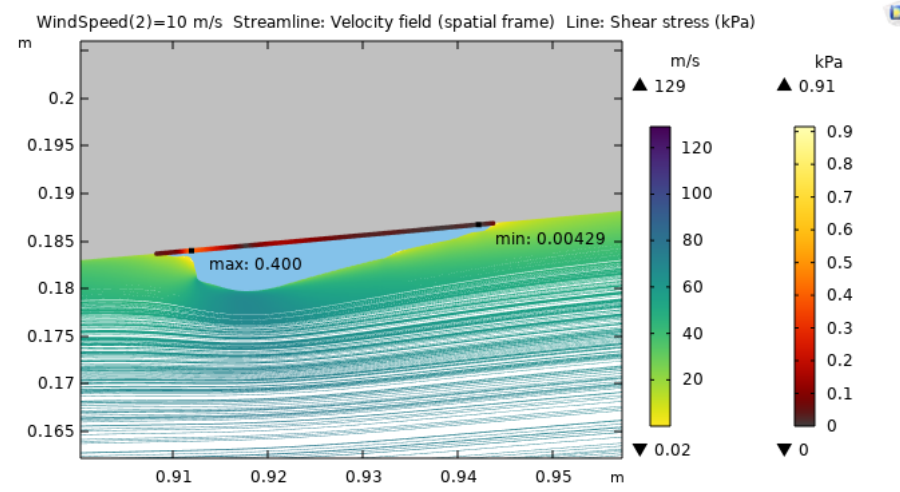
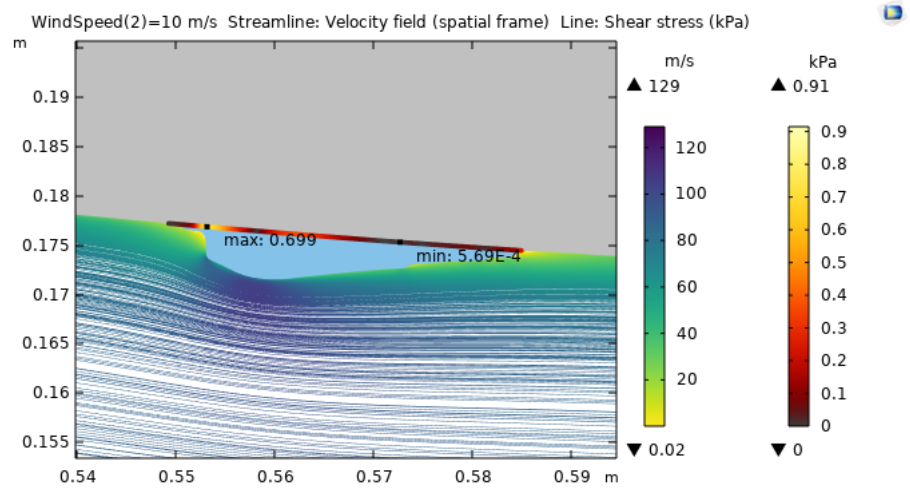
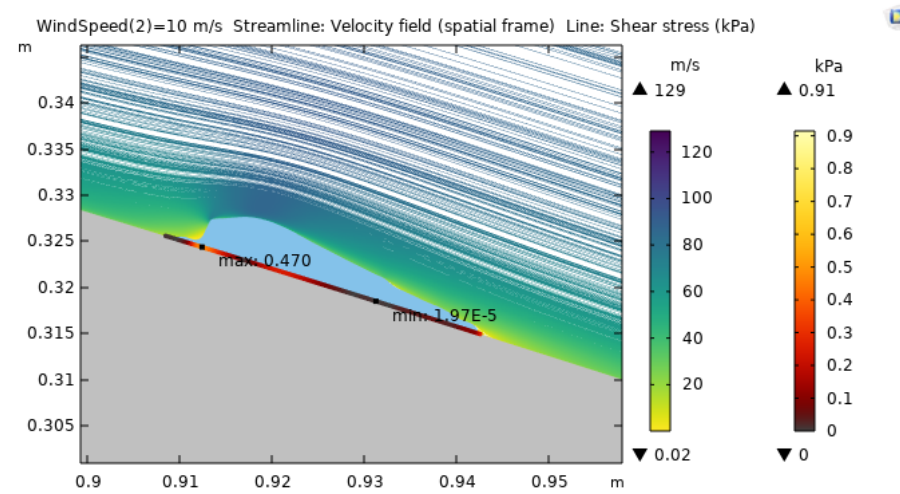
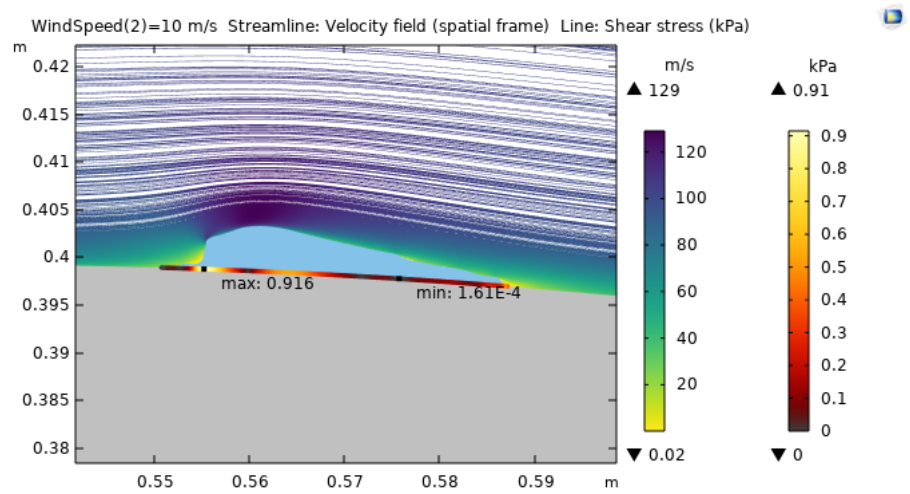
Geometry = Runback Ice; Height = 1 mm; Wind Speed = 20 mm/s



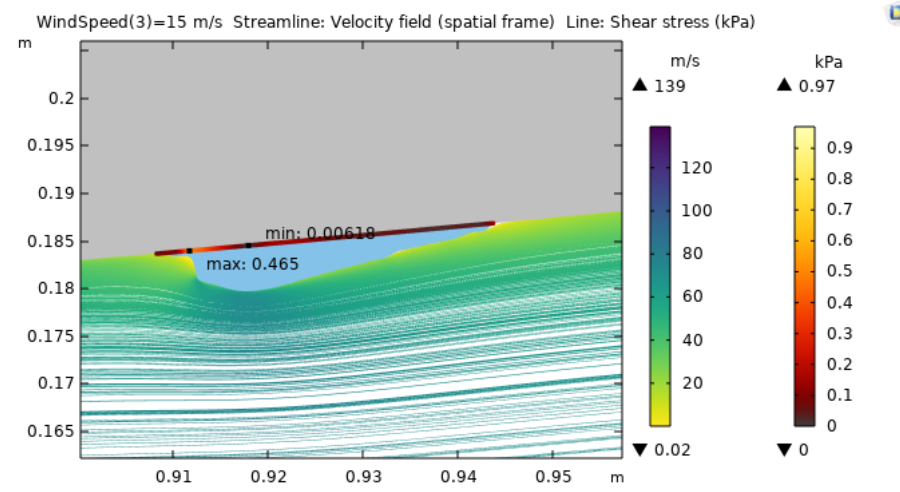
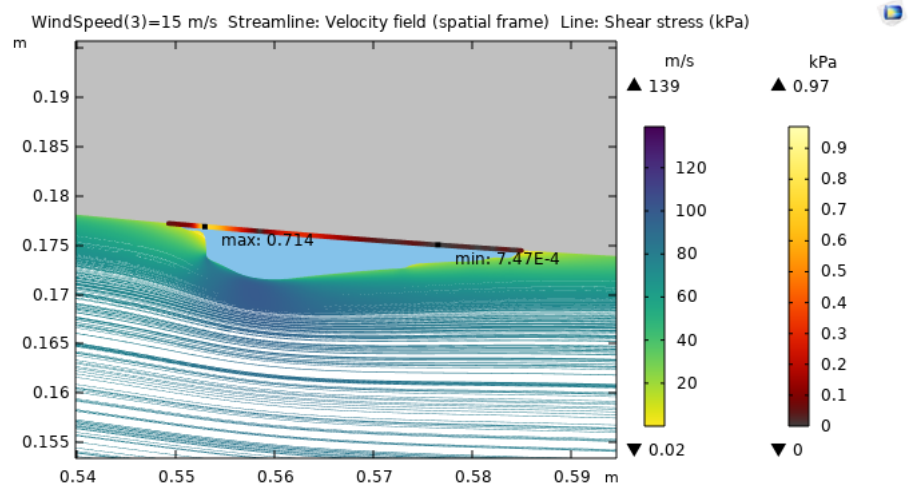
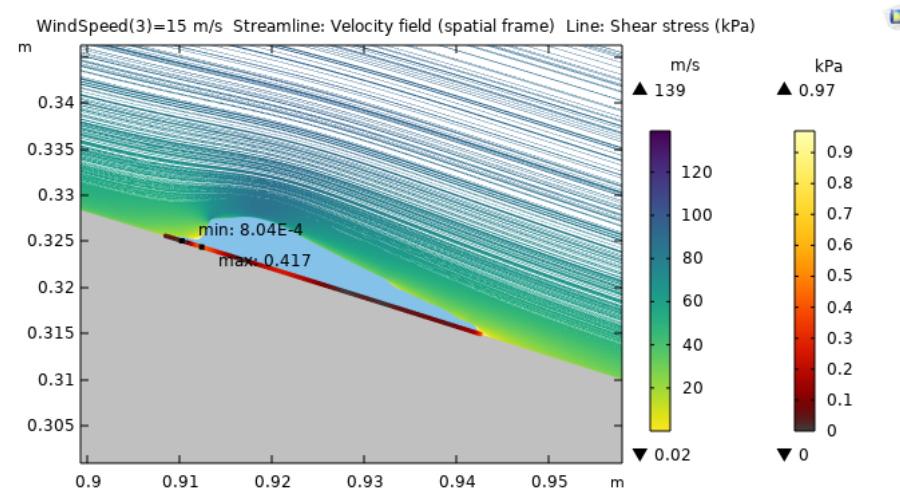
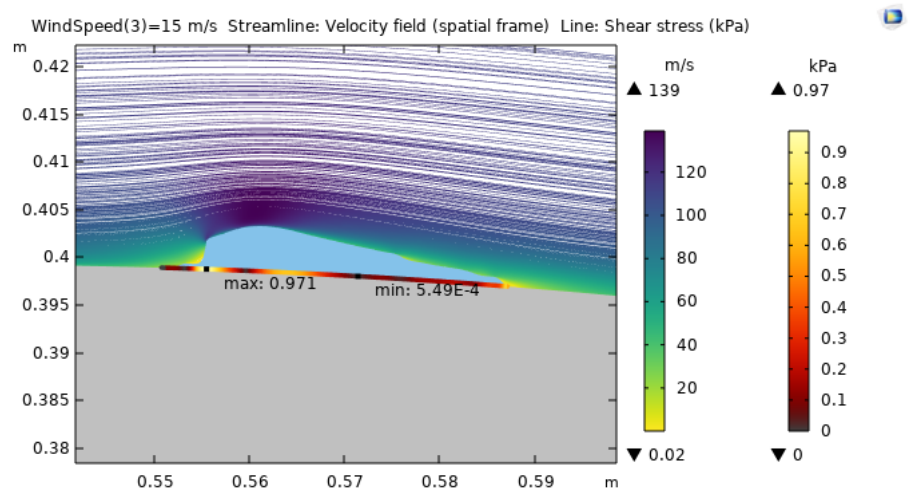
Geometry = Runback Ice; Height = 5 mm; Wind Speed = 5 m/s



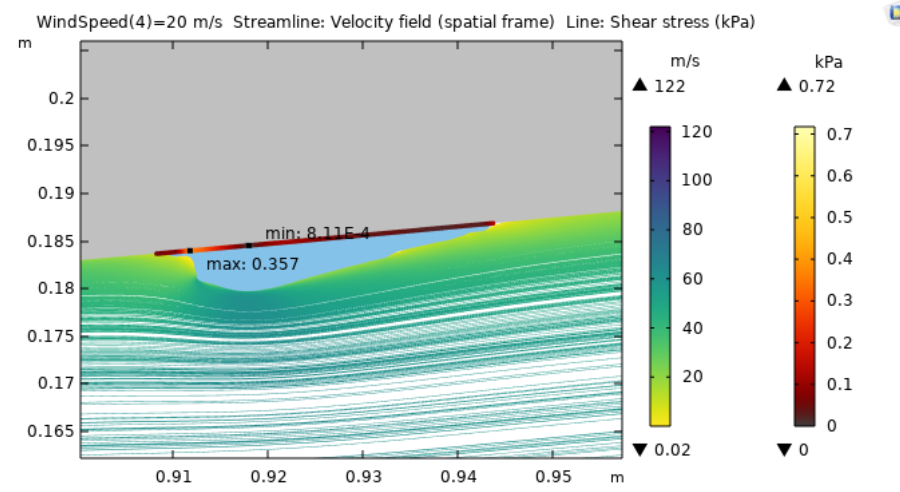
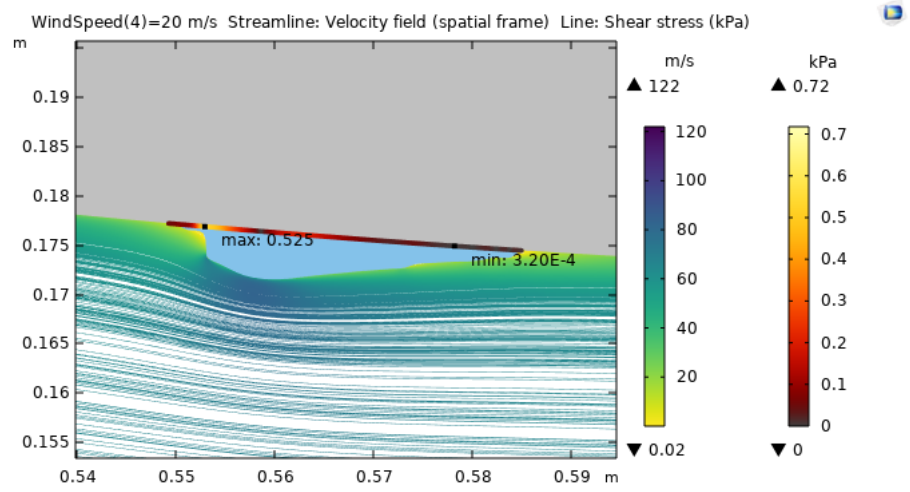
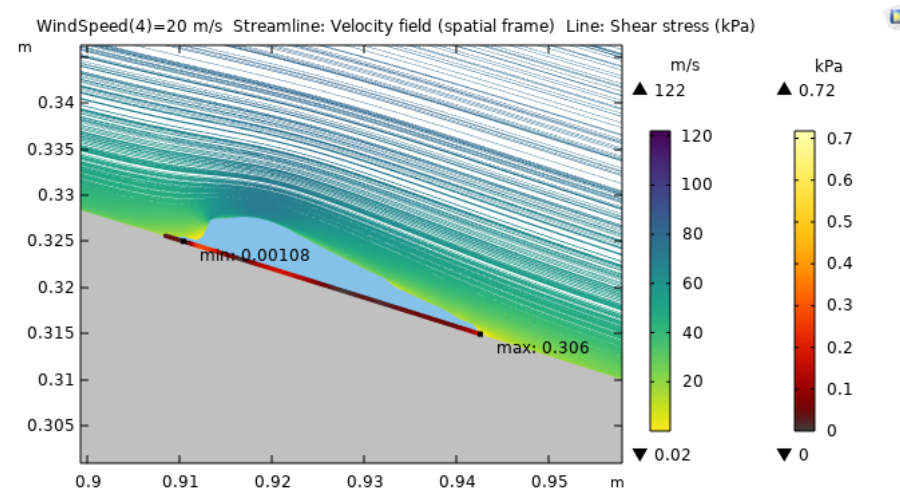
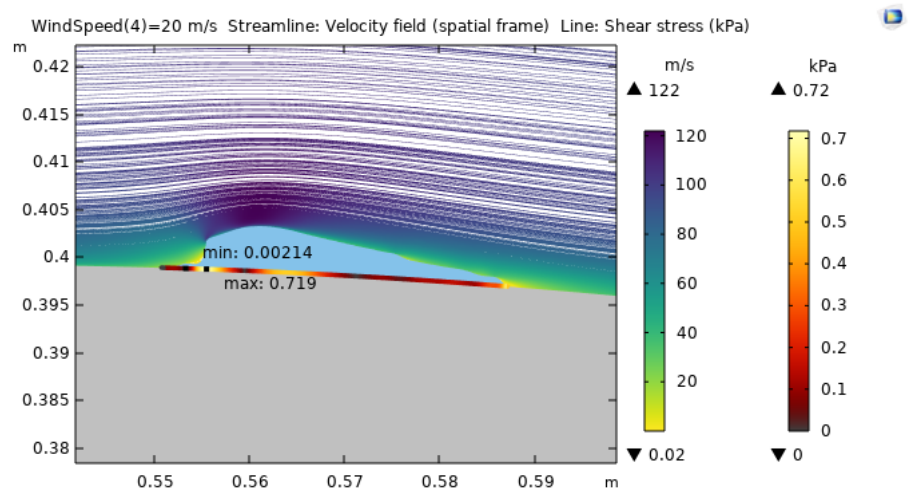
Geometry = Runback Ice; Height = 5 mm; Wind Speed = 10 mm/s



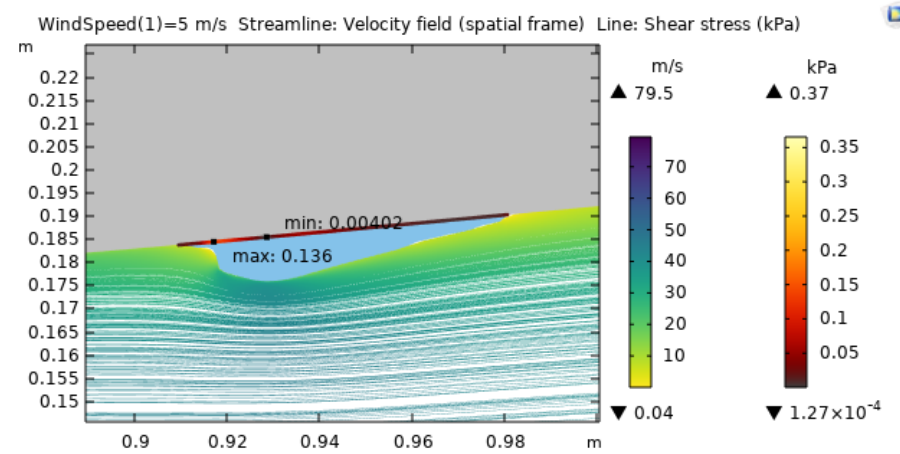
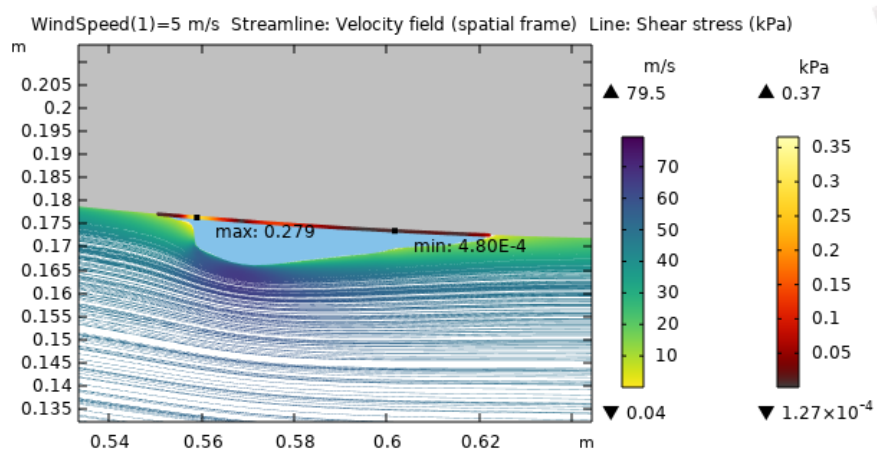
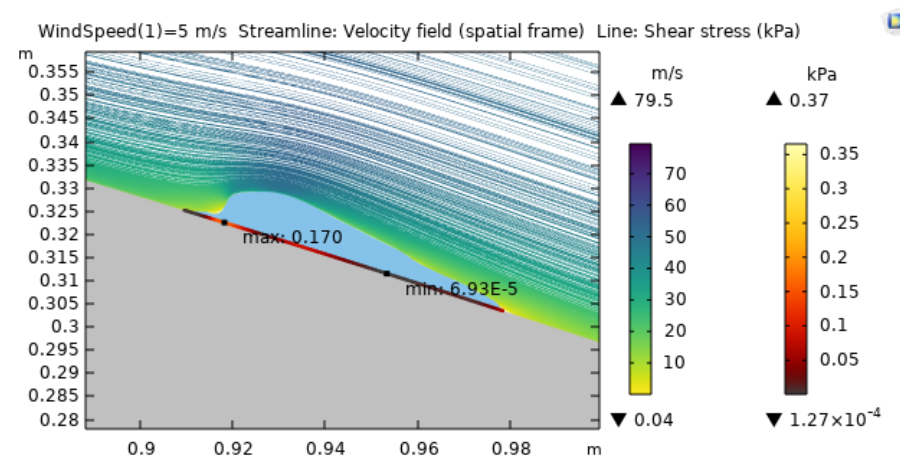
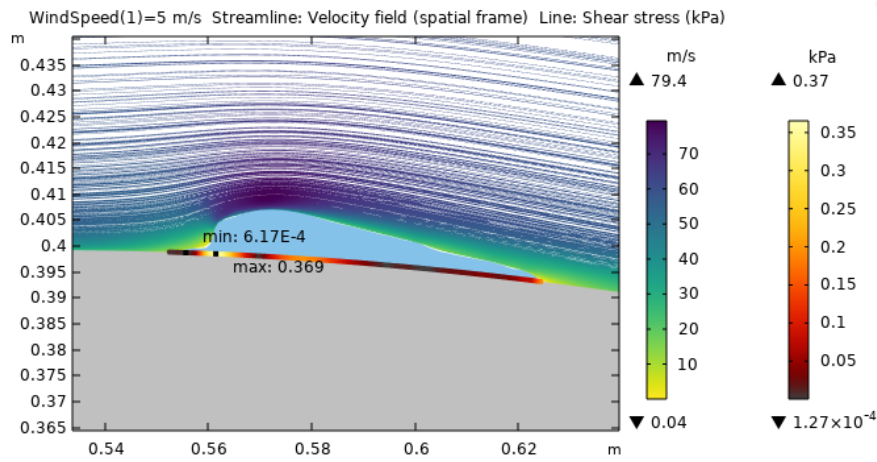
Geometry = Runback Ice; Height = 5 mm; Wind Speed = 15 mm/s



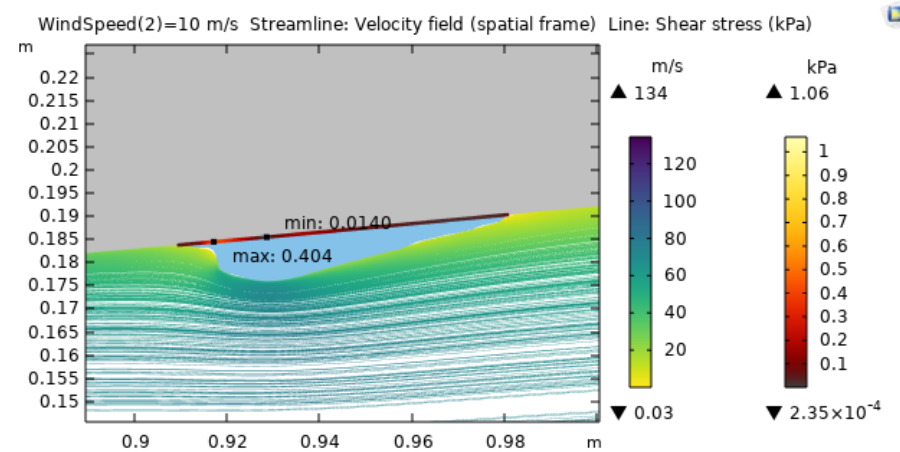
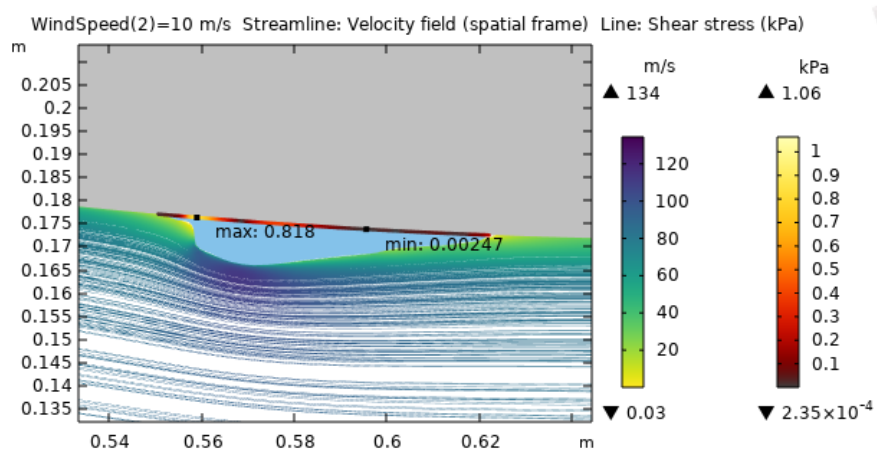
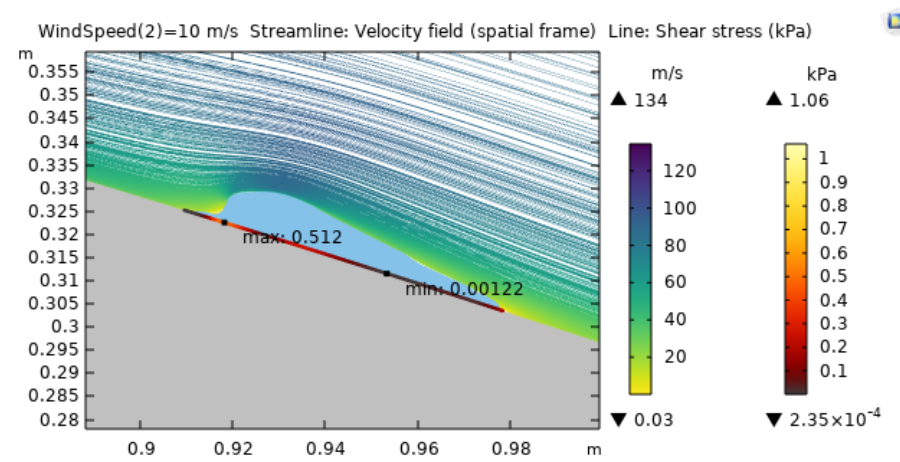
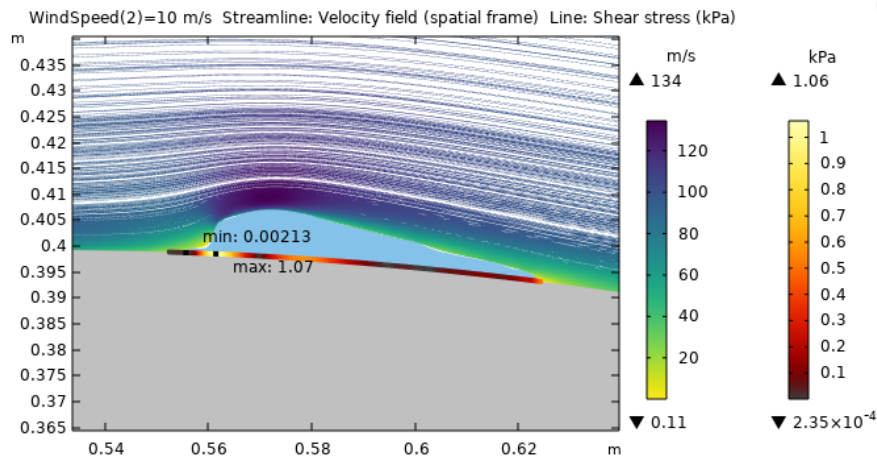
Geometry = Runback Ice; Height = 5 mm; Wind Speed = 20 mm/s



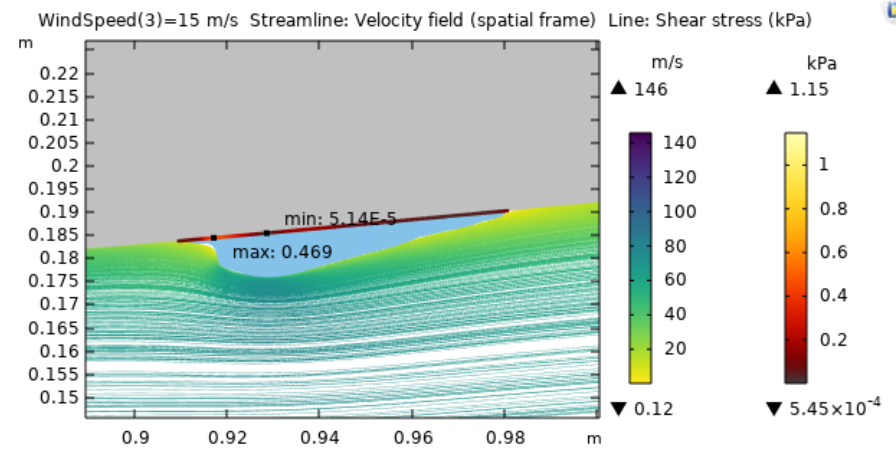
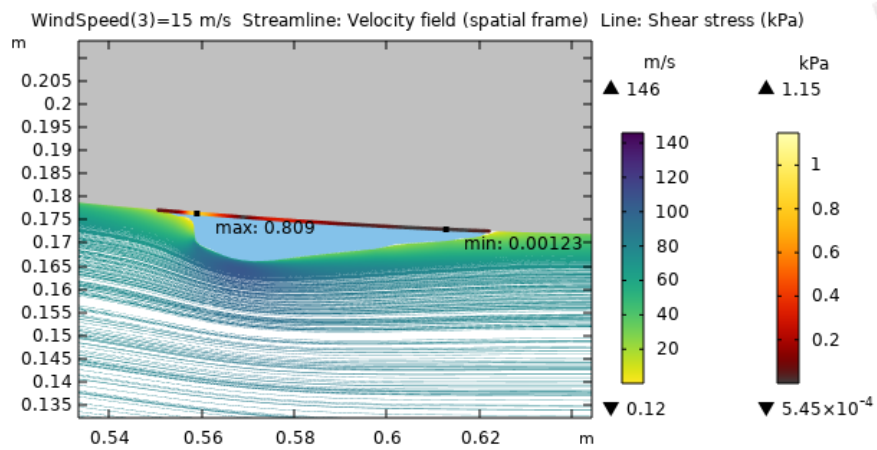
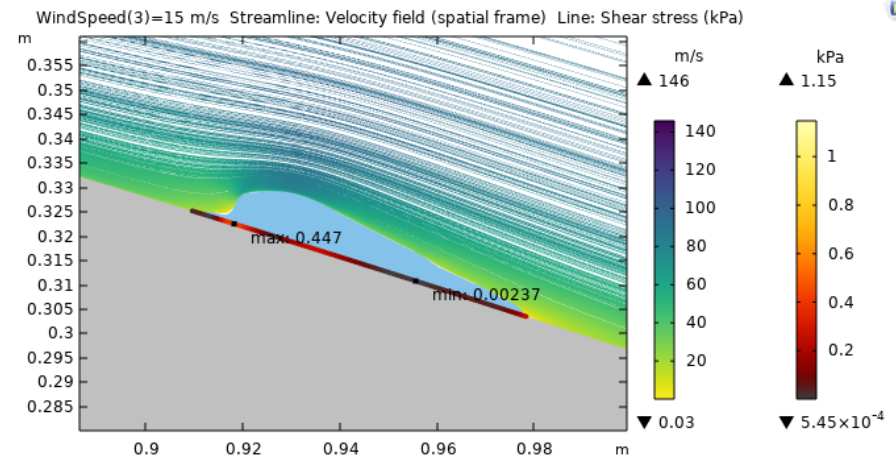
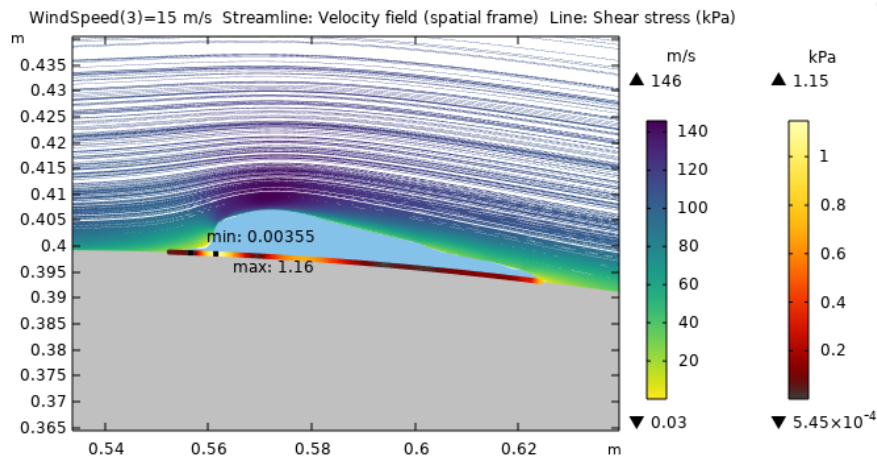
Geometry = Runback Ice; Height = 10 mm; Wind Speed = 5 mm/s



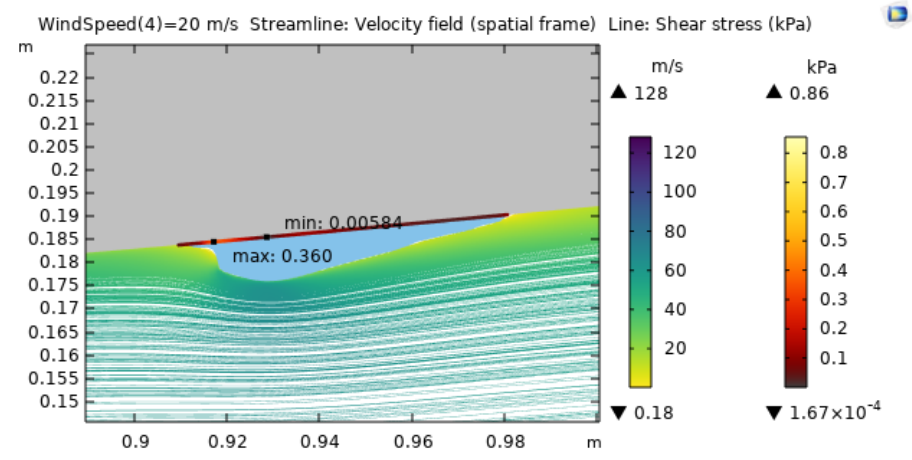
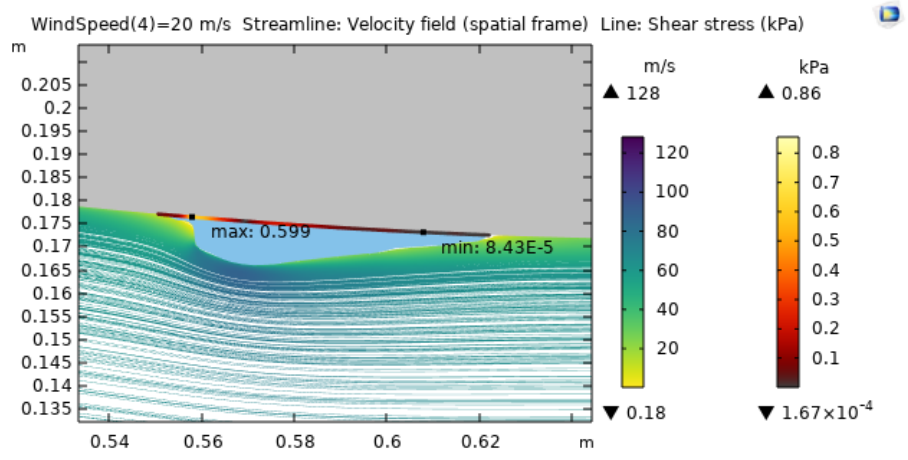
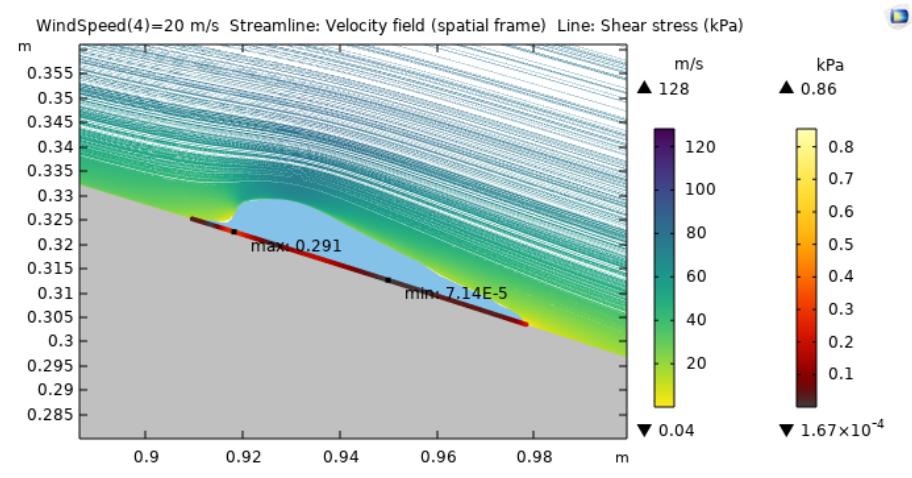
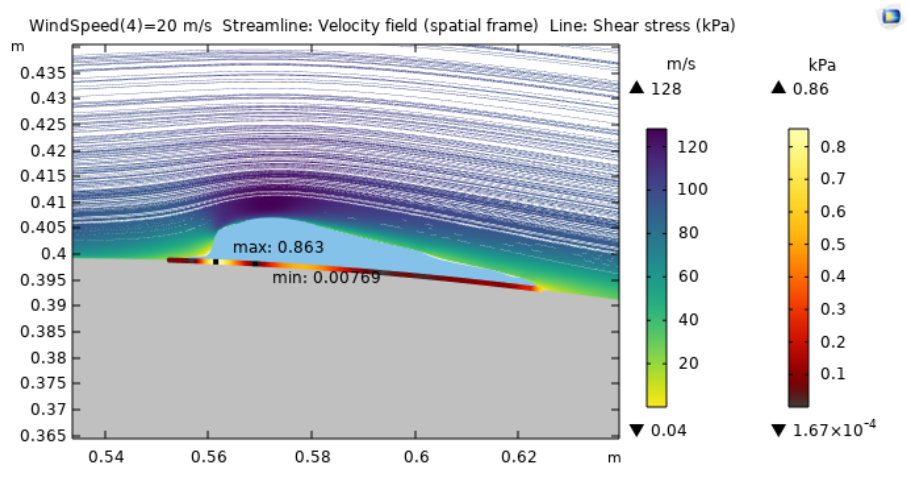
Geometry = Runback Ice; Height = 10 mm; Wind Speed = 10 m/s



Geometry = Runback Ice; Height = 10 mm; Wind Speed = 15 m/s



Geometry = Runback Ice; Height = 10 mm; Wind Speed = 20 mm/s



ANNEX G: COMSOL SHEAR STRESS RESULTS

Circular Geometry – Radius = 1 mm								
Velocity (mm/s)	5		10		15		20	
Shear Stress (kPa)	Max	Min	Max	Min	Max	Min	Max	Min
Position 1	0.515	0.091	1.430	0.234	1.940	0.291	1.590	0.238
Position 2	0.224	0.043	0.631	0.111	0.758	0.123	0.591	0.096
Position 3	0.264	0.054	0.772	0.143	0.835	0.096	0.653	0.055
Position 4	0.179	0.015	0.514	0.037	0.633	0.016	0.499	0.005

Circular Geometry – Radius = 5 mm								
Velocity (mm/s)	5		10		15		20	
Shear Stress (kPa)	Max	Min	Max	Min	Max	Min	Max	Min
Position 1	0.567	0.031	1.480	0.002	1.970	0.002	1.640	0.022
Position 2	0.234	0.017	0.622	0.005	0.727	0.024	0.570	0.033
Position 3	0.401	0.017	1.180	0.001	1.400	0.000	0.979	0.002
Position 4	0.221	0.000	0.657	0.000	0.812	0.0014	0.634	0.001

Circular Geometry – Radius = 10 mm								
Velocity (mm/s)	5		10		15		20	
Shear Stress (kPa)	Max	Min	Max	Min	Max	Min	Max	Min
Position 1	0.661	0.004	1.970	0.002	1.900	0.028	1.450	0.013
Position 2	0.245	0.002	0.793	0.012	0.629	0.004	0.511	0.002
Position 3	0.552	0.005	1.620	0.005	1.760	0.005	1.320	0.004
Position 4	0.268	0.002	0.805	0.009	1.040	0.017	0.817	0.014

Runback Ice Geometry – Radius = 1 mm								
Velocity (mm/s)	5		10		15		20	
Shear Stress (kPa)	Max	Min	Max	Min	Max	Min	Max	Min
Position 1	0.222	0.001	0.667	0.004	0.726	0.005	0.651	0.000
Position 2	0.110	0.000	0.340	0.000	0.323	0.001	0.264	0.002
Position 3	0.165	0.001	0.490	0.000	0.532	0.000	0.394	0.000
Position 4	0.105	0.000	0.310	0.000	0.365	0.004	0.280	0.000

Runback Ice Geometry – Radius = 5 mm								
Velocity (mm/s)	5		10		15		20	
Shear Stress (kPa)	Max	Min	Max	Min	Max	Min	Max	Min
Position 1	0.312	0.000	0.916	0.000	0.971	0.000	0.719	0.002
Position 2	0.154	0.000	0.470	0.000	0.417	0.000	0.306	0.001
Position 3	0.238	0.000	0.699	0.000	0.714	0.000	0.525	0.000
Position 4	0.135	0.002	0.400	0.004	0.465	0.006	0.357	0.000

Runback Ice Geometry – Radius = 10 mm								
Velocity (mm/s)	5		10		15		20	
Shear Stress (kPa)	Max	Min	Max	Min	Max	Min	Max	Min
Position 1	0.369	0.000	1.07	0.002	1.160	0.004	0.863	0.008
Position 2	0.170	0.000	0.512	0.001	0.447	0.002	0.291	0.000
Position 3	0.279	0.000	0.818	0.002	0.809	0.001	0.599	0.000
Position 4	0.136	0.004	0.404	0.014	0.469	0.000	0.360	0.006

REFERENCES

- [1] Vestas, “Vestas ranked the most sustainable company in the world 2022,” 2022. <https://www.vestas.com/en/sustainability/mostsustainablecompany> (accessed Jun. 07, 2022).
- [2] Inspire Clean Energy, “Who Discovered Wind Energy?” <https://www.inspirecleanenergy.com/blog/clean-energy-101/who-discovered-wind-energy> (accessed May 04, 2022).
- [3] Z. Shahan, “History of Wind Turbines,” 2014. <https://www.renewableenergyworld.com/storage/history-of-wind-turbines/#gref> (accessed May 04, 2022).
- [4] Fábio Alexandre Amorim Melo, “Doubly-fed Induction Generator Wind Turbine System,” 2019.
- [5] M. Gustavo and P. Enrique, “Modelling and Control Design of Pitch-Controlled Variable Speed Wind Turbines,” *Wind Turbines*, no. May, 2011, doi: 10.5772/15880.
- [6] A. Ilinca, “Analysis and Mitigation of Icing Effects on Wind Turbines.” doi: 10.5772/15484.
- [7] M. Klemm, “Economic Feasibility of Wind Turbines’ Anti-icing Systems: Development and Application of a Simple Heuristic Method and Tool,” *Uppsala Universitet*, vol. 39, no. 1, pp. 1–24, 2014, [Online]. Available: <https://uu.diva-portal.org/smash/get/diva2:1037164/FULLTEXT01.pdf>
- [8] O. Fakorede, Z. Feger, H. Ibrahim, A. Ilinca, J. Perron, and C. Masson, “Ice protection systems for wind turbines in cold climate: characteristics, comparisons and analysis,” *Renewable and Sustainable Energy Reviews*, vol. 65. Elsevier Ltd, pp. 662–675, Nov. 01, 2016. doi: 10.1016/j.rser.2016.06.080.
- [9] A. G. Kraj and E. L. Bibeau, “Measurement method and results of ice adhesion force on the curved surface of a wind turbine blade,” *Renew Energy*, vol. 35, no. 4, pp. 741–746, Apr. 2010, doi: 10.1016/j.renene.2009.08.030.
- [10] R. Cattin, “Icing of Wind Turbines,” Stockholm, 2012. [Online]. Available: http://winterwind.se/2012/wp-content/uploads/2012/08/Icing_of_windturbines_elforsk_report_12_13_draftversion_120127.pdf

- [11] O. Parent and A. Ilinca, "Anti-icing and de-icing techniques for wind turbines: Critical review," *Cold Reg Sci Technol*, vol. 65, no. 1, pp. 88–96, Jan. 2011, doi: 10.1016/j.coldregions.2010.01.005.
- [12] N. Dalili, A. Edrisy, and R. Carriveau, "A review of surface engineering issues critical to wind turbine performance," *Renewable and Sustainable Energy Reviews*, vol. 13, no. 2, pp. 428–438, Feb. 2009. doi: 10.1016/j.rser.2007.11.009.
- [13] C. Callahan, "What is rime ice? See the cool formations popping up in the Midwest," *Today*, 2021. <https://www.today.com/news/rime-ice-appearing-midwest-what-it-today-t205333> (accessed Jun. 08, 2022).
- [14] L. Ma, Z. Zhang, L. Gao, Y. Liu, and H. Hu, "An exploratory study on using Slippery-Liquid-Infused-Porous-Surface (SLIPS) for wind turbine icing mitigation," *Renew Energy*, vol. 162, pp. 2344–2360, Dec. 2020, doi: 10.1016/j.renene.2020.10.013.
- [15] Wikipedia, "Glaze (ice)." https://www.wikiwand.com/en/Glaze_%28ice%29 (accessed Jun. 08, 2022).
- [16] Oloufemi. Fakorede, Adrian. Ilinca, Hussein. Ibrahim, and Jean. Perron, *Modelling Ice Accretion and Its Effects on Wind Turbine Blades*. 2013.
- [17] Q. Hongwu -PhD and A. Professor, "Research on the Mechanism of Wind Turbine Blades Ice Coating and Anti-icing Methods."
- [18] Enercon, "Windblatt," *Enercon Magazine for wind energy*, 2011.
- [19] K. Al-Khalil, "Thermo-mechanical expulsion deicing system - TMEDS," *Collection of Technical Papers - 45th AIAA Aerospace Sciences Meeting*, vol. 12, pp. 8562–8574, 2007, doi: 10.2514/6.2007-692.
- [20] V. Daniliuk, Y. Xu, R. Liu, T. He, and X. Wang, "Ultrasonic de-icing of wind turbine blades: Performance comparison of perspective transducers," *Renew Energy*, vol. 145, pp. 2005–2018, 2020, doi: 10.1016/j.renene.2019.07.102.
- [21] Delce-UT, "Summary description of project context and objectives," 2014. <http://www.deice-ut.eu/publications/> (accessed Jul. 07, 2022).
- [22] Ewind, "Wind power in Finland: wind farm will be powered by 93MW of Vestas wind turbines," 2015. <https://www.ewind.es/2015/09/30/wind-power-in-finland-wind-farm-will-be-powered-by-93mw-of-vestas-wind-turbines/54253> (accessed Jul. 07, 2022).

- [23] S. T. Examiners, P. Vuoristo, and H. Koivuluoto, "CHRISTIAN STENROOS PROPERTIES OF ICEPHOBIC SURFACES IN DIFFERENT ICING Master ' s Degree Programme Materials Science," p. 108, 2015, [Online]. Available: <https://trepo.tuni.fi/bitstream/handle/123456789/23364/Stenroos.pdf?sequence=3&isAllowed=y>
- [24] M. Froese, "The cold, hard truth about ice on turbine blades," 2018. <https://www.windpowerengineering.com/the-cold-hard-truth-about-ice-on-turbine-blades/> (accessed Jul. 17, 2022).
- [25] T. Weis and J. Maissan, "The effects of black blades on surface temperatures for wind turbines," 2003.
- [26] C. Gessel, "Research into the effect of black blade in wind turbine," 2022. <https://group.vattenfall.com/press-and-media/newsroom/2022/black-turbine-blades-reduce-bird-collisions> (accessed Jul. 06, 2022).
- [27] Reve, "Black paint on wind turbines helps prevent bird deaths," 2020. <https://www.evwind.es/2020/08/25/black-paint-on-wind-turbines-helps-prevent-bird-deaths/76783> (accessed Jun. 17, 2022).
- [28] X. Huang *et al.*, "A survey of icephobic coatings and their potential use in a hybrid coating/active ice protection system for aerospace applications," *Progress in Aerospace Sciences*, vol. 105. Elsevier Ltd, pp. 74–97, Feb. 01, 2019. doi: 10.1016/j.paerosci.2019.01.002.
- [29] L. Gao, Y. Liu, L. Ma, and H. Hu, "A hybrid strategy combining minimized leading-edge electric-heating and superhydro-/ice-phobic surface coating for wind turbine icing mitigation," *Renew Energy*, vol. 140, pp. 943–956, Sep. 2019, doi: 10.1016/j.renene.2019.03.112.
- [30] D. Weston, "Vestas launches electrothermal anti-ice system," 2018. <https://www.windpowermonthly.com/article/1456241/vestas-launches-electrothermal-anti-ice-system>
- [31] Vestas, "Vestas Anti-Icing System™ Part of Vestas Cold Climate Solutions," 2018.
- [32] K. Gregory, "Vestas Cold Climate Solutions," 2020.
- [33] L. Boinovich and A. Emelyanenko, "Anti-icing potential of superhydrophobic coatings," *Mendeleev Commun*, vol. 23, pp. 3–10, 2013.

- [34] W. Huang, J. Huang, Z. Guo, and W. Liu, "Icephobic/anti-icing properties of superhydrophobic surfaces," *Advances in Colloid and Interface Science*, vol. 304. Elsevier B.V., Jun. 01, 2022. doi: 10.1016/j.cis.2022.102658.
- [35] M. Shamshiri, R. Jafari, and G. Momen, "Potential use of smart coatings for icephobic applications: A review," *Surf Coat Technol*, vol. 424, Oct. 2021, doi: 10.1016/j.surfcoat.2021.127656.
- [36] H. Sojoudi, M. Wang, N. D. Boscher, G. H. McKinley, and K. K. Gleason, "Durable and scalable icephobic surfaces: Similarities and distinctions from superhydrophobic surfaces," *Soft Matter*, vol. 12, no. 7. Royal Society of Chemistry, pp. 1938–1963, Feb. 21, 2016. doi: 10.1039/c5sm02295a.
- [37] Z. He, Y. Zhuo, Z. Zhang, and J. He, "Design of icephobic surfaces by lowering ice adhesion strength: A mini review," *Coatings*, vol. 11, no. 11. MDPI, Nov. 01, 2021. doi: 10.3390/coatings11111343.
- [38] Properla, "The Lotus Effect," 2017. <https://www.properla.co.uk/lotus-effect/> (accessed Jun. 15, 2022).
- [39] B. Boston, "How duck feathers could inspire warmer raincoats," 2017. <https://www.futurity.org/heat-exchange-superhydrophobicity-1464212/> (accessed Jun. 15, 2022).
- [40] V. Okulov, I. Kabardin, D. Mukhin, K. Stepanov, and N. Okulova, "Physical de-icing techniques for wind turbine blades," *Energies*, vol. 14, no. 20. MDPI, Oct. 01, 2021. doi: 10.3390/en14206750.
- [41] S. Farhadi, M. Farzaneh, and S. A. Kulinich, "Anti-icing performance of superhydrophobic surfaces," *Appl Surf Sci*, vol. 257, no. 14, pp. 6264–6269, 2011, doi: 10.1016/j.apsusc.2011.02.057.
- [42] N. Wang, D. Xiong, Y. Deng, Y. Shi, and K. Wang, "Mechanically robust superhydrophobic steel surface with anti-icing, UV-durability, and corrosion resistance properties," *ACS Appl Mater Interfaces*, vol. 7, no. 11, pp. 6260–6272, 2015, doi: 10.1021/acsami.5b00558.
- [43] T. Verho, C. Bower, P. Andrew, S. Franssila, O. Ikkala, and R. H. A. Ras, "Mechanically Durable Superhydrophobic Surfaces," *Advanced Materials*, vol. 23, no. 5, pp. 673–678, 2011, doi: 10.1002/adma.201003129.

- [44] P. Irajizad, S. Nazifi, and H. Ghasemi, "Icephobic surfaces: Definition and figures of merit," *Advances in Colloid and Interface Science*, vol. 269. Elsevier B.V., pp. 203–218, Jul. 01, 2019. doi: 10.1016/j.cis.2019.04.005.
- [45] C. Antonini, M. Innocenti, T. Horn, M. Marengo, and A. Amirfazli, "Understanding the effect of superhydrophobic coatings on energy reduction in anti-icing systems," *Cold Reg Sci Technol*, vol. 67, no. 1–2, pp. 58–67, Jun. 2011, doi: 10.1016/j.coldregions.2011.02.006.
- [46] Ramé-hart, "Information on Contact Angle," 2022. <http://www.ramehart.com/contactangle.htm> (accessed Jun. 06, 2022).
- [47] T. Young, "An Essay on the Cohesion of Fluids," in *Philosophical Transactions of the Royal Society of London*, 1805, pp. 65–87.
- [48] M. Raquel De Vasconcelos and B. Jardim, "Development of Superhydrophobic Coatings for Textile and Glass Surfaces," 2018.
- [49] F. Mussano, T. Genova, and S. Carossa, "Possible Role of Microcrystallinity on Surface Properties of Titanium Surfaces for Biomedical Application," 2016. <https://www.intechopen.com/chapters/50483> (accessed May 03, 2022).
- [50] W. N, "Resistance of solid surfaces to wetting by water," 1936, pp. 988–994.
- [51] J. Andersson, "Evaluation of Capillary Flow in Gels-The Liquid Uptake of Capillaries and Gelation Mechanisms in Alginate Gels", doi: 10.13140/RG.2.2.31074.73920.
- [52] Z. Wang, M. Elimelech, and S. Lin, "Environmental Applications of Interfacial Materials with Special Wettability," *Environ Sci Technol*, vol. 50, no. 5, pp. 2132–2150, 2016, doi: 10.1021/acs.est.5b04351.
- [53] C. D and B. S, "Wettability of porous surfaces," 1944, pp. 546–51.
- [54] J. Heriberto, O. Nascimento, P. Machado, E. F. de Freitas, and P. A. A. Pereira, "Aplicação de um novo compósito biomimético nanoparticulado com propriedades superhidrofóbicas e anti-gelo para pavimentos rodoviários," 2011.
- [55] L. Makkonen, "Surface melting of ice," *Journal of Physical Chemistry B*, vol. 101, no. 32, pp. 6196–6200, 1997, doi: 10.1021/jp963248c.
- [56] L. Makkonen, "Ice adhesion - Theory, measurements and countermeasures," *J Adhes Sci Technol*, vol. 26, no. 4–5, pp. 413–445, 2012, doi: 10.1163/016942411X574583.

- [57] M. Nosonovsky and V. Hejazi, "Why superhydrophobic surfaces are not always icephobic," *ACS Nano*, vol. 6, no. 10, pp. 8488–8491, Oct. 23, 2012. doi: 10.1021/nn302138r.
- [58] A. Elzaabalawy and S. A. Meguid, "Development of novel icephobic surfaces using siloxane-modified epoxy nanocomposites," *Chemical Engineering Journal*, vol. 433, no. P3, p. 133637, 2022, doi: 10.1016/j.cej.2021.133637.
- [59] A. Laroche, M. J. Grasso, A. Dolatabadi, and E. Bonaccorso, "Tensile and Shear Test Methods for Quantifying the Ice Adhesion Strength to a Surface," *Ice Adhesion*, pp. 237–284, 2020, doi: 10.1002/9781119640523.ch9.
- [60] X. Tan *et al.*, "A simple fabrication of superhydrophobic PVDF/SiO₂ coatings and their anti-icing properties," *J Mater Res*, vol. 36, no. 3, pp. 637–645, 2021, doi: 10.1557/s43578-020-00034-z.
- [61] Y. Hou and K. L. Choy, "Durable and robust PVDF-HFP/SiO₂/CNTs nanocomposites for anti-icing application: Water repellency, icing delay, and ice adhesion," *Prog Org Coat*, vol. 163, no. November 2021, p. 106637, 2022, doi: 10.1016/j.porgcoat.2021.106637.
- [62] M. Bleszynski, R. Woll, J. Middleton, and M. Kumosa, "Effects of crosslinking, embedded TiO₂ particles and extreme aging on PDMS icephobic barriers," *Polym Degrad Stab*, vol. 166, pp. 272–282, 2019, doi: 10.1016/j.polymdegradstab.2019.06.005.
- [63] R. Menini and M. Farzaneh, "Elaboration of Al₂O₃/PTFE icephobic coatings for protecting aluminum surfaces," *Surf Coat Technol*, vol. 203, no. 14, pp. 1941–1946, 2009, doi: 10.1016/j.surfcoat.2009.01.030.
- [64] R. Karmouch, S. Coudé, G. Abel, and G. G. Ross, "Icephobic PTFE coatings for wind turbines operating in cold climate conditions," in *2009 IEEE Electrical Power and Energy Conference, EPEC 2009*, 2009. doi: 10.1109/EPEC.2009.5420897.
- [65] M. Zou, S. Beckford, R. Wei, C. Ellis, G. Hatton, and M. A. Miller, "Effects of surface roughness and energy on ice adhesion strength," *Appl Surf Sci*, vol. 257, no. 8, pp. 3786–3792, 2011, doi: 10.1016/j.apsusc.2010.11.149.
- [66] T. Bharathidasan, S. V. Kumar, M. S. Bobji, R. P. S. Chakradhar, and B. J. Basu, "Effect of wettability and surface roughness on ice-adhesion strength of hydrophilic, hydrophobic and superhydrophobic surfaces," *Appl Surf Sci*, vol. 314, pp. 241–250, 2014, doi: 10.1016/j.apsusc.2014.06.101.

- [67] Z. He, Y. Zhuo, F. Wang, J. He, and Z. Zhang, "Design and preparation of icephobic PDMS-based coatings by introducing an aqueous lubricating layer and macro-crack initiators at the ice-substrate interface," *Prog Org Coat*, vol. 147, no. November 2019, p. 105737, 2020, doi: 10.1016/j.porgcoat.2020.105737.
- [68] Z. A. Janjua *et al.*, "Performance and durability tests of smart icephobic coatings to reduce ice adhesion," *Appl Surf Sci*, vol. 407, pp. 555–564, 2017, doi: 10.1016/j.apsusc.2017.02.206.
- [69] R. Khammas and H. Koivuluoto, "Durable Icephobic Slippery Liquid-Infused Porous Surfaces (SLIPS) Using Flame- and Cold-Spraying," *Sustainability (Switzerland)*, vol. 14, no. 14, 2022, doi: 10.3390/su14148422.
- [70] E. Tetteh and E. Loth, "Reducing static and impact ice adhesion with a self-lubricating icephobic coating (SLIC)," *Coatings*, vol. 10, no. 3, Mar. 2020, doi: 10.3390/coatings10030262.
- [71] S. A. Kulinich, S. Farhadi, K. Nose, and X. W. Du, "Superhydrophobic surfaces: Are they really ice-repellent?," *Langmuir*, vol. 27, no. 1, pp. 25–29, Jan. 04, 2011. doi: 10.1021/la104277q.
- [72] Z. Ghalmi and M. Farzaneh, "Experimental investigation to evaluate the effect of PTFE nanostructured roughness on ice adhesion strength," *Cold Reg Sci Technol*, vol. 115, pp. 42–47, 2015, doi: 10.1016/j.coldregions.2015.03.009.
- [73] S. A. Kulinich and M. Farzaneh, "On ice-releasing properties of rough hydrophobic coatings," *Cold Reg Sci Technol*, vol. 65, no. 1, pp. 60–64, 2011, doi: 10.1016/j.coldregions.2010.01.001.
- [74] C. Peng, S. Xing, Z. Yuan, J. Xiao, C. Wang, and J. Zeng, "Preparation and anti-icing of superhydrophobic PVDF coating on a wind turbine blade," *Appl Surf Sci*, vol. 259, pp. 764–768, Oct. 2012, doi: 10.1016/j.apsusc.2012.07.118.
- [75] M. J. Toh, P. C. Oh, and M. I. S. Mohd Shaufi, "Preparation of Highly Hydrophobic PVDF-HFP Membrane with Anti-Wettability Characteristic," *IOP Conf Ser Mater Sci Eng*, vol. 778, no. 1, 2020, doi: 10.1088/1757-899X/778/1/012176.
- [76] Wearlon Plastic Maritime Corporation, "Wearlon® Super F-1 - Ice Prevention Coating," 2022. http://www.wearloncorp.com/index.php/datasheet/Wearlon_Super_F-1 (accessed Jul. 31, 2022).

- [77] Chemona Nanocoat Technologies, “Multi-Coat Technical Data Sheet.” https://www.chemona.us/wp-content/uploads/2019/12/Multi-Coat_EN-2-1.pdf (accessed Jul. 31, 2022).
- [78] Chemona Nanocoat Technologies, “Multi Coat Safety Data Sheet,” vol. 2022, pp. 1–13, 2022, [Online]. Available: https://www.chemona.us/wp-content/uploads/2022/02/SDS_Multi-Coat_2.0_EN.pdf
- [79] NTT Advanced Technology Corporation, “HIREC® 100 Super Water Repellent Coatings NTT-AT Datasheet,” 2020.
- [80] E. J. Y. Ling, V. Uong, J. S. Renault-Crispo, A. M. Kietzig, and P. Servio, “Reducing Ice Adhesion on Nonsmooth Metallic Surfaces: Wettability and Topography Effects,” *ACS Appl Mater Interfaces*, vol. 8, no. 13, pp. 8789–8800, 2016, doi: 10.1021/acsami.6b00187.
- [81] A. Ramachandran, “Relative Standard Deviation.” <https://www.wallstreetmojo.com/relative-standard-deviation-formula/> (accessed Nov. 12, 2022).
- [82] M. Huré, P. Olivier, and J. Garcia, “Effect of Cassie-Baxter versus Wenzel states on ice adhesion: A fracture toughness approach,” *Cold Reg Sci Technol*, vol. 194, no. April 2021, 2022, doi: 10.1016/j.coldregions.2021.103440.
- [83] Solvay, “Solef® PVDF Typical Properties Overview,” 2020.
- [84] K. Parmar, “The Aerodynamic Effects of Runback Ice,” no. September, 2013, [Online]. Available: <https://dspace.lib.cranfield.ac.uk/handle/1826/8429>
- [85] Cadence, “What is Signal to Noise Ratio and How to calculate it?” <https://resources.pcb.cadence.com/blog/2020-what-is-signal-to-noise-ratio-and-how-to-calculate-it> (accessed Nov. 26, 2022).
- [86] C. M. Bentz, L. Baudzus, and P. M. Krummrich, “Signal to noise ratio (SNR) enhancement comparison of impulse-, coding- and novel linear-frequency-chirp-based optical time domain reflectometry (OTDR) for passive optical network (PON) monitoring based on unique combinations of wavelength selective mirro,” *Photonics*, vol. 1, no. 1, pp. 33–46, 2014, doi: 10.3390/photonics1010033.

- [87] Empiria Studio, “Signal-to-Noise Ratio.”
https://www.licor.com/bio/help/empiria_studio/software/empiria_studio/calculate/blot/signal-to-noise.html (accessed Nov. 28, 2022).
- [88] M. Bleszynski and E. Clark, “Current Ice Adhesion Testing Methods and the Need for a Standard: A Concise Review,” *Standards*, vol. 1, no. 2, pp. 117–133, 2021, doi: 10.3390/standards1020011.